RPSEA
FINAL REPORT

Authors: Marc Mansfield, Seth Lyman, Huy Tran
Bingham Research Center, Utah State University

Measurement of Hydrocarbon and Greenhouse Gas Emissions from Uncharacterized Area Sources

Contract Number 12122-15

31 August 2016

Principal Investigator: Seth Lyman, PhD
Director, Bingham Research Center
Utah State University
320 N. Aggie Blvd., Vernal, Utah 84078

LEGAL NOTICE

Abstract for:
RPSEA Final Report: Measurement of Hydrocarbon and Greenhouse Gas Emissions from Uncharacterized Area Sources

We have measured emissions of a suite of organic compounds and carbon dioxide to the atmosphere from several uncharacterized area sources associated with the natural gas or oil production industry. The geographic setting of the study was several gas or oil producing basins in Eastern Utah (Uintah, Clay, and Paradox Basins) and West Central Wyoming (Upper Green River Basin). These sources include produced water surface impoundments ("ponds"), subsurface leakage from natural gas wells, natural seepage, land farms, and emissions from the snowpack. We have also measured concentrations of a suite of organic compounds in produced water ponds. The measurement techniques consisted of flux chamber and plume characterization combined with inverse modeling.

The emissions from the ponds included methane, non-methane hydrocarbons (NMHC), alcohols, and carbon dioxide. The NMHC emission is dominated by the aromatics (benzene, toluene, ethylbenzene, and xylenes; BTEX) and by C5 to C8 alkanes. The alcohol emission is dominated by methanol. The strongest hydrocarbon emissions are observed from water that has recently entered the facility, while carbon dioxide emissions persist as the water ages. Assuming that our results can scale to all the ponds in the Uintah Basin, we estimate a total non-methane organic emission of 2800 tonnes/year. The methane emission constitutes 0.1% and 0.2%, respectively, of two separate emissions inventories, while the non-methane organic emission constitutes 1.5% and 2.8%, respectively.

We measured methane emissions at 27 different natural gas well pads, some of which had previously exhibited large combustible soil gas concentrations. On average, emissions of methane drop off with distance from the well pad, suggesting that we are detecting wellbore leakage. When these results are scaled up to the entire Uintah Basin, we find that this leakage mode is an insignificant contribution ($\approx 0.004\%$) to the total CH_4 flux. It is also an insignificant portion ($\approx 0.0003\%$) of total natural gas production. In an effort to detect natural seepage, we deployed the flux chamber over surface outcrops of coal, oil shale, gilsonite, and over a fault system. No significant fluxes of methane or NMHC were observed.

We performed 21 flux chamber measurements at a facility that contained two land farms. Based on our measurements, we estimate that a 2-hectare (ha) active land farm would emit about 100 kg/day of total hydrocarbons, including about 10 kg/day of BTEX compounds.

It is well known that exchange of compounds between the atmosphere and the snowpack in polar regions has an influence on the chemistry and physics of the troposphere. Similar measurements in oil- or gas-producing basins are practically non-existent. Our flux chamber measurements indicate an average NMHC emission (including methanol) from Uintah Basin snowpacks of about 2 mg m^{-2} h^{-1}, equivalent to 2×10^3 kg/h over a total area of 10^3 km^2, meaning that snowpack physics and chemistry should probably not be ignored in models of the winter ozone phenomenon.

THIS PAGE INTENTIONALLY LEFT BLANK

ACKNOWLEDGEMENTS

Funding for various components of this project was provided by

Research Partnership to Secure Energy for America/U.S. Department of Energy (Contract No. 12122-15)
Bureau of Land Management (Cooperative Agreement No. L13AC00292)
Uintah Impact Mitigation Special Service District
GSI, Inc./State of Wyoming
Utah State and Institutional Trust Lands Administration

The authors would also like to acknowledge the contributions from the entire Bingham Center Air Quality Research Team, all of whom contributed in some way to this project:

Randy Anderson	Marc Mansfield
Jordan Evans	Trevor O'Neil
Colleen Jones	Huy Tran
Jerimiah Lamb	Trang Tran
Seth Lyman	Cody Watkins

Several collaborators from other organizations also assisted with fieldwork:

Mike McKinley, Bureau of Land Management
Ryan Rowland, US Geological Survey
Cara Keslar, Wyoming DAQ
Ann Smith, GSI
Ric Bowers, GSI

Site access and logistical support was provided by many generous energy companies.

MEASUREMENT OF HYDROCARBON AND GREENHOUSE GAS EMISSIONS FROM UNCHARACTERIZED AREA SOURCES

Table of Contents

I. INTRODUCTION

Atmospheric emissions from the oil and gas industry include the greenhouse gases methane and carbon dioxide [Karion et al., 2013; Howarth et al., 2011; Brandt, et al., 2014], as well as volatile organic compounds (VOC) and nitrogen oxides (NO_x) [Lyman & Tran, 2015; Rappenglück, et al., 2014; Edwards, et al., 2014; Prenni, et al., 2016; McDuffie, et al., 2016], which can react together in the atmosphere to form ozone and particulate pollution. Emissions from the oil and gas sector, and oil and gas impacts on air quality and climate, have been studied extensively [Karion et al., 2013; Howarth et al., 2011; Brandt et al., 2014; Allen et al., 2013; Kang et al., 2014; Colborn, et al., 2014; Hendler, et al., 2009; Warneke et al., 2014]. However, in many cases emissions inventories underestimate field-wide or basin-wide emissions measurements [Karion et al., 2013; Brandt et al., 2014; Ahmadov et al, 2015]. This discrepancy could be due to underestimates in the emission factors or activity data used to generate emissions inventories. It could also be due to emission source categories that are excluded from current emissions inventories. This report summarizes our results for several uncharacterized emissions sources that we studied in the Rocky Mountain Region of the Western USA.

Produced Water Surface Impoundments

One emission source neglected in current emissions inventories is produced water surface impoundments [Friesen et al, 2009; Stoeckenius et al, 2014]. The only publicly-available study of atmospheric emissions from this source category included only two facilities over a few days [Thoma, 2009]. In the absence of information about emissions, some regulatory agencies have required operators to assume 100% of organic compounds that enter disposal ponds are emitted into the atmosphere, an assumption that almost certainly overestimates true emissions [Dicataldo et al, 2009]. Without emissions data, it will be impossible to include produced water surface impoundments in emissions inventories or adequately account for them in regulations.

Produced water is a complex solution containing hydrocarbons and other organic and inorganic compounds [Benko & Drewes, 2008; Dórea et al., 2007; Lu et al., 2006; Neff et al, 2011; Tibbetts et al, 1992; Utvik, 1999; Clark & Veil]. Because constituents of produced water vary by region, well location, treatment methods and well depth, no absolute compositional definition exists for produced water [Veil et al., 2004]. Total dissolved solids (TDS) in produced water range in concentrations from near zero to more than 75,000 ppm [Zhang et al., 2009], with a median of 13,200 for Utah's Uintah Basin, where much of the work presented below was conducted [Benko & Drewes, 2008], and inorganic ions tend to be dominated by Na-Cl [Zhang et al., 2009]. It tends to be rich in hydrocarbons, especially aromatics [Dórea et al., 2007], and can contain high concentrations of water-soluble organics like methanol [Veil et al., 2004]. Water disposed of or stored in surface impoundments often includes both produced water and fluid that flows back from the well to the surface after hydraulic fracturing.

Produced water represents a large portion of the material brought to the surface during the oil and gas production process. More than five barrels of water are produced per barrel of oil in the United States, and 182 barrels of water are produced per Mmcf of natural gas [Clark & Veil, 2009]. Most produced water in the United States is injected back into the subsurface, but about 2% is disposed of by depositing it in surface ponds and allowing it to evaporate into the atmosphere. In arid Western states, the percentage of produced water disposed of by evaporation is higher. In the Uintah Basin, 11% is disposed of this way [Chidsey, 2015]. Water is also often stored in surface impoundments prior to subsurface injection.

Here we report on emissions measurements of a suite of organic compounds from produced water surface impoundments at eight produced water disposal facilities in the Uintah Basin of Utah and the Upper Green River Basin of Wyoming during 2013-2016. This study included measurements from surface impoundments only and did not consider emissions from tank storage, transport, or processing of produced water.

Because all methods for measuring emissions have drawbacks, we have employed both flux chamber measurements and techniques for plume measurement and characterization to complement each other. Although the flux chamber provides accurate measurements at the point of sampling, it covers just a limited area and is prone to altering environmental conditions (e.g., temperature, pressure). This fact raises the need to validate the flux chamber measurements. In this study, we apply an inverse-dispersion modeling technique with evacuated canister sampling of the emission plume to validate the flux-chamber measurements. This modeling technique applies an initial and arbitrary emission rate to estimate pollutant concentrations at pre-defined receptors, and adjusts the emission rate until the estimated pollutant concentrations approximates measured concentrations at the receptors. The derived emission rates are then compared with flux-chamber measurements and differences are analyzed.

The inverse-dispersion modeling technique has been widely used with variety of dispersion model types [Hensen et al. 2009; Flesch et al. 2009; O'Shaughnessy & Altmaier 2011]. This method works well with constant wind conditions and simple terrain. Furthermore, receptor sites should be carefully chosen so that the impact of the source of interest on the receptor can be isolated from impacts of surrounding sources. It is not suited for a comprehensive characterization of many different pond sites or land farms in many different conditions, but it is well suited to provide a check on chamber measurements.

Subsurface Leakage from Natural Gas Wells and Natural Seepage

Subsurface leakage from natural gas wells, both active and abandoned; from pipelines; and from natural gas storage facilities is probably also underreported in emissions inventories [Karion et al., 2013; Brandt et al., 2014]. It represents an economic loss to natural gas providers, and better techniques for identifying subsurface well leakage are needed to avoid catastrophic events such as the 2001 Yaggy leak in Kansas or the 2015 Aliso Canyon leak in Southern California [Evans & West 2008; Miyazaki, 2009; Conley et al., 2016].

Researchers have reported that a small fraction of natural gas wells in Eastern Utah show very high concentrations of methane in the soil near natural gas wells [Stolp, et al. 2006], which probably indicates leakage of the wellbore or of adjoining pipelines. Our interest has been to quantify emissions of greenhouse gases and VOCs from the soil in proximity to natural gas wells through flux chamber measurements, and to quantify correlations between soil gas concentrations and flux measurements. Some related studies have occurred in Pennsylvania and Australia [Kang et al., 2014; Day et al. 2014], but still much needs to be done to quantify the contributions of subsurface leakage to emissions inventories.

Furthermore, there are many documented instances of natural seepage of petroleum liquids or gases to the surface, with some estimates indicating that this is an important component of the global greenhouse gas budget [Etiope & Klusman, 2000; Etiope 2004, 2005]. Our interest here has also been to examine whether natural seepage might be an important component of the local emissions inventory or have an effect on local air quality problems.

We measured methane, non-methane hydrocarbons (NMHC), and CO_2 emissions using the flux chamber at 27 oil and gas well sites in Eastern Utah, including the Paradox Basin and Uintah Basin oil and gas fields, and the natural gas storage facility at Clay Basin, see Figure I.1, generally with multiple visits to the same site. In an effort to quantify natural seepage and to obtain control measurements, emissions from non-well soil surfaces within oil and gas fields and from hydrocarbon bearing outcrops were also measured.

At oil and gas production sites, sources of methane and NMHC emissions could be poor construction or subsequent failure of an oil or gas well, re-emission from liquid hydrocarbon spills, or bacterial methane production. At non-well sites, emissions may be due to surface geologic features that directly emit CO_2 or hydrocarbons [Kirchgessner et al., 2000], migration pathways that allow these gases to reach the surface from subsurface reservoirs [Selley, 1985], or bacterial methane production [Leson and Winer, 1991].

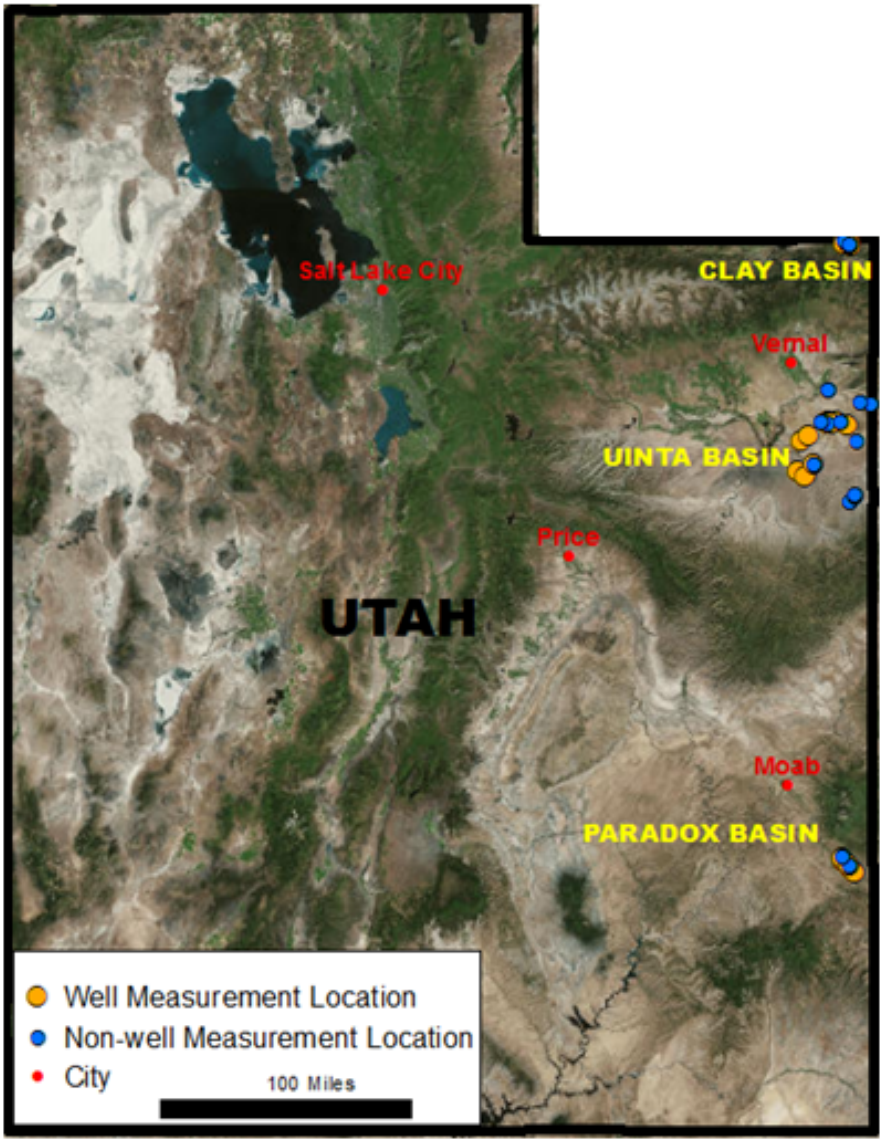

Figure I.1. Well pads at which emissions from the soil were measured.

Land Farms

Land farms are sites where hydrocarbon-contaminated solid waste from the oil and gas industry is applied to and mixed with surface soil as a method of bioremediation [Gurska et al., 2009]. Oil and gas solid waste disposed of at land farms may include drilling waste, solid material accumulated in liquid storage tanks, or other materials. Usually, fertilizers or other additives are used [Callaham et al., 2002] and the soil is periodically tilled [Ausma et al., 2001] to promote decomposition of hydrocarbons in land farm soils. Volatile hydrocarbons tend to be emitted from land farms into the atmosphere, rather than being degraded [Hejazi et al., 2003]. Emissions from land farms decrease rapidly after application of solid waste [Ausma et al., 2002; Pardue & Valsaraj 2000], likely because the supply of volatiles becomes depleted. Tilling increases emissions of hydrocarbons from land farm soils [Ausma et al., 2001, 2003]. Emissions from land farms have been modeled

by Thibodeaux and Hwang [1982], Dupont [1986], and Pardue and Valsaraj [2000]. We report below on measurements of emissions from a land farm facility in the Uintah Basin.

Snowpack Emissions

It is well documented that the snowpack in polar regions has an impact on atmospheric chemistry and physics [Sumner & Shepson, 1999; Sumner et al., 2002; Grannas et al., 2009; Bartels-Rausch et al., 2014]. There are many different physical and chemical mechanisms through which the snowpack and the atmosphere interact. It is known that snow crystals, either as they grow, as they fall, or after they reach the ground, scavenge pollutants from the atmosphere. Because of the granular, porous nature of the snowpack, the effective surface area between it and the atmosphere is much larger than the area of the horizontal boundary surface. The surface of ice crystals between about -20° to about 0° C is known to be disordered and liquid-like [Petrenko & Whitworth, 1999] and it is expected that this quasi-liquid layer can dissolve ions and small, polar organics such as methanol and formaldehyde. Solar energy is able to penetrate to some depth through the snowpack, and there is evidence in artic regions for photochemical reactions, such as the production of formaldehyde and nitrous acid, in the snowpack [Sumner & Shepson, 1999; Grannas et al., 2009]. The carbon feedstock for the formaldehyde reaction has not been positively identified, but it is hard to imagine how it could be anything but organics previously scavenged from the atmosphere.

Presumably, any adsorbates or solutes are re-released to the atmosphere when the snowpack sublimes, or when they are transformed chemically to a more volatile species. Therefore, we might see accumulation and storage of impurities in the snowpack throughout the winter, with a net release in late winter. This is interesting because winter ozone production also peaks in late winter. The explanation for this has always been the higher solar angle, but perhaps a net release of ozone precursors from the snow pack in late winter is a contributing factor. Perhaps a diurnal cycle is superimposed on this seasonal cycle as water vapor freezes onto the snowpack overnight and sublimes during the day.

Not surprisingly then, snowpack emissions of VOC, NO_x, NO_y, and other compounds have been measured in polar regions. These are comparatively small, measured in the range of $\mu g\ m^{-2}\ hr^{-1}$ [Grannas et al., 2009], below the detection limit of our flux chamber. However, we can expect such emissions to scale-up when the snowpack interacts with the atmosphere of a natural gas or oil field, although we are unaware of any such measurements. Below we report measurements of VOC emissions from the snowpack in the Uintah Basin of Eastern Utah that lie in the range of a few $mg\ m^{-2}\ h^{-1}$. More extensive measurements are needed to understand the full impact and extent of these emissions, but since the active oil and natural gas fields of the basin extend over about 10^3 to 10^4 km^2, a few $mg\ m^{-2}\ h^{-1}$ could be significant.

II. METHODS

Meteorological Measurements

We measured temperature and relative humidity (Campbell CS215 or New Mountain NM150WX), wind speed and direction (Gill WindSonic or New Mountain NM150WX), barometric pressure (Campbell CS100 or New Mountain NM150WX), and total incoming solar radiation (Campbell CS300) at each measurement location at 6 m above ground level and recorded these with a Campbell Scientific CR1000 data logger. To characterize atmospheric stability for many of the plume characterization/inverse modeling measurements, we measured the change in temperature with height using aspirated temperature probes (Apogee TS-110) at 1 and 6 m above ground.

Flux Chamber Measurements

We measured emissions of carbon dioxide, methane, non-methane hydrocarbons, and light alcohols (methanol, ethanol, and isopropanol) using a modified version of the commonly-used [Hafner et al., 2010; Wang et al., 2011; Leduc et al., 2009] EPA Emission Isolation Flux Chamber [Eklund, 1992]. Two views of our flux chamber are shown in Figure II-1. For the complete list of compounds measured, see the Appendix. While flux chambers have been widely used for emissions measurements from water and other surfaces, including emissions of greenhouse gases [Denmead, 2008; Kasimir, 1997], methanol [de Gouw et al., 1999], and various hydrocarbons [Boudries et al., 2002; Gallego et al., 2014], they are known to suffer from biases. Turbulence inside flux chambers is constant, so effects of wind speed on emissions may not be fully accounted for by chamber methods [Denmead, 2008]. Chamber flow rates and the presence or absence of mixing fans can alter measured emissions [Parker et al., 2013]. Also, chambers can alter temperatures of the surface being studied and the air above it.

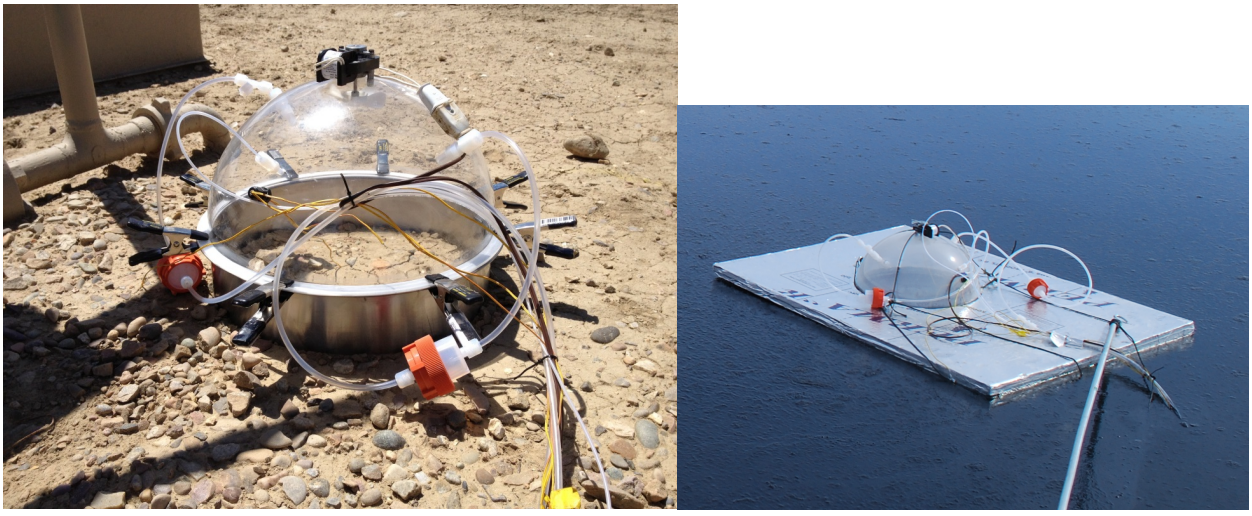

Figure II-1. Field snapshots of our flux chamber. With simple modifications, it can be deployed over soil, water, snow, or ice.

In spite of these limitations, chambers are the only surface flux measurement method that can be used in any meteorological or topographical conditions, or among any number of sources [Parker et al., 2013]. Produced water disposal facilities typically contain many ponds and additional sources of the compounds studied in this work, and isolating a single source or differentiating among sources is difficult with the plume characterization/inverse modeling family of methods, and adequately incorporating complex terrain and structures in the models can also be difficult [Theobald et al., 2012]. Also, produced water ponds usually have berms that are well above the water level, making it difficult to achieve the large, uniform fetch required for micrometeorological methods [Twine et al., 2000]. Also, neither of these methods works well in conditions with low and meandering wind [Twine et al., 2000; Marchant et al., 2011], which are common during winter in the study areas [Lyman & Tran, 2015]. Thus, we used a flux chamber for most of our measurements, and we periodically conducted plume characterization/inverse modeling measurements to determine the extent of any bias in the flux chamber measurements.

We used a dynamic flux chamber, Figure II-1, which was an acrylic hemispherical dome with a 41 cm diameter. A polystyrene sheet with dimensions of 3 cm × 122 cm × 122 cm with a hole cut from the center for the chamber provided for floatation, and strings attached to the chamber anchored it in place. The chamber had a fan at the top with a polyethylene blade that turned at about 200 rotations per minute to provide mixing within the chamber. The fan was designed to achieve a uniform concentration of measured compounds within the chamber (as in Pape et al. [2009]). We tested the impact of fan speed on measured fluxes by comparing measured fluxes from produced water at the same location while the fan was rotating fast enough to agitate the water within the chamber and at the normal speed (n = 3 for high speed, n = 4 for normal speed). Fluxes were significantly higher for ethane and propane (1.8, and 1.5 times higher, respectively) with the fan rotating at high speed, but were not significantly different for any of the other measured compounds.

A 1.2 cm hole on one side allowed ambient air to enter the chamber. Air was pulled through the chamber via a 1 cm × 45 m perfluoroalkoxy (PFA) copolymer resin line connected to the opposite side of the chamber, continually supplying the chamber with ambient air. Air outside the chamber was sampled via a 1 cm diameter × 45 m PFA line near the 1.2 cm hole. Total flow through each line was 10 standard L min^{-1} (standard conditions of 1 atm and 21°C). Flow through the outside line was regulated with a rotameter (the rotameter was positioned downstream of analytical instrumentation), and flow through the inside line was regulated with an Alicat MC stainless steel mass flow controller. 47 mm in-line PTFE filters with 0.5 µm pore size were installed at the beginning of sample lines to prevent particle contamination of sample air.

The 45 m PFA lines both connected to solenoid valves and then to a laser-based methane and carbon dioxide analyzer (LGR Ultraportable Greenhouse Gas Analyzer), which switched between the lines every two minutes. PFA tees also connected the inside and outside lines to 6 L stainless steel air sampling canisters. During 2013 and 2014, SUMMA canisters were used. During 2015 and 2016, canisters coated with deactivated fused silica

were used. Flow into the canisters was regulated with Alicat MC stainless steel mass flow controllers. Canisters were collected over 30-60 minutes, and flows were regulated at 60-150 standard mL min^{-1}. All mass flow controllers used in this study were checked annually with BIOS DryCal flow meters that were calibrated against a NIST-traceable standard, and were always within ± 5% of the expected value.

The chamber emission rate was calculated as

$$E = \frac{(\Delta C \times F)}{S}$$

where E is the emission rate in mg m^{-2} h^{-1}, ΔC is the difference in concentrations of the compound of interest inside versus outside the chamber in mg m^{-3}, F is the flow rate in m^3 h^{-1}, and S is the surface area covered by the chamber in m^2 [Denmead, 2008] Concentrations of measured compounds were converted from ppm to mg m^{-3} using standard conditions of 1 atm and 21°C.

Four type K thermocouples measured the temperature of air and water inside and outside the chamber. Air and water inside the chamber were 5.1 ± 0.8°C (mean ± 95% confidence interval) and 0.3 ± 0.7°C higher than outside, respectively.

A Campbell CR1000 data logger recorded flows, thermocouple temperatures, and the LGR analyzer output at five-second intervals. We washed the chamber, tubing and wires, and foam floatation device periodically with soap and water and then rinsed them in methanol and flushed the system overnight to remove oil and grease. We measured emissions periodically from a clean, 1/8" thick Teflon surface (including before and after cleaning) to assess system contamination.

The LGR analyzer was checked daily against a National Institute of Standards and Technology (NIST)-traceable standard at two calibration points (0 and 30 ppm for methane, 0 and 5610 ppm for carbon dioxide) and periodically, including after instrument repairs and maintenance, at four calibration points (0, 6, 30, and 1000 ppm for methane, 0, 570, 1120, and 5610 ppm for carbon dioxide). Hydrocarbon and carbon dioxide-free air was generated by passing ambient air through a nafion-based drying tube, two canisters that were each filled with 500 mL indicating Drierite, a hydrocarbon scrubber that catalytically converted hydrocarbons to carbon dioxide and water (Teledyne P/N 73380200), a canister filled with 500 mL activated charcoal, and a canister filled with 500 mL indicating soda lime. This scrubbed air was used for zero calibration checks and was used to dilute air from compressed gas standards. Flow of scrubbed air and flow from compressed gas standards were regulated with Alicat MC stainless steel mass flow controllers.

Calibration checks in scrubbed air (n = 67) resulted in 15 ± 10 ppb for methane and 1.0 ± 0.3 ppm for carbon dioxide. Calibration checks from compressed gas standards (n = 86) resulted in 100 ± 1% recovery for methane (6 and 30 ppm; 90^{th} and 10^{th} percentiles of 101% and 97%, respectively) and 100 ± 2% recovery for carbon dioxide (90^{th} and 10^{th} percentiles of 104% and 96%). Methane concentrations inside the chamber occasionally

approached 1000 ppm, and methane calibrations at 1000 ppm (n = 14) resulted in only 93 ± 3% recovery, since 1000 ppm is slightly outside the linear range of the LGR analyzer. The LGR analyzer was not calibrated for water vapor. Software correction of methane and carbon dioxide values for water vapor resulted in 0.1% greater methane and carbon dioxide per 1000 ppm of water vapor. Water vapor was up to 12000 ppm higher inside the chamber than outside, so lack of calibration for water vapor could introduce as much as 1.2% uncertainty in methane and carbon dioxide ΔC. Using 3 times the standard deviation of the instrument response when subjected to scrubbed air, the detection limits were 3 ppb for methane and 1.4 ppm for carbon dioxide.

After sampling, canisters were analyzed within 30 days. In 2013 and 2014, SUMMA canisters were analyzed for hydrocarbons by gas chromatography - flame ionization detection (GC-FID) according to EPA Photochemical Assessment Monitoring Stations (PAMS) analysis protocols [EPA, 1998], and alcohols were analyzed according to EPA TO-15 protocols [EPA, 1999] by a commercial laboratory (AAC, Ventura, California). In 2015 and 2016, canisters were analyzed in our laboratory. We used an Entech 7200 preconcentrator and 7016D autosampler to concentrate samples and introduce them to a gas chromatograph (GC) system for analysis. We used cold trap dehydration to reduce water vapor in the sample, as described by Wang and Austin [2006]. Hydrocarbons and alcohols passed through an empty deactivated fused silica-coated tube kept at -40°C to remove most water and were collected on a subsequent Tenax-filled trap kept at -110°C. The empty tube was then heated to 10°C as helium passed over it to transfer additional hydrocarbons and alcohols into the Tenax-filled trap. Next, the Tenax-filled trap was heated to 230°C to transfer hydrocarbons and alcohols to an empty silonite-coated tube kept at -195°C. Finally, that tube was heated rapidly to 75°C to introduce the trapped sample into the GC system.

The GC system consisted of two Shimadzu GC-2010 GCs with a flame ionization detector (FID) and a Shimadzu QP2010 Mass Spectrometer (MS). Sample introduced to the GC system first passed through a Restek rtx1-ms column (60 meter, 0.32 mm ID), and then entered a VICI four-port GC valve with a Valcon T rotor. For the first 5.7 min after injection, the sample then passed into a Restek Alumina BOND/Na_2SO_4 PLOT column (50 m, 0.32 mm ID) and into an FID. After 5.7 min, the valve position changed and the sample was directed into another Restek rtx1-ms column (30 m, 0.25 mm ID). Light hydrocarbons (ethane, ethylene, acetylene, propane, and propylene) were quantified by FID, while all other compounds were quantified by MS. The temperature of the GC that housed the PLOT column was held at 45°C for the first 25 minutes of each analysis, then increased to 170°C at a rate of 10°C per minute, and then increased to 200°C at a rate of 17°C per minute, and remained at 200°C for the last 19 minutes. The temperature of the GC that housed the other columns was held at 45°C for the first 15 minutes of each analysis, then increased to 170°C at a rate of 6°C per minute, and then increased to 250°C at a rate of 15°C per minute, and remained at 250°C for the last 17 minutes. Bromochloromethane, 1,4-difluorobenzene, chlorobenzene-d5, and 1-bromo-4-fluorobenzene were added to each sample by the Entech 7200 and used as internal standards.

The beginning of every batch analyzed consisted of a five-point calibration curve (0-400 ppb for hydrocarbons, 0-600 ppb for ethanol and isopropanol, and 0-1200 ppb for methanol), with two calibration checks, a duplicate, and a blank check at the end of the batch. Calibration and internal standards were prepared by diluting NIST-traceable compressed gas standards in high-purity nitrogen using an Entech 4600. Canisters with analyzed concentrations more than 50% higher than the highest calibration point were diluted in high-purity nitrogen with the Entech 4600 and reanalyzed.

The average Pearson's-r^2 value for calibration curves was 0.99 ± 0.00 (average of all compounds). Calibration checks had an average recovery of 104 ± 1%. Duplicate samples were 2 ± 2% different (calculated for all compounds as the difference between the original and duplicate divided by the average of the two; only calculated for values greater than 3 ppb). The extent of variability in duplicate samples decreased as the study progressed. In 2015 the difference between duplicate samples had 90th and 10th percentiles of 21% and -27%, respectively, while in 2016 the 90th and 10th percentiles were 8% and -14%. We analyzed six canisters in an inter-comparison between our laboratory and AAC. We excluded one of these canisters due to contamination. Of the remaining canisters, the duplicate samples were 7 ± 7% different (90th and 10th percentiles were 40% and -24%, respectively).

Detection limits for the compounds analyzed by GC were 1.1 ± 0.2 ppb (calculated as 3 times the standard deviation of repeated analysis of a calibration sample with concentrations near the detection limit), with no significant trend with elution order ($p = 0.16$). The detection limits for alcohols were not significantly different from those for hydrocarbons (student's t-test, $p = 0.12$).

We cleaned canisters with an Entech 3100, which heated them to 55°C and repeatedly evacuated them and then pressurized them with humidified high-purity nitrogen (between 5 and 8 repetitions). After cleaning, we pressurized some canisters with high-purity nitrogen and analyzed them. The average concentration of analyzed compounds in cleaned canisters was 0.2 ± 0.1 ppb. The highest recovered compound from cleaned canisters was methanol, at 1.8 ± 1.6 ppb. Brymer et al. [1995] showed a 10% decrease in methanol after 30 days of storage of an air sample in a SUMMA canister, while Pate et al. [1992] showed a 46% decrease after 31 days. We collected a canister sample and analyzed the sample four times within 15 and 18 days of collection, and four more times between 45 and 48 days after collection. We observed a loss of 1 ± 15% of methanol over that time period.

Flux detection limits were calculated using twice method detection limits for methane, carbon dioxide, and non-methane organic compounds as ΔC, and were 0.02, 22.71 and 0.05 ± 0.01 mg m^{-2} h^{-1}, respectively. We also measured fluxes while the chamber rested on a 3 mm thick PTFE sheet. When the flux chamber was operated on a PTFE sheet, emission rates for methane, carbon dioxide, hydrocarbons, and alcohols were 0.02 ± 0.03, 15.88 ± 94.43, 0.24 ± 0.55, and 0.11 ± 0.11 mg m^{-2} h^{-1}, respectively ($n = 8$).

To verify that compounds emitted into the chamber could be quantitatively recovered by the measurement system, and as a practical estimate of uncertainty in flux measurements,

we filled a small pool (1.5 m diameter) with tap water to a depth of about 0.2 m and placed the flux chamber in the water. We injected undiluted gas from the same compressed gas standards used for calibration into the center of the chamber via a PFA tube that extended 1 cm above the water level. During these tests and during many of the flux chamber sampling periods, condensation was present on the inside of the chamber. We injected methane, carbon dioxide, hydrocarbon, and alcohol calibration gases at 200 mL min^{-1} at concentrations of 1620, 152000, 1, and 43 ppm, respectively (balance nitrogen). Recovery was 101 ± 4% for methane (n = 5), 103% for carbon dioxide (n = 2), 100 ± 5% for alkanes, 99 ± 5% for alkenes, 114 ± 3% for aromatics, and 48 ± 10% for alcohols (n = 5 for hydrocarbons and alcohols). We expect that the low recovery for alcohols was due to dissolution of emitted alcohols into water. That expectation will be tested shortly by injecting alcohols with the chamber on a PTFE sheet.

Flux Chamber Measurements from Soils and Snowpacks

Flux chamber emissions measurements from soils were conducted in the same way as emissions measurements from water, except that the float was removed and the chamber was instead affixed to a ring constructed of 3 mm thickness stainless steel (Figure II-1). The ring was the same diameter as the chamber and 10 cm in height. The ring was pressed about 1 cm into the soil before the chamber was attached.

The same thermocouples that were used to measure water temperature were pressed 1 cm into the soil during soil emissions measurements. For soil measurements, air and soil inside the chamber were 6.5 ± 0.7°C and 0.9 ± 0.5°C higher than outside, respectively.

Plume Characterization by Canister Sampling

A set of evacuated canisters was placed along the borders of the produced water ponds. The number of canisters assigned for each facility varies depending on the geometry and number of the ponds. Air intake was set at 1 m above the ground surface. The duration of the sample was one hour.

For each canister sampling, a canister was placed upwind of the ponds to characterize the background organic compound concentrations. However, in many cases we found that the background canister may have been contaminated with the pond's plumes as wind direction changed unexpectedly. We examined such circumstances carefully when performing inverse-modeling analyses.

The GC/MS procedure to analyze canister concentrations is identical to that given above for the flux chamber analysis.

Plume Characterization and Inverse Modeling

The latest version of AERMOD (EPA, 2004), an EPA approved plume dispersion model, serves as the dispersion model for the inversion – dispersion modeling technique. Geophysical parameters (surface roughness, albedo, Bowen ratio, elevations, etc.) are processed by AERSURFACE version 13016 to generate geophysical parameters for

AERMOD's meteorological module (AERMET). AERSURFACE currently only supports input from the National Land Cover Database (NLCD) 1992 version while more recent land-use databases (NLCD2006, NLCD2011) are available. We created a customized computer program to transform the NLCD2011 land-use classifications into the NLCD1992 classifications, allowing the use of NLCD2011 in AERSURFACE. More importantly, the customized program inserted produced water ponds (open water) into the NLCD2011 to better represent the surface characteristics of the study area. The required input meteorological data for the AERMOD model were collected at an approximately 18 ft. tower located close by the produced-water pond. Ambient temperatures were measured at 3 ft and 18 ft heights. Data were collected every 15 seconds.

AERMOD allows options to calculate pollutant concentrations for various averaging times (i.e., annually, monthly, daily, hourly) and 1-hour averaged concentration is its standard calculation. Accordingly, the meteorological parameters are processed by AERMOD to produced 1-hour inputs for AERMOD. The canister samplings are therefore conducted for 1-hour periods.

However, we often found that wind direction changed significantly during the sampling period, especially during wintertime and under weak wind conditions. Under such conditions, the single-vector 1-hour wind field poorly represents the actual wind field during the sampling period. To better represent the pollutant dispersion, we disengaged the 1-hour period into four 15-minutes sub-periods and processed the meteorological inputs and performed AERMOD simulations accordingly. We took averaging of the four 15-minutes AERMOD outputs to obtain the 1-hour modeled concentrations before evaluations with canister samples. The 15-seconds on-site meteorological measurements were used for the 15-minutes aggregation without significant losses in the meteorological variability.

Depending on the location of the collecting water ponds, upper air profile data were collected either at stations located in Salt Lake City, UT or in Grand Junction, CO which are more than 160 km away from the study area. Because of such large distances, we had concerns that data from these two stations might not represent the vertical structure of the sampling sites. In investigating an alternative approach, we performed a sensitivity study in which we adopted the Weather Research and Forecasting (WRF) meteorological model to simulate meteorological and geophysical parameters for AERMOD. The meteorological interface (MMIF v3.1) was used to extract output from WRF and generated surface and vertical profile output files for direct use in AERMOD without the need of running AERMET. However, we found no significant differences in AERMOD simulations with observed and with WRF-simulated meteorological quantities for receptors (canister placements) that are close to the ponds. Because of this finding and the constraints in labor and computer resources in running WRF models, we decided not to employ WRF-simulated meteorological quantities for the inverse modeling in this study.

Hydrocarbon concentrations were converted from ppb (volume mixing ratio) to ug/m^3 for direct comparison with AERMOD estimated concentrations. The unit conversion is as follows:

$$ug/m^3 = (ppb * Mw * Ts * Pm)/(22.4136 * Tm * Ps)$$

with standard temperature (Ts) of 273 K, standard pressure (Ps) of 1013.25 hPa, measured temperature (Tm), measured pressure (Pm) and Mw is the molecular weight of the hydrocarbon compounds.

As a regulatory dispersion model, AERMOD is developed for evaluating critical pollutants (NO_x, SO_2, PM, Pb) but not for VOC. In this study, all hydrocarbon species are modeled as OTHER pollutant. As such, all species were modeled in same manner except for dry and wet deposition which take specific inputs for each species including: diffusivity in air (D_a, cm^2/s), diffusivity in water (D_w, cm^2/s), cuticular resistance to uptake by lipids for individual leaves (Rcl, s/cm), and Henry's Law constant (H, $Pa.m^3/mol$). Values of D_a, D_w, Rcl, and H were adopted from literature review. Other required gas deposition inputs are treated similarly among species.

Water Analyses

We collected water samples from the ponds at each facility we visited. We collected these samples with a 500 mL polyethylene jar attached to a 3 m pole. All samples were collected 3 m or less from the edge of ponds. Water was transferred from the jar into 40 mL amber vials with septum lids without headspace. Because this collection method agitated collected water, it may have resulted in the loss of some volatiles to the atmosphere.

In 2013, samples collected in 40 mL vials were analyzed for methane by method RSK-175 [Kampbell & Vandegrift, 1998], for methanol by EPA Method 8015B [EPA, 1996a] by ALS Environmental in Fort Collins, Colorado, and for other organics by EPA Method 8260B [EPA, 1996b] by American West Analytical Laboratories in Salt Lake City, Utah. After 2013, we analyzed water samples for the same organic compounds for which we analyzed air canister samples, except that we did not analyze water samples for alkenes, undecane, or isopropyl benzene, and we did analyze water samples for methane. Water samples were analyzed using the same GC/MS system that was used to analyze air samples, with the same configuration and columns. 0.8 g NaCl was added to 20 mL septum-top autosampler vials, and then 10 mL of sample was transferred from the 40 mL amber sample vial into the autosampler vials. Samples were then analyzed via headspace analysis with a PAL COMBI-xt autosampler. Each sample was heated to 60°C and agitated for 10 min, then 1 mL of headspace was extracted from the vial with a syringe heated to 100°C and injected into the injection port of the GC, which utilized a 1:14 split ratio.

We performed a five-point instrument calibration prior to each analysis. Calibration standards were prepared by adding 0.8 g NaCl and 10 mL of 18.2 megaohms cm^{-1} water to 20 mL autosampler vials, then adding calibration standards in the gas or liquid phases. All compounds used for preparation of calibration standards were obtained from Sigma Aldrich. Methane, ethane, propane, n-butane, and isobutane were added by drawing gas with a gas-tight syringe from a gas stream generated from pure compressed gas analytical standards and then injecting the gas into the calibration autosampler vials. For other compounds, we injected liquid-phase analytical standards for each compound into a 40 mL

vial with methanol so that the entire filled volume of the vial was 40 mL. We then injected varying amounts of this prepared standard into calibration autosampler vials. We prepared internal standards (the same internal standards that were used for air sample analysis) by injecting liquid-phase analytical standards of each compound in a 5 mL vial with methylene chloride, and we added 1 µL of internal standard solution to each autosampler vial. For each batch, we analyzed one sample in duplicate. Also, for each batch we prepared a matrix spike by adding calibration standards to a duplicate sample. The r^2 value for calibration curves was 0.99 ± 0.00. The difference between duplicate samples was 26 ± 8%, and the recovery of matrix spikes was 93 ± 10%. We used four water samples to conduct an inter-comparison with TestAmerica Laboratories in Arvada, Colorado. TestAmerica used method RSK-175 [Kampbell & Vandegrift, 1998] for methane, ethane, propane, and n-butane, EPA Method 8015B [EPA, 1996a] for alcohols, and EPA Method 8260B [EPA, 1996b] for benzene, cyclohexane, methylcyclohexane, toluene, ethylbenzene, and xylenes. The difference between the results reported by the two laboratories was 9 ± 12%.

For samples analyzed by commercial laboratories using EPA Method 8260B [EPA, 1996b], results for compounds other than hydrocarbons and alcohols were obtained, including carbonyls, acetates, carbon disulfide, and naphthalene.

During 2013, we collected water samples in 50 mL polyethylene vials and analyzed them within a few hours of collection using a Hanna Instruments Model HI 4521 for specific conductivity, salinity, and pH. Calibration of this instrument was conducted immediately prior to analysis at four points with certified standards. For 2014-2016, we used a YSI EXO2 sonde to collect in-situ measurements of specific conductivity, total dissolved solids (TDS), pH, oxidation-reduction potential (ORP), and turbidity. These measurements were collected within 2 m of the water's edge. The EXO2 sonde was calibrated prior to each sample collection day with certified standards.

Water samples were also collected in sealed, sterilized 50 mL jars and analyzed by the IDEXX SimPlate method [Vulindlu et al, 2004]. This method involves adding water sample and media to a growth plate with a number of wells, incubating the plate for 48 hours, and then counting the number of wells that fluoresce under a UV light. Results are reported as the most probable number (MPN) of culturable bacteria.

Well Pad Soil Emission Measurement Locations

Three oil and gas-bearing basins in Eastern Utah were sampled for soil emissions at well sites, the Clay, Uintah, and Paradox Basins, see Figure I.1. Thirteen, nine, and five wells were examined, respectively, in these basins. The wells were selected, based on previous USGS measurements of total combustible soil gas concentrations, to include wells with a range of combustible soil gas concentrations in the soil. Producing, shut-in, and gas storage wells were all sampled. Between two and eight flux chamber measurements were collected at each well pad during each site visit, and each well pad was visited a number of times during the study, for a total of 195 flux measurements of soil emissions on well pads. Also, eleven non-well sites within the oil and gas fields of the Clay, Uintah and Paradox Basins

were visited in order to determine baseline emissions for comparison with well-pad measurements. The distance and direction of the measurement locations relative to the wellhead were recorded, and flux chamber sampling periods had durations of 30 minutes or longer.

Total Combustible Soil Gas Measurements

Measurements of the amount of total combustible gas in soil interstitial space were collected at many well sites using a Bascom-Turner Gas-Rover model VGI-201. The Bascom-Turner Gas-Rover detects natural gas from 10 ppm to 100% gas with a ±2% of accuracy and a detection limit of ± 10 ppm (manufacturer specifications). This portion of the project was carried out in cooperation with the United States Geological Survey (USGS). USGS installed temporary total combustible soil gas probes at most of the wells visited for this study. USGS installed probes at well sites at various distances and directions from the wellhead. Between four and twelve probes were installed at each well site. The probes consisted of PVC pipe and perforated Teflon tubing placed into the ground at a depth of 0.3-1 m. The lowest 12 cm of the Teflon tubing was perforated, and it was closed off at the bottom. Clean sand was placed between the tubing and the outer PVC pipe. The perforated Teflon tubing had a screw-on cap that connected to the Bascom-Turner Gas-Rover via a sampling tube. The Bascom-Turner Gas-Rover was calibrated daily using clean ambient air and 100 ppm and 100% methane certified calibration gas.

III. RESULTS AND DISCUSSION

III.A. Produced Water Impoundments

Study Locations

The produced water disposal facilities sampled for this study were located in the Uintah Basin in Utah and the Upper Green River Basin in Wyoming. We used 2014 National Agriculture Imagery Program (NAIP) imagery to determine the location of produced water ponds in the Uintah Basin. After identifying the facility locations, we attempted to contact operators of facilities and visited each facility to determine ownership and verify that the ponds observable in imagery were produced water disposal facilities. While the majority of produced water is injected into the subsurface without spending time in surface impoundments ("ponds"), the facilities sampled in this study all incorporated surface impoundments, either for storage of water prior to injection or for evaporative disposal. We were granted access to some of the facilities on condition of anonymity, so facility names and other identifying information are not disclosed. Table III.A.1 provides information about the types of sampling that occurred at each facility.

Table III.A.1. Number and season of campaigns carried out at the facilities sampled for this study. Number of flux chamber and inverse modeling measurements of emissions are also shown.

Facility ID	Number and Season of Campaigns	Flux Chamber Measurements	Inverse Modeling Measurements
A	2 in Spring 1 in Fall	34	1
B	1 in Winter	7	0
C	1 in Winter 1 in Summer	42	0
D	1 in Winter	12	0
E	1 in Winter 1 in Fall	22	0
F	1 in Spring 2 in Summer	16	3
G	1 in Summer 1 in Winter	12	0
H	1 in Summer 1 in Winter	18	0

The produced water disposal facilities sampled in this study functioned as follows: (1) At well sites, produced water was separated from hydrocarbon liquids and natural gas by gravity and collected in a storage tank at an oil or gas well site. In some cases, water was piped directly to the disposal facility, rather than being stored in a tank. (2) Produced

water was trucked or piped to a disposal facility, where it was released into a tank or vessel for additional gravity-based separation of water and oil. Some facilities employed more sophisticated techniques to separate water from oil. Because water in well-site storage tanks is usually heated during winter, water released into separation tanks can be warm (sometimes exceeding 40°C). (3) Water was transferred from separation tanks into open ponds. Ponds varied from well under 1 hectare to several hectares in size. (4) Once in a pond, water was often transferred to additional ponds. Facilities had from two to ten individual ponds. Most facilities utilized a small, netted pond downstream from the separation tank to catch additional residual oil before transfer to larger evaporation or storage ponds. (5) For some facilities, water was injected into the subsurface from the storage ponds. For others, water remained at the surface to evaporate. In at least one case, a portion of the water was further treated and then reused in the oil and gas industry.

During winter, much of the water surface at disposal facilities froze. Some ponds, however, were so saline that despite subfreezing air temperatures the water remained unfrozen. Also, since produced water storage tanks are heated during winter months, areas of ponds that regularly received new water did not freeze or developed a layer of ice at night that thawed during the day.

We measured emissions from a variety of surfaces at produced water disposal facilities, including ponds with water recently received from well sites, ponds with briny water that retained very little organic compounds, ice surfaces, a few fresh water surfaces (i.e., water from fresh sources, not produced water), and a pond that had been reclaimed by covering with dirt and vegetation.

Properties of Emissions from Produced Water Impoundments

Emissions of methane, carbon dioxide, non-methane hydrocarbons, and alcohols from produced water surface impoundments varied widely across and within facilities because of differences in the quality and volume of water received at facilities, differences in water management practices, in meteorological conditions, and in the interval of time over which a given body of water had been stored at the site. In this section, we use flux chamber measurements to explore the extent and drivers of this variability.

For convenience, ponds at produced water facilities were categorized as *skim ponds*, which were the first pond in a series, were usually netted, and were usually at least partially covered with oil (these are called skim ponds because oil is periodically skimmed from the ponds' surfaces); *other active ponds*, which were actively receiving new produced water but were not the first pond in a series, and *inactive ponds*, which had water in them but were not receiving new water. At the time of sampling, inactive ponds had not received new produced water for weeks to months, but the exact age of water in inactive ponds could not be determined. Figure III.A.1 shows that the flux of organic compounds from skim ponds was much higher than the flux from other active ponds, and that the flux from inactive ponds was by far the lowest, or about 4000 ± 2700, 930 ± 470, and 27 ± 11 mg m^{-2} h^{-1}, respectively.

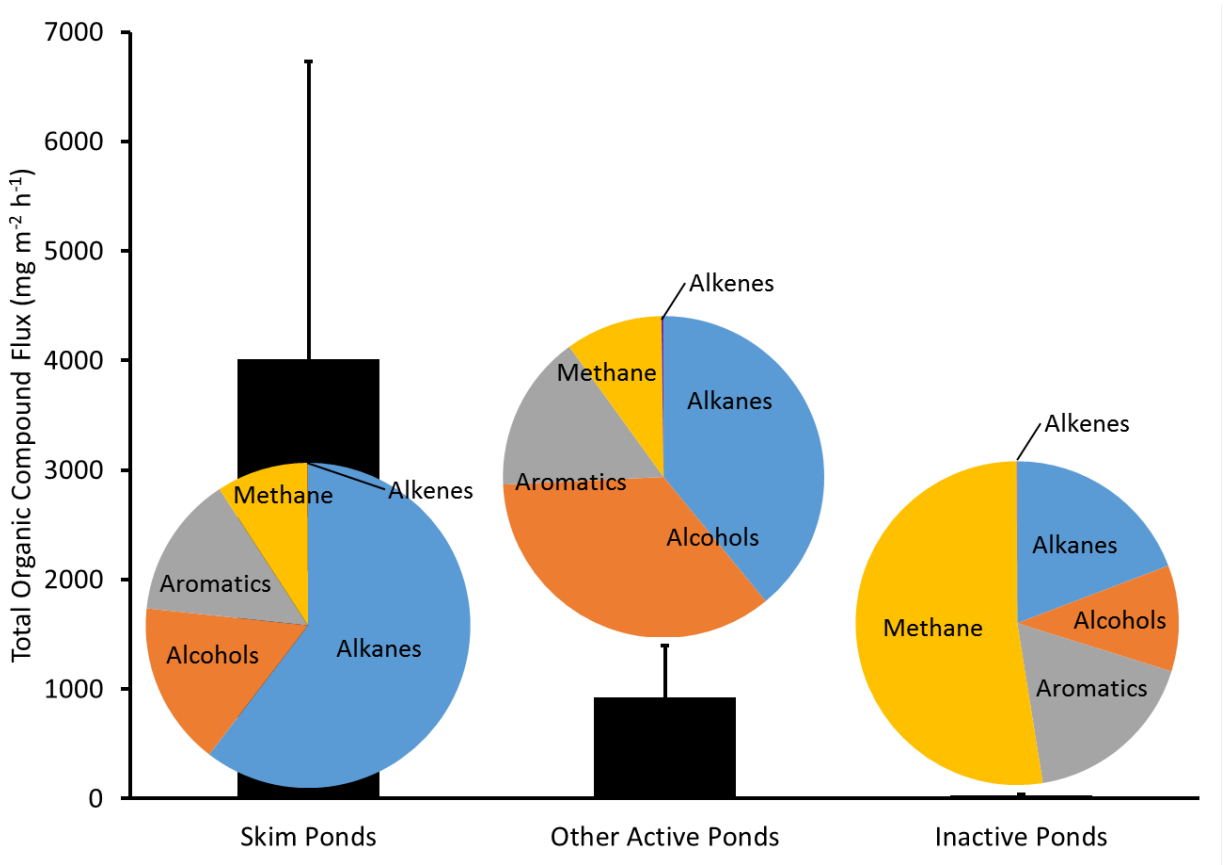

Figure III.A.1. Average flux of total organic compounds (sum of methane, hydrocarbons and alcohols) from different types of ponds at produced water disposal facilities visited for this study (black bars). Whiskers show 95% confidence intervals. Overlain pie charts show the fraction of total emissions that were due to alkanes, alcohols, aromatics, methane, and alkenes. Measurements over ice are excluded.

Figure III.A.1 shows that the speciation of organic compound fluxes was different for skim, other active, and inactive ponds. Fluxes from skim ponds tended to be dominated by alkane emissions, while emissions of alcohols and aromatics made up the majority of fluxes from other active ponds. This may have occurred because alkanes are more volatile and less water soluble than alcohols and aromatics, so they can be expected to emit from skim ponds quickly, leaving fewer alkanes in solution to be emitted from downstream ponds. Fluxes from skim ponds were the most variable. The 95% confidence interval for total organic compound flux from skim ponds was 68% of the mean, but was only 51% and 39% of the mean for other active and inactive ponds, respectively. One cause of this variability was that a portion of the surface of skim ponds was usually covered with oil, and some flux chamber measurements were collected from oil surfaces. Oil surfaces were occasionally observed on other active ponds, also. For a subset of measurements that were collected from oil surfaces and nearby water surfaces, oil surfaces resulted in total NMHC, alcohol, and methane emissions that were 32 ± 33, 13 ± 56, and 6 ± 8 times higher, respectively, than nearby water surfaces.

While methane fluxes were greatest from skim ponds, followed by other active ponds, the percent of total organic compound flux that was due to methane was highest for inactive ponds, followed by other active ponds. The most likely explanation for this is that methanogenic bacteria produced an increasing portion of emitted methane as (1) methane that was dissolved in produced water when it arrived at the disposal facility was volatilized from the water, and (2) the water had time to develop a larger population of bacteria. The bacterial MPN value for skim ponds was 79 ± 51, while the values for other active and inactive ponds were 250 ± 53 and 258 ± 48, respectively, providing evidence for this hypothesis. Carbon dioxide flux from skim ponds was not significantly different from all other ponds (student's t-test, $p = 0.95$). Some produced water disposal facilities add bacteria to promote degradation of organic compounds. We were only able to determine whether bacteria were added at a few of the facilities we sampled. However, MPN values for a facility that did not add bacteria were not significantly different from two facilities that did add bacteria ($p = 0.31$).

The speciation of non-methane hydrocarbon fluxes stayed roughly the same for skim ponds, other active ponds, and inactive ponds (Figure III.A.2). The speciation of alcohol fluxes from skim and other active ponds was similar, but inactive ponds showed more ethanol and isopropanol emissions relative to methanol emissions.

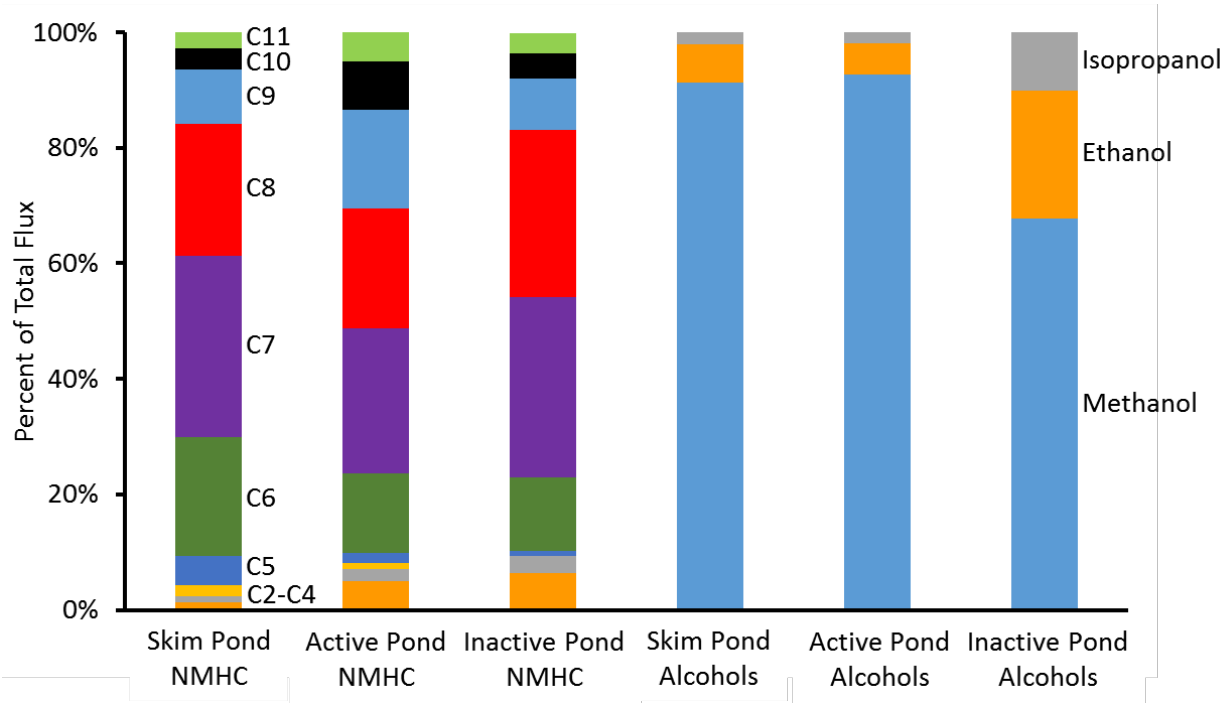

Figure III.A.2. Percent of total NMHC fluxes from skim, active, and inactive ponds at produced water disposal facilities that were due to C2-C11 hydrocarbons (three leftmost bars), and percent of total alcohol fluxes that were due to methanol, ethanol, and isopropanol (three rightmost bars). Measurements over ice are excluded.

Figure III.A.3 displays the average speciation of hydrocarbon emissions from the ponds in greater detail. The hydrocarbon signature is dominated by the BTEX compounds and by the C6-C9 alkanes. Fluxes of the lower alkanes, C2 - C5, are relatively low. These probably have a higher concentration in produced water when it first comes out of the ground, but flash quickly in separators or during transport and are absent as soon as the water reaches the ponds.

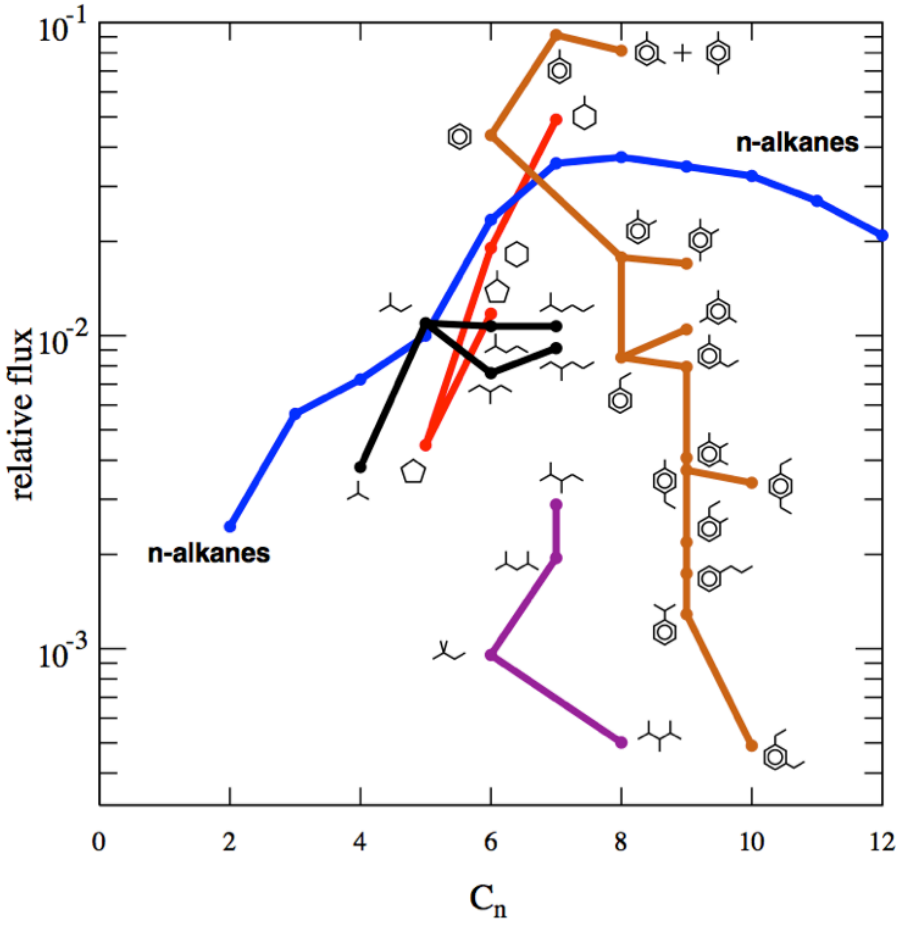

Figure III.A.3. Hydrocarbon speciation signature in fluxes from produced water ponds. Coloration is by compound class: blue = n-alkanes, black = once-branched alkanes, mauve = twice-branched alkanes, red = cyclic alkanes, rust = aromatics. Compound classes are connected by straight lines as a guide to the eye.

We divided fluxes for each compound by the concentrations of each compound in water and calculated correlations between the concentration-weighted fluxes and meteorological parameters measured, but none of the correlations were statistically significant. Ice cover, however, lowered emissions dramatically. For a subset of measurements of fluxes from active ponds that had some ice cover and some unfrozen water, the unfrozen portion had 174 times higher methane flux (24.9 ± 20.3 versus 0.1 ± 0.2 mg m^{-2} h^{-1}), 131 times higher total hydrocarbon flux (9.2 ± 4.7 versus 1201.8 mg m^{-2} h^{-1}), and 12 times higher methanol flux (14.0 ± 14.9 versus 167.4 ± 99.5 mg m^{-2} h^{-1}). On one occasion, we observed the capping effect of ice over the course of a single morning. Figure III.A.4 shows measurements from an active produced water pond from 8:45 to 14:00 local time during winter. This portion of this pond was covered with a 2 cm layer of ice when the day began, and as temperatures warmed the ice melted, leading to a substantial increase in emissions.

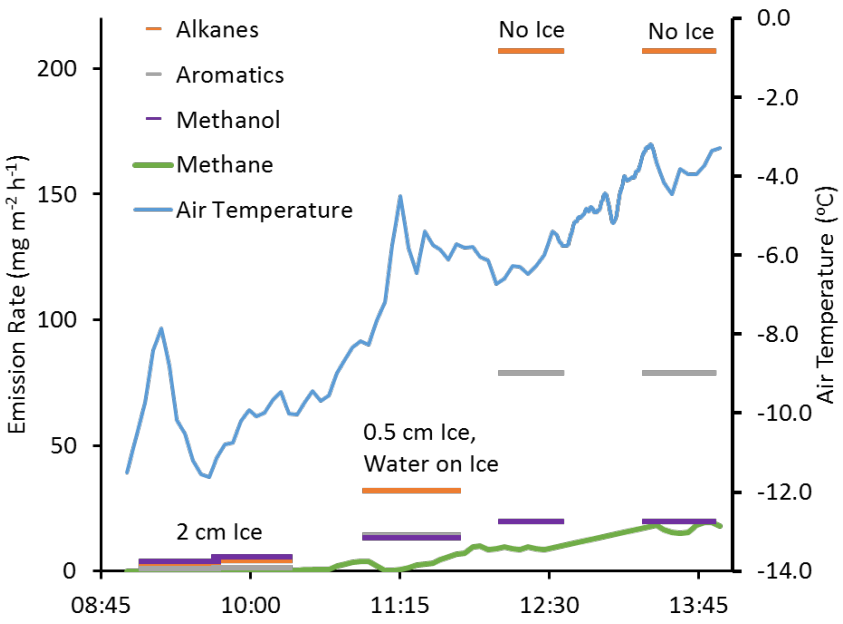

Figure III.A.4. Emission rates and air temperature at a produced water pond during winter. The pond had a layer of ice in the morning, but the ice melted by midday. Times are Mountain Standard Time.

We used GIS software and NAIP imagery to determine the acreage of produced water ponds at each facility. We used the average surface area of each pond type at the Uintah Basin facilities that we sampled to scale up measured fluxes into emission rates, with units of kg day^{-1}. For ponds that had some ice cover and some water cover, we collected flux measurements from both surfaces and weighted pond-level emission rates based on the percent of the pond covered by each surface.

For the six sampled facilities that were in the Uintah Basin, skim ponds comprised 1 ± 4% of the total pond surface area, ponds that were actively receiving water from the skim ponds comprised 22 ± 41% of pond surface area, and inactive ponds comprised 77 ± 43% of pond surface area. In contrast, skim ponds were responsible for 15% of total organic compound emissions from these facilities, while other active ponds and inactive ponds were responsible for 83% and 2%, respectively (Table III.A.2).

Table III.A.2. Emissions from produced water disposal facilities (average ± 95% confidence interval of measurements collected in the Uintah Basin).

kg day^{-1}	Skim ponds	Other active ponds	Inactive ponds	Total
Methane	6 ± 9	23 ± 17	1 ± 2	29 ± 21
Carbon dioxide	13 ± 28	149 ± 68	212 ± 484	374 ± 309
Alkanes	35 ± 73	89 ± 95	2 ± 3	126 ± 102
Alkenes	0 ± 0	0 ± 1	0 ± 0	0 ± 1
Aromatics	9 ± 17	87 ± 127	1 ± 2	96 ± 119
Alcohols	8 ± 90	114 274	3 ± 35	125 ± 172
Non-methane organics	52 ± 96	290 ± 251	5 ± 7	347 ± 261

Methane, alkane, and aromatic emissions were lower during winter than during other seasons, while alcohol emissions were higher. While some ponds froze during winter, effectively capping the pond and prohibiting most emissions, we never observed frozen skim ponds, and we observed that at least a portion of other active ponds always remained unfrozen during daytime. The extent of ice cover at produced water disposal facilities can be expected to vary from year to year, and this study only takes into account conditions observed during sampling periods.

Table III.A.2 shows that, while a high degree of variability was observed among the facilities sampled, emissions of organic compounds from ponds at produced water disposal facilities are significant. Emissions of non-methane organic compounds (including methanol) from all ponds at the facilities sampled were 347 ± 261 kg day^{-1}. Since no significant seasonal trends in facility-level emissions were observed, this value can be used as an annual average, and would lead to total annual emissions of 126 ± 95 tonnes. Methanol emissions from the facilities sampled would lead to annual emissions of 45 ± 48 tonnes. We have observed methanol emissions in excess of 1.2 g m^{-2} h^{-1} (Figure III.A.16), equivalent to about 300 kg day^{-1} for a one-hectare pond, although this appears to be a relatively rare occurrence. On the other hand, because methanol is classified as a hazardous air pollutant (HAP) subject to more stringent regulation, more study is needed to understand the source and extent of methanol emissions by the ponds.

The only other published measurements of emissions of organic compounds from produced water ponds are those of Thoma [2009]. Thoma measured emissions from three produced water ponds in Colorado during August, 2008 using two open path Fourier transform infrared spectrometers, SUMMA canisters, and vertical radial plume mapping. Figure III.A.5 shows the average emission rate of a few select organic compounds from the three ponds measured by Thoma (which included one pond identified as a skim pond and two ponds identified as evaporation ponds), in comparison with our measurements. Emission rates of all compounds measured by Thoma were in the same range as those from this study, with the exception of methanol. Methanol emission rates in this study were two orders of magnitude greater than those measured by Thoma (16.1 ± 17.2 vs 0.1 ± 0.2).

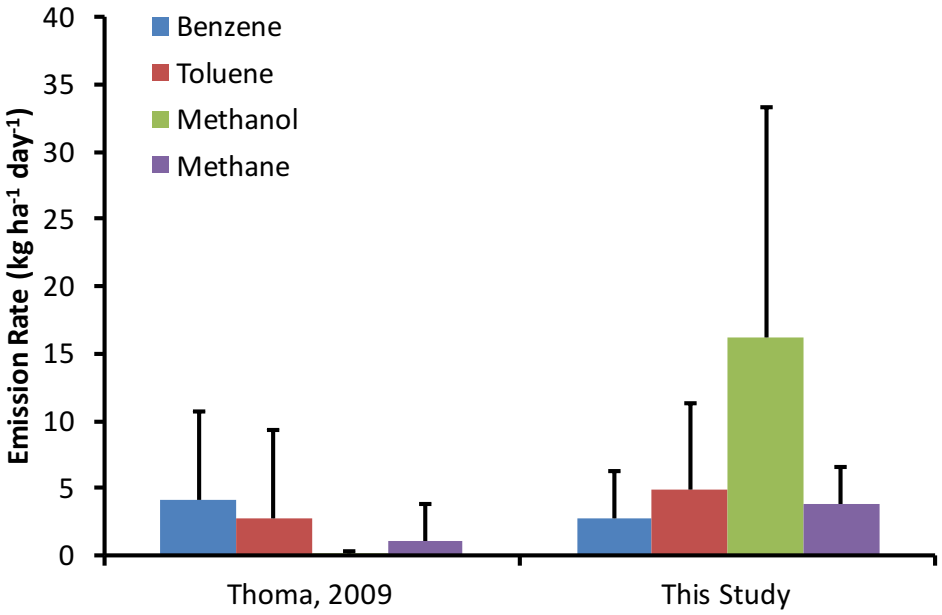

Figure III.A.5. Emissions of select organic compounds from three produced water disposal ponds, as reported by Thoma [2009] compared with emissions from this study (whole-facility average). Whiskers show 95% confidence intervals.

Correlations Among Emitted Compounds

The plots shown in Figures III.A.6-17 illustrate many properties of the emissions. The emissions of different compounds or classes of compounds are displayed either as rank correlation plots or as ordinary correlation plots on log-log scales. (There is no perfect graphical representation for datasets that span many orders of magnitude and that simultaneously may be either positive or negative. For example, all negative or zero points have been excluded from the log-log plots. Rank correlations permit us to display all points in the dataset, but completely obscure the variable spacing between points.) The correlations shown are across all facilities, seasons, and pond types, although variable coloration is often used to indicate different facilities, seasons, and pond types. All emissions appearing in Figures III.A.6-17 are in mg m^{-2} h^{-1}.

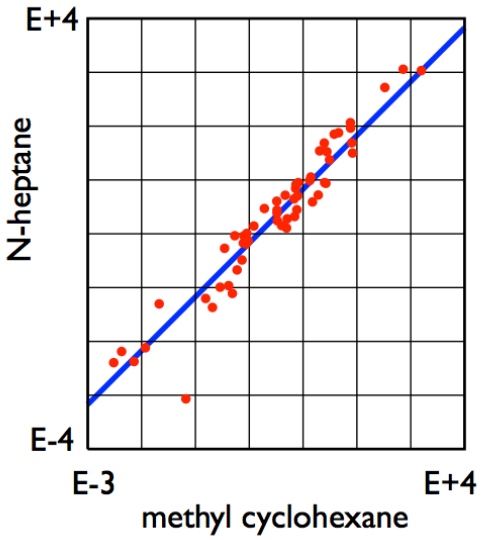

Figure III.A.6. Correlation plot of the indicated compounds.

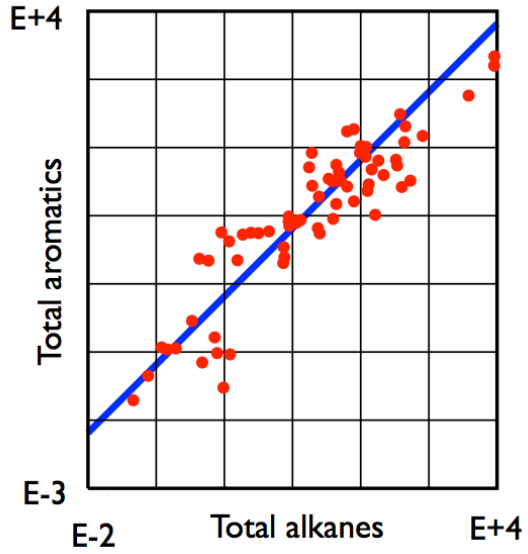

Figure III.A.7. Correlation plot of total alkanes and aromatics.

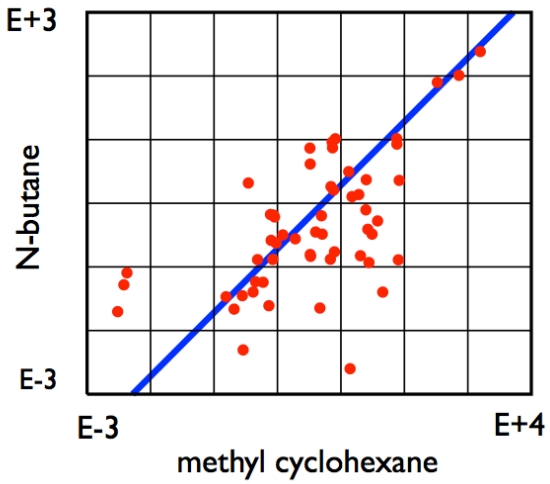

Figure III.A.8. Correlation plot of the indicated compounds.

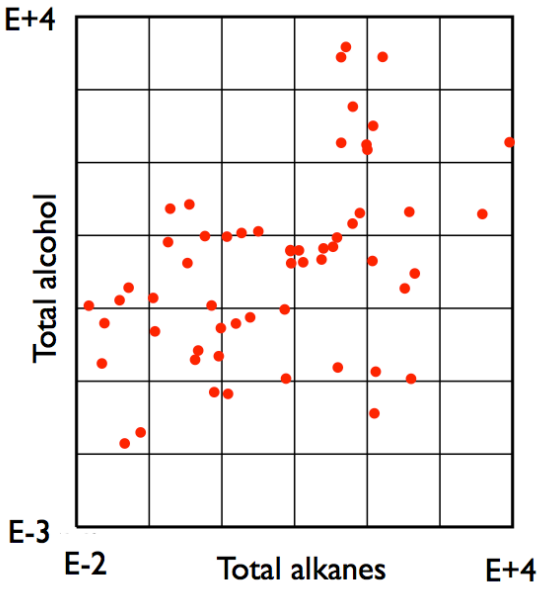

Figure III.A.9. Correlation plot of total alkanes and alcohols.

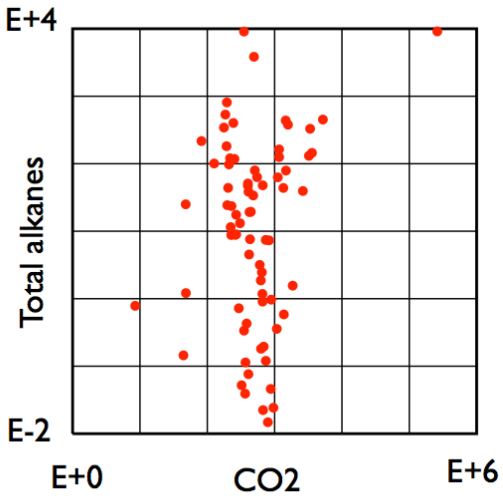

Figure III.A.10. Correlation plot of CO_2 and total alkanes.

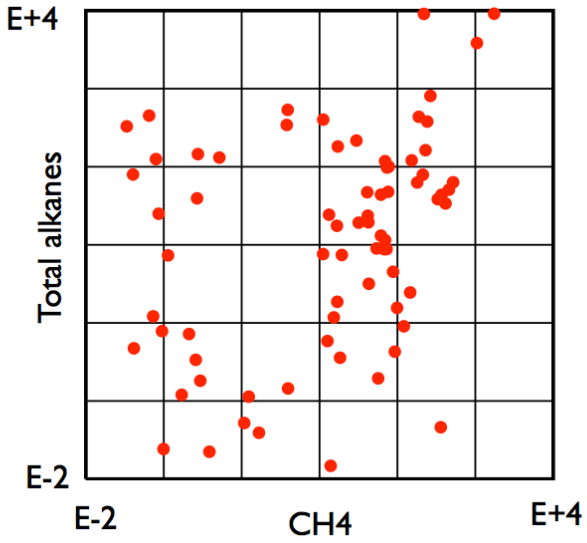

Figure III.A.11. Correlation plot of total alkanes and alcohols.

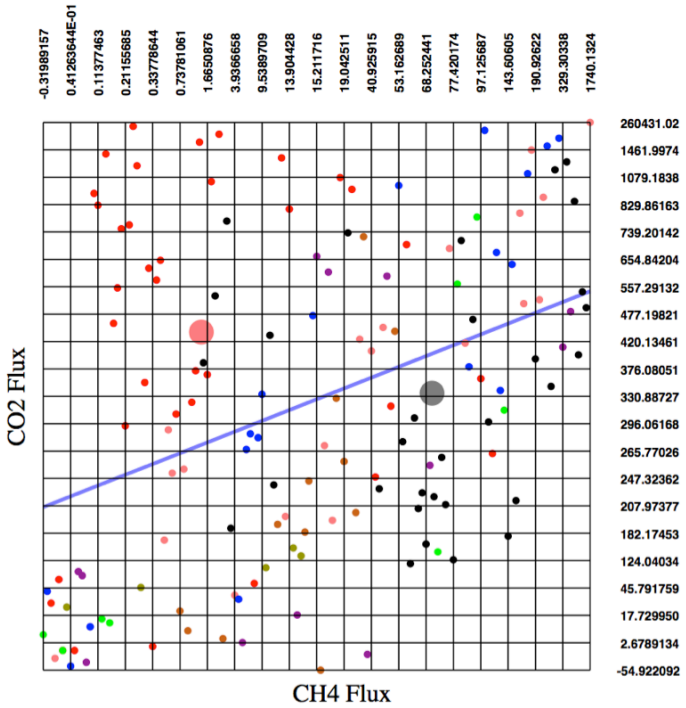

Figure III.A.12. Rank correlation plot of CO_2 and CH_4 fluxes. Coloration is by facility. The larger pink and gray filled circles show the centroids of the smaller red and black symbols, respectively.

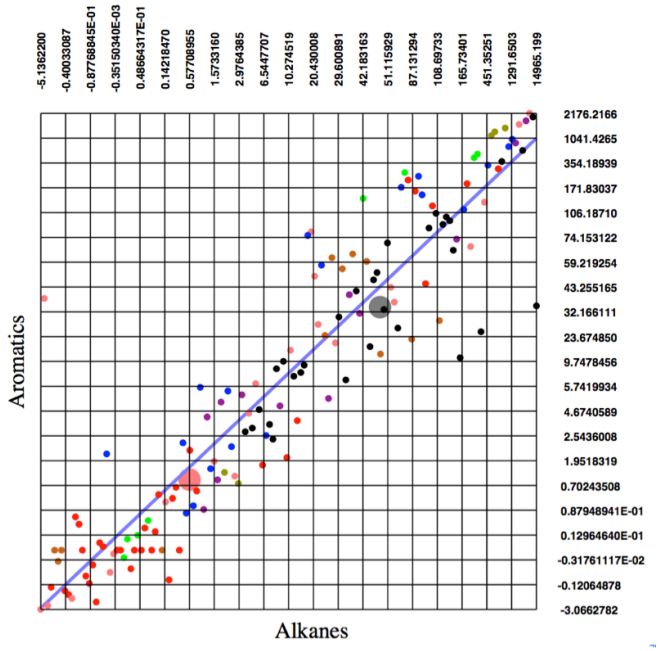

Figure III.A.13. Rank correlation plot of total alkanes vs. total aromatics. Coloration is by facility. The larger pink and gray filled circles show the centroids of the smaller red and black symbols, respectively.

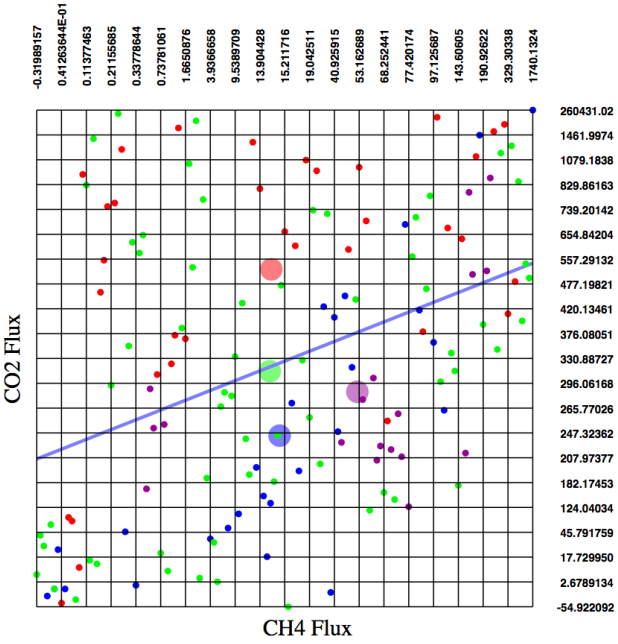

Figure III.A.14. Rank correlation plot of CO_2 and CH_4 fluxes. Coloration is by season (green = spring, red = summer, mauve = autumn, blue = winter). Larger, lighter filled circles are centroids of each collection of seasonal symbols.

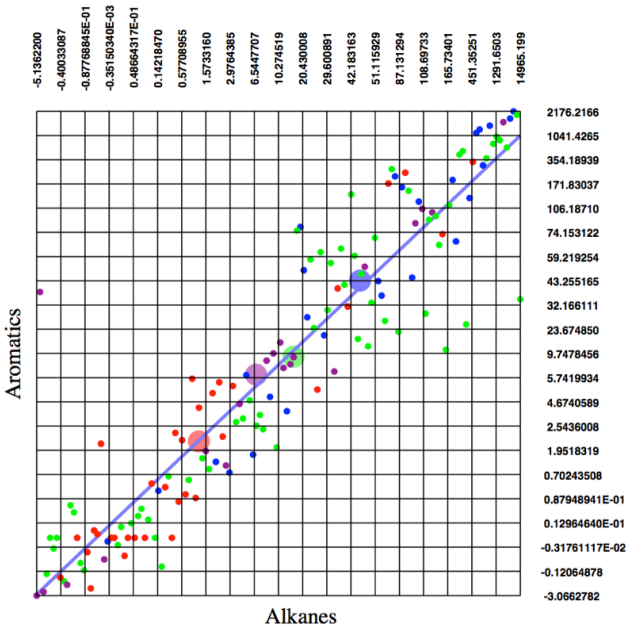

Figure III.A.15. Rank correlation plot of total aromatics vs. total alkanes. Coloration is by season (green = spring, red = summer, mauve = autumn, blue = winter). Larger lighter symbols are centroids of the smaller corresponding symbols.

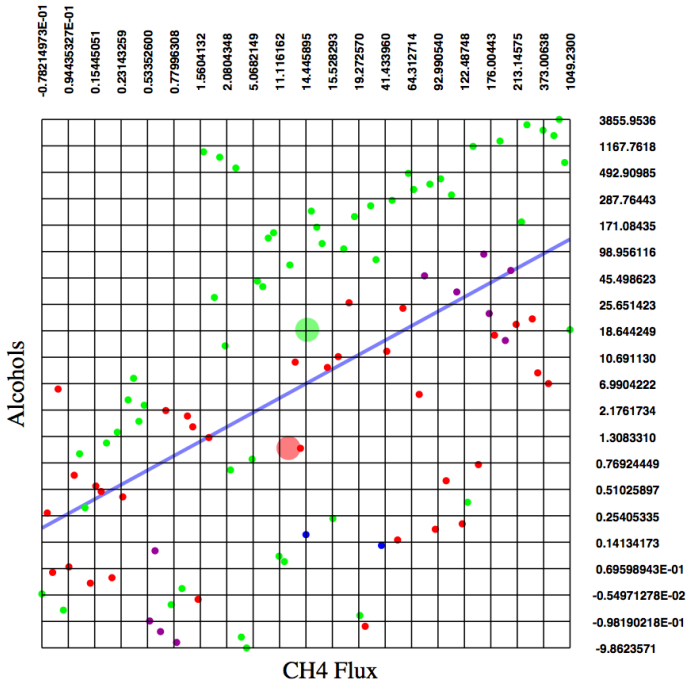

Figure III.A.16. Rank correlation plot of total alcohols vs. CH_4. Coloration is by season (green = spring, red = summer, mauve = autumn, blue = winter. The larger, light green and pink filled circles are the centroids of the smaller green and red symbols respectively.

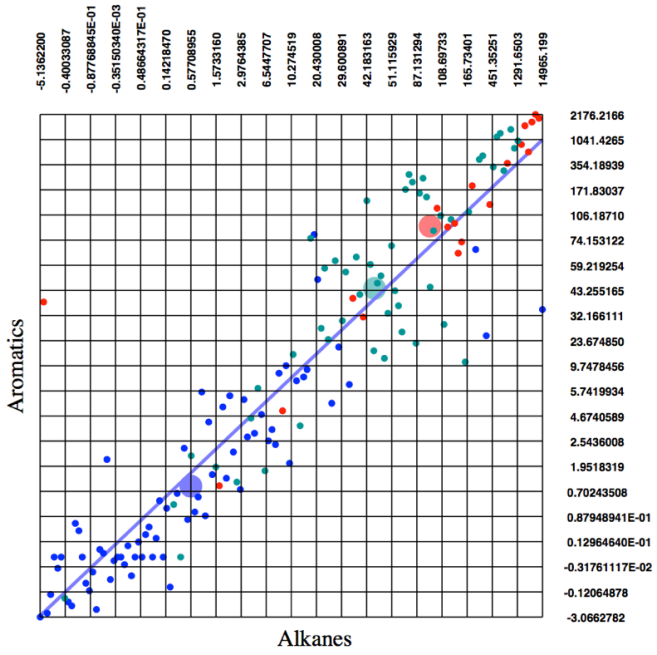

Figure III.A.17. Rank correlation plot of total aromatics vs. total alkanes. Coloration is by pond type (red = skim ponds, green = other active ponds, blue = inactive ponds). The larger, light blue, light green and pink filled circles are the centroids of the smaller blue, green, and red symbols, respectively.

In Figures III.A.14, 15, and 16, spring is defined as the three months March, April, and May; summer as the three months June, July and August; autumn as September, October, and November; and winter as December, January, and February.

The above figures illustrate that flux measurements vary over many orders of magnitude depending on the condition of the water. However, we nevertheless see strong correlations in the fluxes among the NMHC, including both alkanes and aromatics (Figures III.A.6-8,13,15,17). These correlations persist throughout all seasons, all treatment facilities, and over various water conditions and over many orders of magnitude in the strength of the total flux. The correlations are stronger when the compounds are closely related (compare, for example, Figures III.A.6 and III.A.8). The subsurface waters possess a particular hydrocarbon speciation signature before they come to the surface, and the fact that the correlations persist over time in the ponds is an indication that all hydrocarbons respond similarly to the physical, chemical, and biological processes that occur in the ponds.

On the other hand, carbon dioxide, methane, and the alcohols (dominated by methanol) are all poorly correlated with hydrocarbons and with each other (Figures III.A.9-12,14,16). Carbon dioxide and methane, and perhaps to a lesser extent, methanol, are produced by aerobic and anaerobic bacteria in the pond. Therefore, the fluxes of these compounds depend on the balance between oxidation and reduction (methanotrophs vs. methanogens) which in turn depends on the oxygen content and temperature of the water. Because of this, strong correlations should not be expected. Figure III.A.1 lends additional support to this finding.

Fluxes of alkenes are very low. No doubt, this is due to the fact that alkenes are present only at very low concentrations in petroleum in general [Tissot & Welte, 1984].

Figures III.A.12 and III.A.13 indicate the effect of different treatment practices on the emissions. The red dots represent a facility that practices aeration and microbial treatment of the water in the ponds, while the black dots represent a facility that practices neither. Such treatments shift the balance of emissions away from hydrocarbons and towards carbon dioxide.

Carbon dioxide emissions are fairly uniform over skim, active, and inactive ponds, usually within about an order of magnitude of 10^3 mg m^{-2} h^{-1} (Figure III.A.10).

Figures III.A.14 and III.A.15 indicate that hydrocarbon fluxes are larger in winter than in summer, while carbon dioxide fluxes are larger in summer than in winter, probably because oxidation is more rapid at higher temperatures.

Figure III.A.16 indicates that methanol emissions are larger than average in the spring. We do not understand this observation.

Basin-Scale Emissions from Produced Water

We identified 174 hectares of produced water ponds in the Uintah Basin, and produced water surface area at the facilities we sampled amounted to more than 25% of this amount. To scale up emissions from this study to the entire Uintah Basin, we assumed all produced water facilities in the Uintah Basin had the same area distribution of skim ponds, active ponds, and inactive ponds as the facilities sampled for this study, leading to the emission rates shown in Table III.A.3.

Table III.A.3. Estimated total annual emissions from all produced water ponds in the Uintah Basin.

Tonnes yr^{-1}	Skim ponds	Other active ponds	Inactive ponds	Total
Methane	47 ± 75	188 ± 144	9 ± 14	243 ± 173
Carbon dioxide	103 ± 227	1232 ± 564	1750 ± 3988	3086 ± 2547
Alkanes	290 ± 603	731 ± 780	13 ± 25	1035 ± 841
Alkenes	0 ± 0	4 ± 8	0 ± 0	4 ± 7
Aromatics	74 ± 140	714 ± 1044	4 ± 12	792 ± 980
Alcohols	64 ± 743	941 ± 2261	22 ± 293	1027 ± 1415
Non-methane organics	428 ± 1479	2390 ± 3792	40 ± 329	2858 ± 2914

To scale emission rates measured in this study to all the produced water ponds in the Uintah Basin, we assumed the facilities sampled in this study were representative of all produced water facilities in the Basin. In reality, we know little about the quality of water and management practices at other facilities, and the true uncertainty in our Uintah Basin-scale emissions estimate may exceed the 95% confidence intervals presented in Table III.A.3. Also, emissions from produced water ponds in the Uintah Basin can be expected to

fluctuate with the amount of drilling and oil and gas production, meteorological conditions, and other factors that are not fully accounted for in this dataset.

Estimates of emissions of organic compounds from oil and gas-related sources contain considerable uncertainty. Ahmadov et al. [2015] used two emissions inventories in their photochemical model of winter air quality in the Uintah Basin: (1) the 2011 U.S. Environmental Protection Agency's National Emissions Inventory and (2) an inventory developed from aircraft-based estimates of basin-wide methane emissions [Karion et al., 2013] and regression analysis of methane with other compounds measured in ambient air. They report 100,279 and 101,184 metric tons of methane and non-methane volatile organic compounds, respectively, emitted annually from the oil and gas sector using the National Emissions Inventory and 482,130 and 184,511 tonnes of methane and non-methane volatile organic compounds, respectively, from their ambient measurement-based inventory. Methane emissions from Table III.A.3 are 0.2% and 0.1% of total oil and gas-related methane emissions in the Uintah Basin in comparison to the National Emissions Inventory and the ambient measurement-based inventory, respectively. Non-methane organic compound emissions (including methanol) from produced water surfaces are 2.8% and 1.5% of the total in comparison to the National Emissions Inventory and ambient measurement-based inventory, respectively.

Correlations Between Water-Phase Concentrations and Emissions to the Atmosphere

We have investigated the correlation between the concentration of a volatile compound dissolved in the pond and its flux into the atmosphere. If a strong correlation exists, then it will be possible to quantify emissions by taking water samples. In most cases, we can expect emissions to satisfy a mass-transfer law of the form

$$f = SC,$$

where C is the concentration of a volatile compound in the water phase and where f is the flux of the compound into the atmosphere [Schwarzenbach, et al., 2003]. The mass-transfer law is a direct proportionality between the water-phase concentration and the emission rate. The proportionality constant, S, is variably called the "mass-transfer coefficient" or, because it has units of a velocity, the "transfer velocity."

For many of our flux chamber measurements, water concentrations were also measured simultaneously. Figures III.A.18-21 display tests of this proportionality for some of our data. On a log-log plot, a proportionality appears as a straight line of slope 1, with the proportionality constant determined by the intercept. The solid red line is the best-fit unit-slope line. The pink band is drawn to have a total width of one order of magnitude centered on the red line and indicates the approximate noise level for these measurements. The blue line is the prediction based on the WATER9 model explained below. Although noisy, many proportionalities hold over 3 or 4 orders of magnitude. Therefore, from an entirely empirical standpoint, we have determined mass-transfer coefficients for each of the compounds studied. These are tabulated in Table III.A.4.

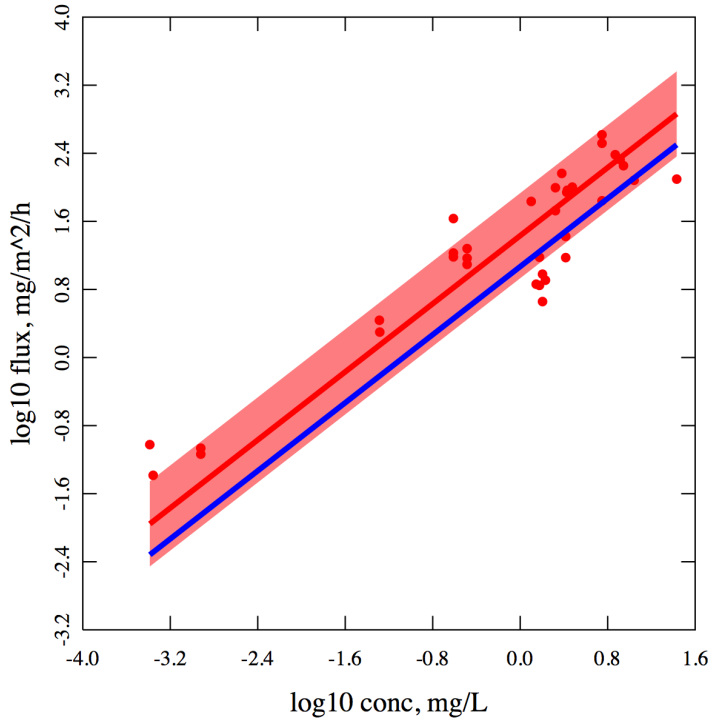

Figure III.A.18. Test of the mass-transfer proportionality for methane.

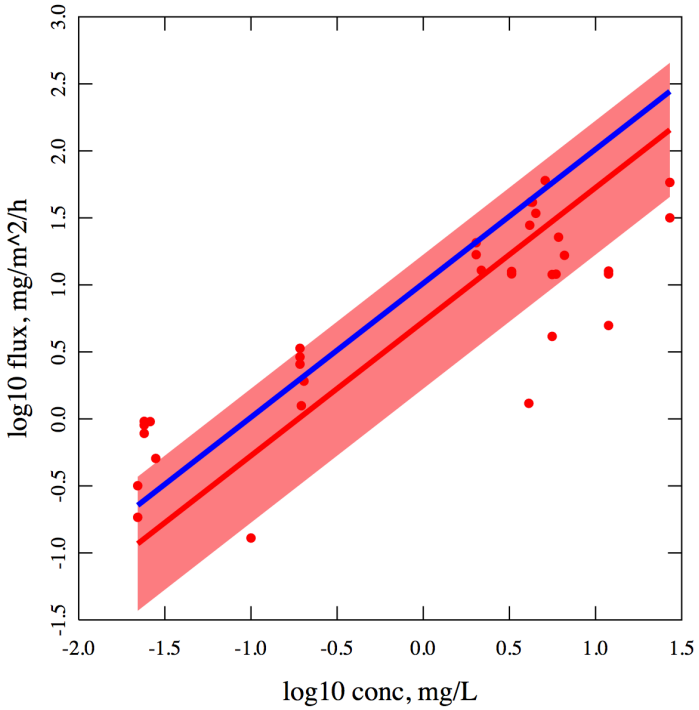

Figure III.A.19. Test of the mass-transfer proportionality for benzene.

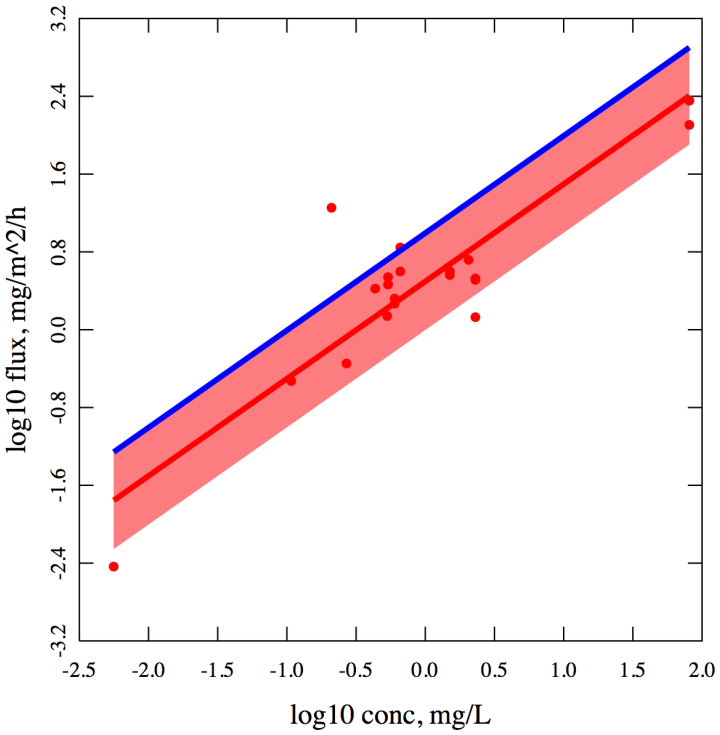

Figure III.A.20. Test of the mass-transfer proportionality for cyclohexane.

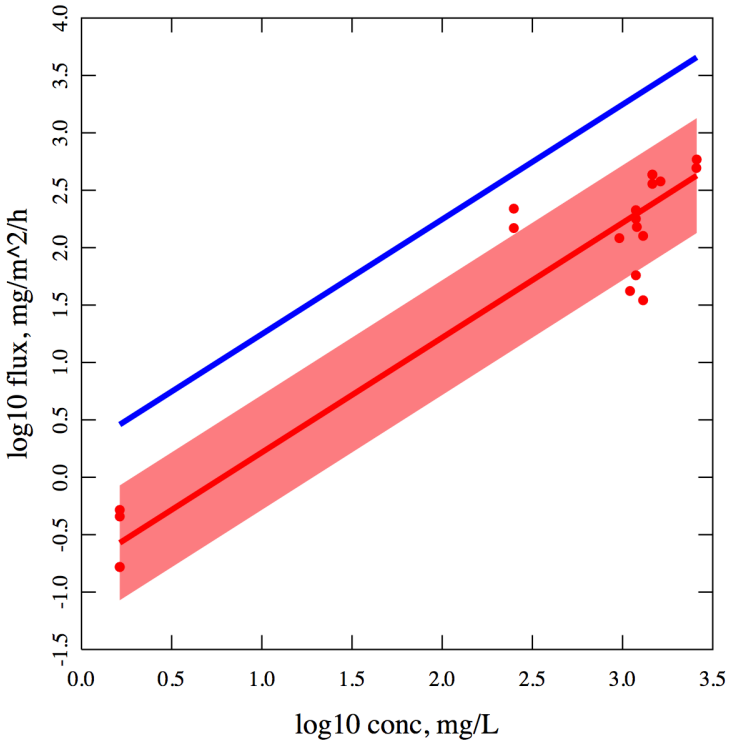

Figure III.A.21. Test of the mass-transfer proportionality for methanol.

Table III.A.4. Empirical *S* as calculated from our data. H_{cc} obtained from Sander (1999).

	S (empirical)	H_{cc}		*S* (empirical)	H_{cc}
methane	27	29	n-heptane	7.9	34
ethane	6.3	21	methylcyclohexane	4.2	
propane	10	28	toluene	5.8	
isobutane	6.5		2-methylheptane	24	
n-butane	7.7	37	3-methylheptane	20	
isopentane	3.3		n-octane	14	144
n-pentane	4.3		ethylbenzene	6.9	
2,2-dimethylbutane	3.9		m/p-xylene	5.4	
cyclopentane	3.4		o-xylene	5.9	
2-methylpentane	5.9		n-nonane	11	
3-methylpentane	5.3		n-propylbenzene	4.2	
n-hexane	5.5	63	1-ethyl-3-methylbenzene	3.0	
2,4-dimethylpentane	4.0		1-ethyl-4-methylbenzene	1.8	0.20
methylcyclopentane	4.1		1,3,5-trimethylbenzene	19	
benzene	5.3	0.22	1,2,4-trimethylbenzene	3.0	
cyclohexane	3.1	7.3	n-decane	2.4	220
2-methylhexane	1.8		1,3-diethylbenzene	2.4	
2,3-dimethylpentane	3.1		methanol	0.16	2.0E-04
3-methylhexane	3.9		ethanol	0.21	2.2E-04
2,2,4-trimethylpentane	9.9		isopropanol	0.25	

Attempts to predict mass-transfer coefficients from molecular theories are now about a century old [Schwarzenbach et al., 2003]. The essential assumption is that both the bulk air and water phases are turbulent and therefore well mixed. However, the turbulence is damped out near the interface, so there are thin stagnant films on each side of the interface through which solute transport is governed by the relatively slow process of molecular diffusion. Passage through these "bottleneck" layers is the rate-determining step. The models involve Henry's Law, the relationship between the partial pressure of the solute in the air in equilibrium with the concentration of the solute in the water phase. Unfortunately, there is no uniform standard formulation of Henry's Law across the physical sciences, and so caution is called for whenever one extracts Henry's constants from the literature. They can appear in three (or more) distinct forms. Let p_A be the partial pressure of the solute in the air phase, and C_A and C_W the molar concentrations of the solute in the air and water phases, respectively. Henry's Law and the gas law state that all three quantities are proportional when the partitioning has attained equilibrium. Therefore, all the following are equivalent expressions of Henry's Law:

$$H^S = \frac{C_W}{p_A}, \quad H^{CC} = \frac{C_W}{C_A}, \quad H_{CC} = \frac{C_A}{C_W}.$$

H^S is Henry's constant as tabulated by Sander [1999], with units mol L^{-1} bar^{-1}. H^{CC} and H_{CC} are dimensionless forms of Henry's constant. We have:

$$H^{CC} = RT\, H^S = 1/H_{CC}$$

where R and T are the gas constant and the absolute temperature. Values of H_{CC} for a few compounds, collected from Sander [1999], are listed in Table III.A.4.

The mass-transfer coefficient governing transport across the double-layer film obeys a "resistivity" relationship [Schwarzenbach, 2003; EPA, 1994]:

$$\frac{1}{S} = \frac{1}{S_W} + \frac{1}{H_{CC} S_A},$$

where S_W and S_A are respectively transfer coefficients defined for either the water or the air film. Henry's constants vary by many orders of magnitude ($H_{CC} \approx 200$ for n-decane, and $\approx 2 \times 10^{-4}$ for methanol, i.e., large for low water solubility, small for high). Unless we are in the crossover domain defined as $S_W \approx H_{CC} S_A$, then only one term in the above is important, and one film or the other dominates:

$S = S_W$ (H_{CC} large, low solubility, control by the water film)

or

$S = H_{CC} S_A$ (H_{CC} small, high solubility, control by the air film).

Figure III.A.22 displays the empirical values of S as functions of H_{CC}. Our empirical data, although noisy, are consistent with these values of S_A and S_W:

$$S_A = 900\ \frac{\text{mm}}{\text{h}}, \quad S_W = 7\ \frac{\text{mm}}{\text{h}}. \qquad \text{Eq. III.A.1}$$

Eq. III.A.1 represents S_A and S_W as constants, whereas they vary from one compound to another and with wind speed. We are only able to use constants because of the noise in our data.

Literature values of H_{CC} are often not well constrained. Different independent measurements are seen to vary by as much as an order of magnitude [Sander, 1999], and entries in Table III.A.4 were selected either as means or as consensus values. Fortunately, most of our compounds are in the regime of control by the water film, and S is insensitive to H_{CC}.

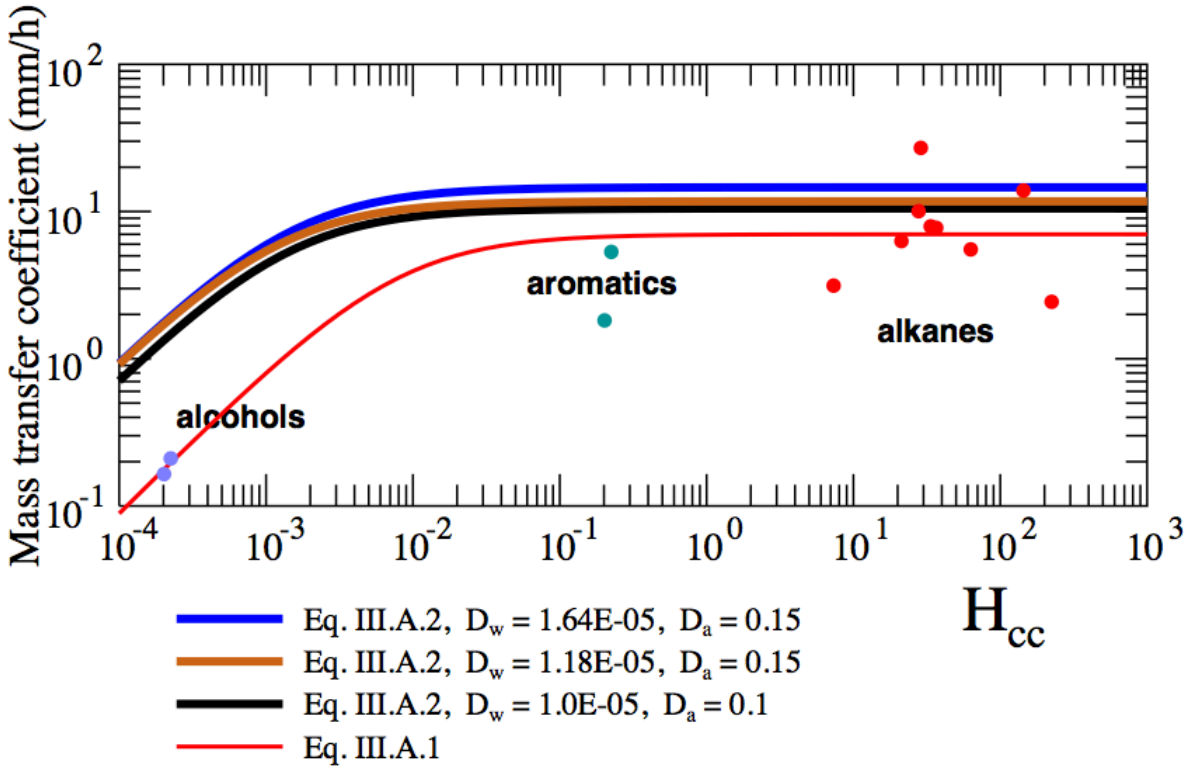

Figure III.A.22. Mass transfer coefficients as functions of Henry's constant. Filled circles represent our empirical results. Solid curves were drawn either according to Eq. III.A.1 or III.A.2.

We next compare our results with a standard model for S_A and S_W, the so-called WATER9 software package [EPA, 1994, 2001]. WATER-9 employs semi-empirical correlations for S_A and S_W that include dependence on wind speed, on the size (fetch) and depth of the pond, and on the molecular diffusivities of the compound in both air and water. However, we expect that the flux chamber masks the effect of the external wind speed, and that flux chamber data should be modeled with an effective wind speed that is a characteristic of the operating parameters of the chamber. We also expect that the effective pond size for chamber measurements is the diameter of the chamber (0.4 m). Therefore, we have chosen to analyze our flux chamber results in WATER9's "deep pond" regime, with depth much greater than fetch, and we have found reasonable agreement when we assume that the effective wind speed u = 1 m/s. With these assumptions, the WATER9 formulas simplify to

$$S_W = \left[10.0\ \frac{mm}{h}\right]\left(\frac{D_W}{D_{RW}}\right)^{2/3}, \qquad \text{Eq. III.A.2(a)}$$

$$S_A = \left[1.00 \times 10^4\ \frac{mm}{h}\right]\left(\frac{D_A}{D_{RA}}\right)^{0.67}, \qquad \text{Eq. III.A.2(b)}$$

where D_W and D_A are the molecular diffusivities of the compound in water and air, respectively. D_{RW} and D_{RA} are reference diffusivities to which we have assigned the values

$$D_{RW} = 9.3 \times 10^{-6} \frac{cm^2}{s}, \; D_{RA} = 0.151 \frac{cm^2}{s}.$$

D_{RW} is the molecular diffusivity of diethyl ether in water (experiments on diethyl ether having served as reference standards). D_{RA} does not correspond to any given compound. Rather it is the ratio of the viscosity and density of air, which has the dimensions of diffusivity. Diffusivities in air and water of a number of compounds were obtained from the WATER9 documentation [EPA, 1999]. These computations also assume T = 298.15 K (Here we are ignoring the temperature dependence of D_A and D_W.) Results for $(D_A, D_W) = (0.15, 1.64 \times 10^{-5})$ (methanol), $(0.15, 1.18 \times 10^{-5})$ (methane), and $(0.1, 1 \times 10^{-5})$, all in $cm^2\ s^{-1}$, are shown in Figure III.A.22. The impact of D_A and D_W is weak, and our data are too noisy to distinguish such small effects.

Figure III.A.23 compares actual flux measurements against WATER9 predictions. The ratios of predicted to actual fluxes have mean and standard deviation 6 ± 15. These results indicate that correlations extending over about six orders of magnitude exist between concentrations in the water and emissions to the air. The WATER9 predictions are valid to within about an order of magnitude, but for reasons we do not understand, they tend to overestimate our results.

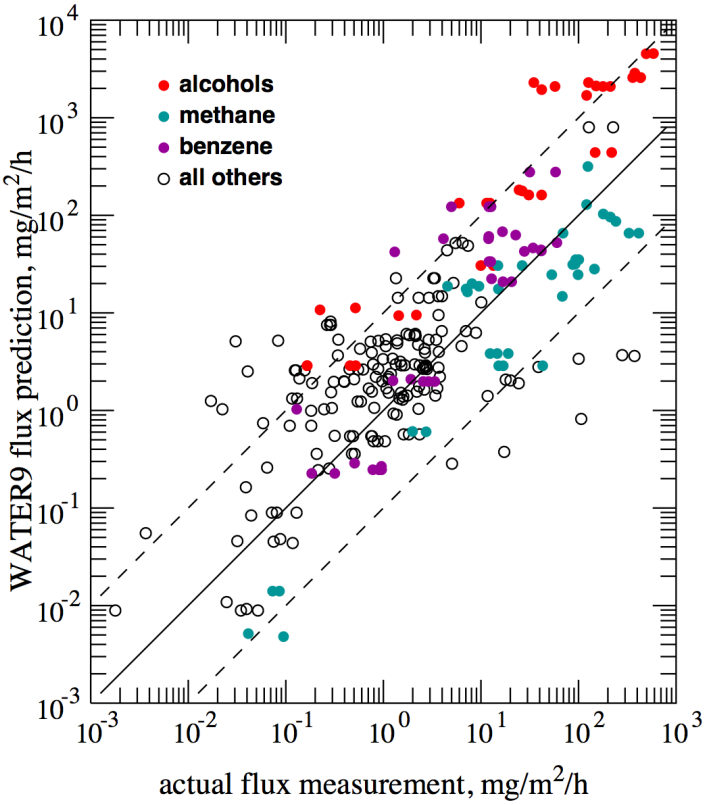

Figure III.A.23. Comparison between actual flux measurements and WATER9 predictions of the flux.

Compounds Dissolved in Produced Water

For convenience, ponds at produced water facilities were categorized as *skim ponds*, which were the first pond in a series, were usually netted, and were usually at least partially covered with oil (these are called skim ponds because oil is periodically skimmed from the ponds' surfaces); *other active ponds*, which were actively receiving new produced water but were not the first pond in a series, and *inactive ponds*, which had water in them but were not receiving new water. At the time of sampling, inactive ponds had not received new produced water for weeks to months, but the exact age of water in inactive ponds could not be determined.

Inactive ponds had higher total dissolved solids (TDS) (47.7 ± 27.8 g L^{-1}) than skim ponds and other active ponds (15.9 ± 6.9 and 23.5 ± 11.4 g L^{-1}, respectively), probably because water in inactive ponds had experienced more evaporation. pH was similar for all three pond types (8.3 ± 0.1 for all pond types). Concentrations of organic compounds were highest and most variable in skim ponds, followed by other active ponds and inactive ponds (Figure III.A.24). For skim ponds and other active ponds, organics in water were dominated by alcohols. Alcohols accounted for 90 ± 6% of all organics measured from these two pond types. For inactive ponds, in contrast, methane made up the largest fraction of organic compounds measured. At least some of this methane was likely produced by methanogenic bacteria.

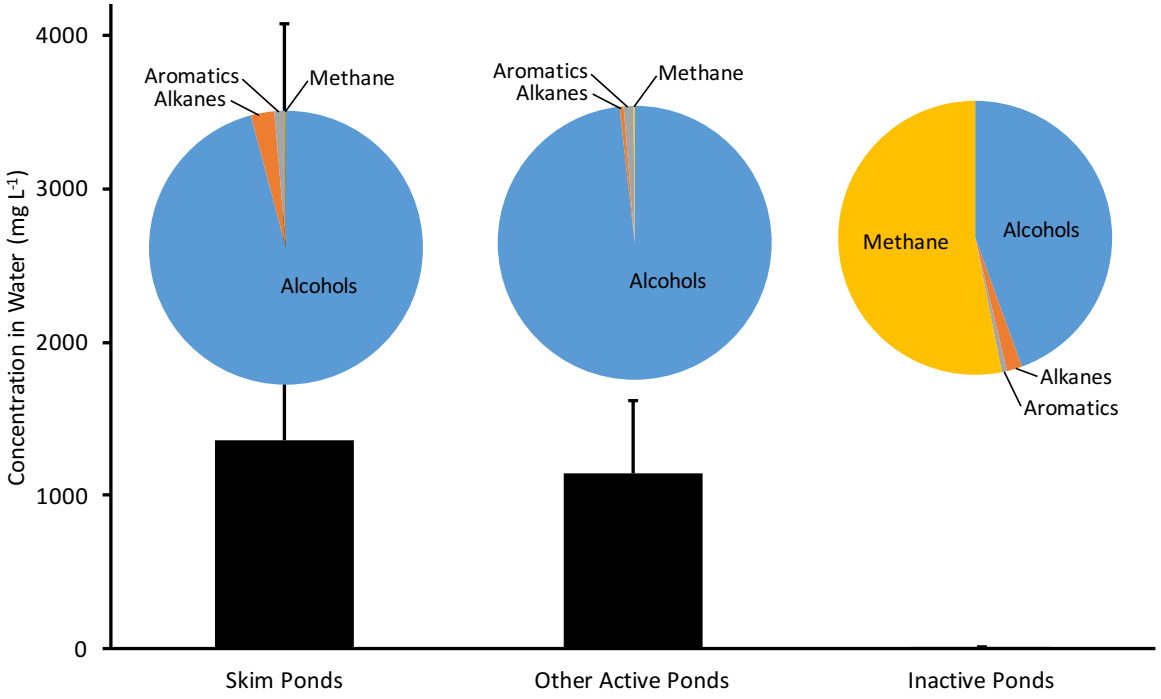

Figure III.A.24. Total organic compound concentrations in water from skim ponds, other active ponds, and inactive ponds (black bars). Whiskers show 95% confidence intervals. Pie charts show the fraction of total concentrations that were due to alcohols, alkanes, aromatics, and methane.

Figure III.A.25 shows the speciation of NMHC and alcohols in skim, other active, and inactive produced water ponds. Speciation did not vary dramatically among the three pond types. C5-C8 compounds made up the vast majority of NMHC observed in produced water.

Methanol concentrations were much higher than those of any other measured non-methane compound in all pond types. Methanol is used in the oil and gas industry to prevent methane hydrate formation and is typically either injected at well heads or added to raw gas transmission pipelines during winter. Methanol is also used as a solvent in antiscaling or other chemical treatment products injected into well bores or at other stages of oil and gas production, and this use of methanol occurs year-round. Methanol is miscible with water and can be expected to partition preferentially with the water phase during gravimetric separation of water from oil and gas. Methane, alkanes and aromatics are much less soluble and so are less likely to remain in the water phase after separation. The source of ethanol and isopropanol in produced water is not clear, but it could be an impurity in methanol used by the oil and gas industry.

For the subset of water samples analyzed by a commercial laboratory using EPA method 8260B [EPA, 1996b], acetone (2.4 ± 0.6 mg L^{-1}), butyl acetate (0.9 ± 0.5 mg L^{-1}), n-butanol (16.5 ± 2.9 mg L^{-1}), and naphthalene (88.7 ± 130.0 mg L^{-1}) were consistently observed.

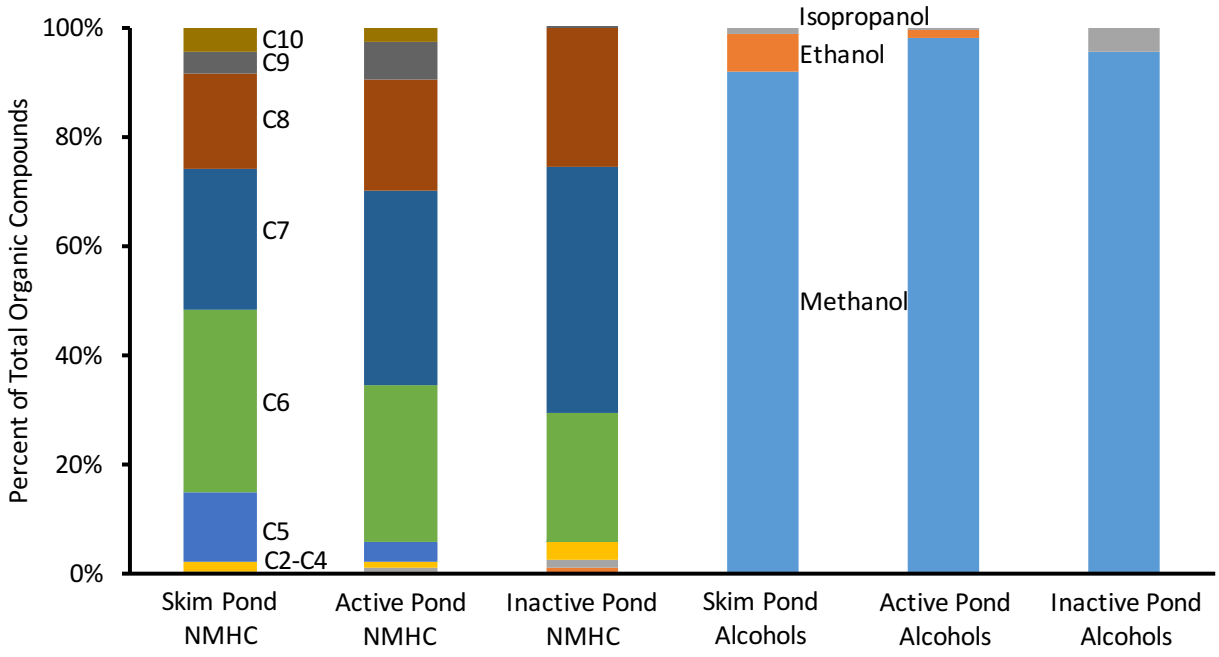

Figure III.A.25. Percent of total NMHC in water from skim, other active, and inactive ponds at produced water disposal facilities that was C2-C11 hydrocarbons (three leftmost bars), and percent of total alcohol in water that was methanol, ethanol, and isopropanol (three rightmost bars).

Benko and Drewes [2008] summarized available information about concentrations of organic compounds in produced water. They report concentrations of 0.39 to 35 mg L^{-1} total volatile organics in produced water. In contrast, we measured total organics in the range of 0.6 to 1356 mg L^{-1}, with an average of 760 mg L^{-1}. The method used to obtain the values reported by Benko and Drewes [2008] likely did not quantify light hydrocarbons or alcohols. Excluding alcohols and C1-C5 hydrocarbons, our results ranged from 0 to 41.5 mg L^{-1}, within the range reported by them.

Plume Characterization and Inverse Modeling

AERMOD model version 15181 (the latest version) was employed to estimate emissions from produced-water ponds. The estimated emission rates (E_{ij}) of a specific HC species (HC_j) from a produced-water pond i are the solutions for minimizing estimation error $\mathcal{E}$ of the following multiple-regression equations:

$$Y_{jk} = Y_{0j} + \sum_{i=1}^{N} E_{ij} \frac{YU_{ijk}}{EU_{ij}} + \varepsilon \qquad \text{(III.A.3)}$$

where Y_{jk} is the measured concentration of hydrocarbon HC_j at canister k; Y_{0j} is the background HC_j concentration, YU_{ijk} is the AERMOD-modeled HC_j concentrations at each canister k with the arbitrarily chosen unit emission rate EU_{ij} for each of the produced-water ponds.

The intercept factor Y_{oj} in Eq. (III.A.3) is the background concentration of chemical j and thus can be solved for in the multi-linear regression equation. However, as discussed above, background concentrations were typically measured upwind of the produced water ponds in each measurement campaign. This gives an alternative way to solve the regression: Treat Y_{0j} as given, using the measured background concentration and subtract it from the measured concentration Y_{jk}. Then solve Eq. (III.A.3) with the Y_{oj} term removed (i.e., the regression line is forced to go through the origin). This can negatively affect the least square solution (decreasing R^2). We performed regression analyses both ways and opted for the solution with best fitting criteria. The agreement between estimated and measured background concentrations is also a criterion to evaluate the fitting of the regression solutions.

Besides the number of evaporation ponds N, the number K of canisters included in Eq. (III.A.3) is an important factor in determining an optimum least-square solution. Keeping only important canisters and removing "bad" canisters can increase the R^2 fitting scores. Canisters are removed if there is clear evidence for doing so (such as a canister located outside the plume).

AERMOD allows several options for modeling pond-like sources, including area, volume, or open-pit sources. We examined scenarios in which the produced-water ponds were modeled as different source types. We found no single source-type that is best to characterize all produced water ponds. For example, for ponds that have water temperature significantly higher than ambient temperature and thus have some initial buoyancy, modeling the ponds as volume sources gave better fitting criteria than modeling

as other source types. For ponds of which the water temperatures are not warmer than the atmosphere, area or open-pit source types gave better fitting scores.

We conducted a sensitivity study to compare AERMOD's estimation to the Heavy Gas Dispersion from Area Sources for Steady-State Conditions (HEGADAS-S). HEGADAS-S is a component model of HGSYSTEM [Post, 1994], a collection of computer programs developed to estimate the dispersion of accidental chemical releases with emphasis on dense gas behavior. In comparison to AERMOD, HEGADAS-S offers explicit dispersion treatments for individual HC species. However, we found several limitations in application of HEGADAS-S: (1) HEGADAS-S can only characterize a pond in a simple rectangular shape, which is inappropriate for an irregularly shaped produced water pond. Additionally, certain dimensional transformations are required to best represent the crosswind width of the pool when wind direction is not ideally normal to the edge of the pond. This results in a shifting of the source-receptor locations, which may cause the evaluation of modeled concentrations against canister samples to be unrealistic. (2) The chemical database of HGSYSTEM (accessible via a DATAPROP module) is limited and is difficult to extend. The database does not cover all organic species collected by the canisters. Consequently, many organic species had to be lumped into groups of species based on their carbon chain length (e.g., C2-C8, C10-C12) and the groups are modeled by a representative species available in the database.

We performed a total of seven inverse modeling studies at two produced water pond facilities and one study at a land farm. At each facility, one study lasted two days and was separated at least one month from the subsequent study to account for differences in disposed water. A single representative case study will be discussed here in detail. The case study was performed at a produced water pond facility in the Uintah Basin in April, 2016. In this case study, a set of nine sampling canisters were placed along the pond immediate boundaries of the pond, and one canister was placed upwind for characterizing background concentrations. Canister samplings and flux chamber measurements were conducted concurrently. During the sampling period, wind directions varied slightly between northwest and northeast with a dominant and steady wind direction of about 30 degrees.

The relative performance of AERMOD and HEGADAS-S for the case study will now be discussed. We initialized the AERMOD and HEGADAS-S models with an arbitrary emission rate of 3×10^4 g m^{-2} s^{-1} of individual hydrocarbons and compared results. Geological parameters and meteorological inputs for HEGADAS-S were taken from corresponding AERMOD inputs. Given all similar input parameters, the HEGADAS-S model estimated a more concentrated and narrow plume relative to the AERMOD estimation (Figure III.A.26). Due to its narrow geometry, the HEGADAS-S plume only reached four of the nine canisters. In contrast, the wider AERMOD plume reached all nine canisters. We also found that hydrocarbon concentrations at receptors located immediately downwind of the ponds were higher as estimated by HEGADAS-S than by AERMOD. For an inverse modeling application, higher estimated concentrations leads to lower estimated emission rates.

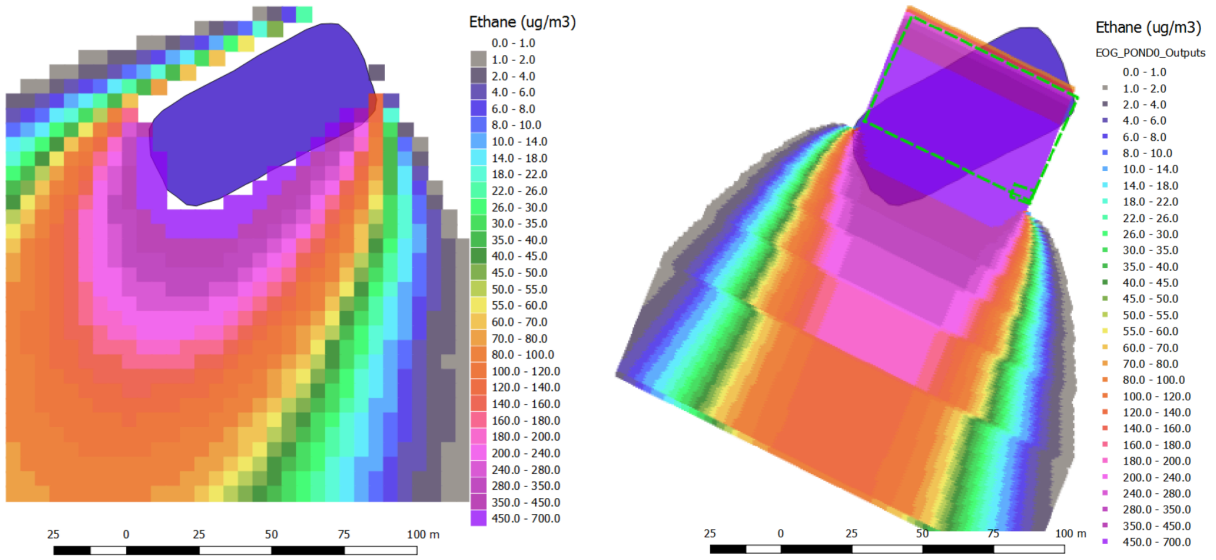

Figure III.A.26. Comparison of plume geometry of ethane as simulated by AERMOD (left) and by HEGADASS (right) at 3ft height above surface. Both models were performed with the dominant wind direction at about 30 degree from true North, and with an arbitrary emission rate of $3x10^{-4}$ g/s-m^2. For HEGADASS, the green rectangle indicates the transformed shape of the produced water pond perpendicular to wind vector.

Additionally, HEGADAS-S and AERMOD show significant differences in simulating the downwind horizontal concentration profiles (Figure III.A.27). For HEGADAS-S, the spatial variation of downwind concentrations differed among hydrocarbons. On the contrary, even with the compound-specific gas deposition included, there was hardly any difference in the horizontal profiles of downwind concentrations among all hydrocarbons in AERMOD (<0.1% of the magnitude). Both models agreed that ethane approximated 100 ug/m^3 at about 120 m downwind. More importantly, both models predicted the highest concentrations at the immediate boundary of the pond.

Both models estimated hydrocarbon emission rates high in comparison with the flux chamber measurements (Figure III.A.28). Largest biases were found for alcohol groups (< 100 ug/m^3 measured, > 2000 ug/m^3 estimated, not shown in Figure III.A.27). As expected, HEGADAS-S gave the lowest emission estimations among all modeling scenarios. AERMOD estimated higher concentrations with characterizing the pond as an area source than as open pit or volume sources. This finding is consistent with common practices of AERMOD applications. The most significant finding is that the flux chamber measured emission rates correlate very well with model's estimations in all modeling scenarios.

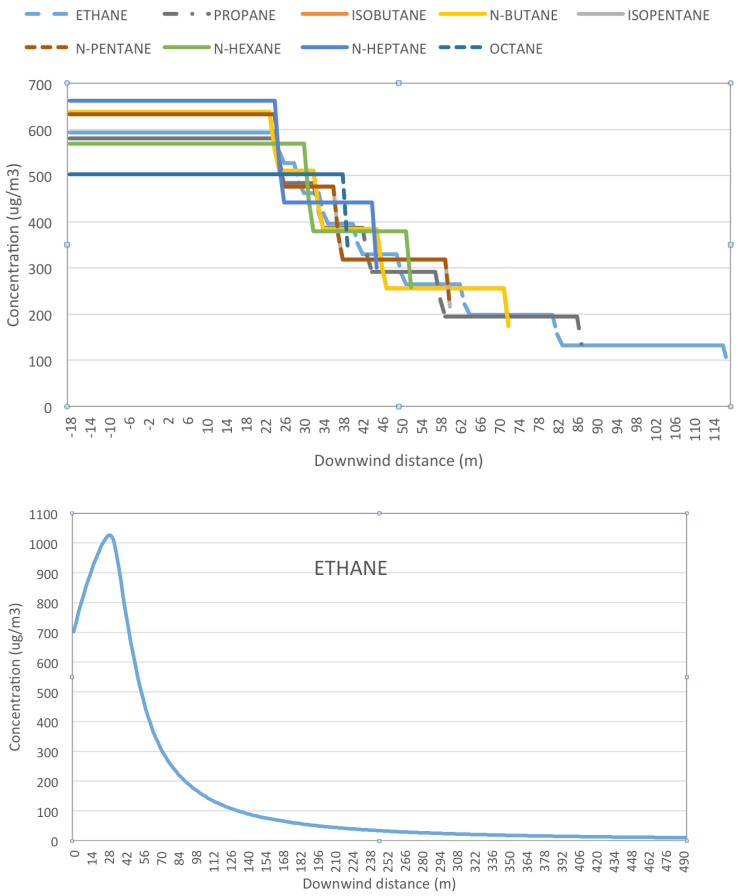

Figure III.A.27. Comparison of spatial variation of hydrocarbon concentrations along the plume center-line downwind of the ponds as estimated by HEGADAS-S (top) and by AERMOD (bottom). For HEGADAS-S, the downwind concentrations do not ultimately extrapolate to zero due to the model's cut-off value (100 ppb). For AERMOD, only the variation in ethane is shown since the variation of other hydrocarbons are almost identical to that of ethane. For both models, the distance of 0 m indicates the center point of the pond, and the distance of 22 m is the pond's boundary.

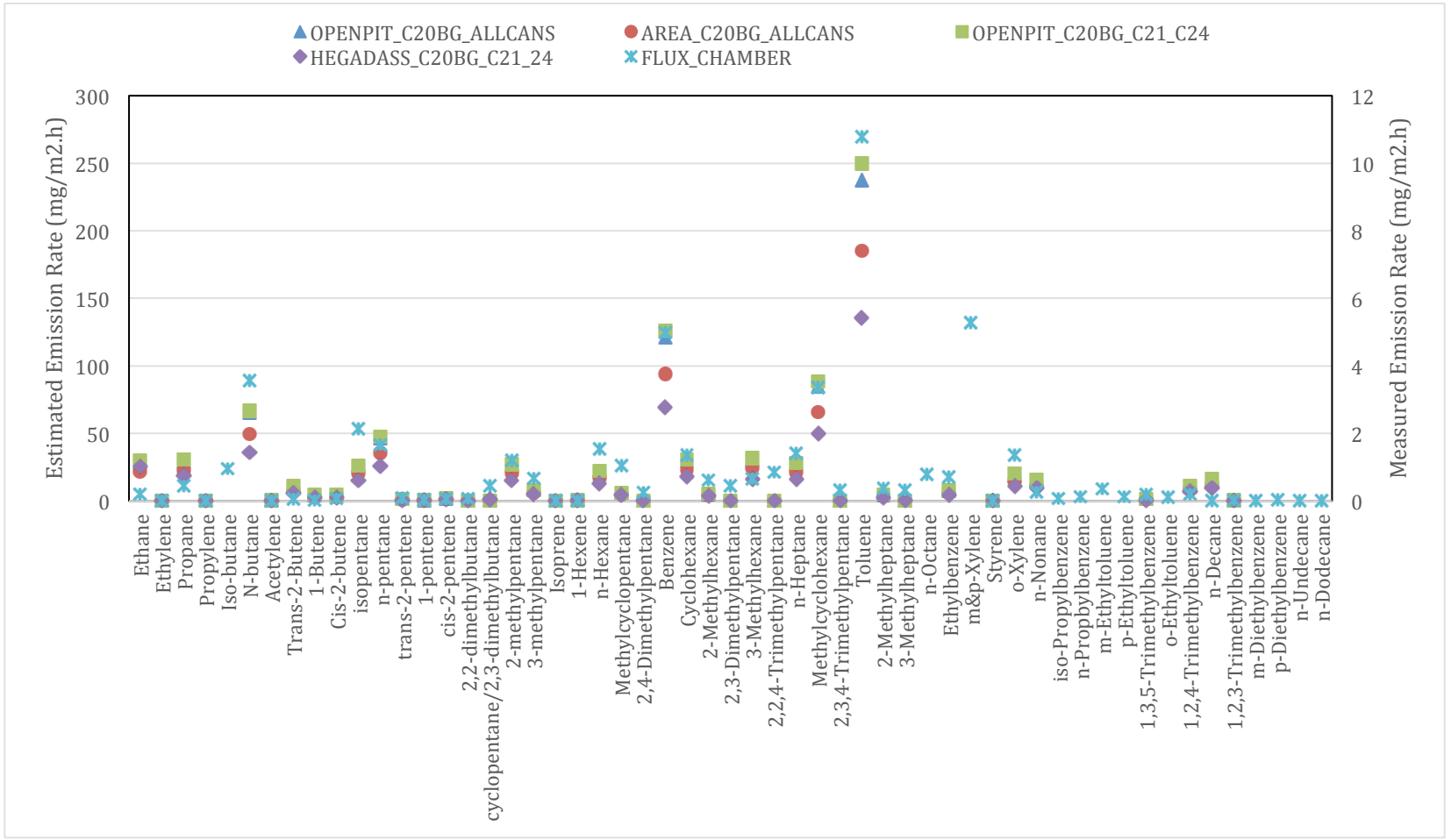

Figure III.A.28. Comparisions of estimated emission rates of invidual hydrocarbons as estimated by AERMOD and HEGADAS-S and as measured by the flux chamber. OPENPIT and AREA indicates AERMOD estimations that characterized the pond as an open-pit and an area source, respectively. As discussed above, HEGADAS-S estimations are the result of linear regression across four canisters. We conducted an equivalent regression with AERMOD across the same four canisters (OPENPIT_C20BG_C21_C24) for direct comparision with HEGADAS-S. Comparisons for alcohols are not shown.

43

We found discrepancies between emission rates as measured by the flux chamber and as estimated by inverse modeling, either with AERMOD or with HEGADAS-S. The discrepancies depended on meteorological conditions (calm vs. steady wind), and the complexity of the ponds themselves. For example, the measurement campaign on 05 May 2015 at a produced water pond facility with five nearby ponds gave very poor agreement between the flux chamber and the model estimations. The campaign on 28 April 2015, on a land farm that is fairly isolated gave good agreement between AERMOD and the flux chamber (Table III.A.5 and Figure III.A.29.)

Three sets of measurements were made on 01 April 2016 at a facility with only one active pond, and in all three sets the model highly overestimated (an order of magnitude) the emission rates in comparison to the estimations from the flux chamber (Table III.A.5 and Figure III.A.29). Among three sets of measurements made on this day, the first set (01APR16_01, Figure III.A.29) was conducted under calm and varying wind conditions and had the weakest performance. Better agreement between model and flux chamber were obtained with the second set as it was conducted under relatively steady wind and this set provides the best correlation between model and flux chamber estimation (Figures III.A.29).

The two sets measurements made on July 2016 are at the same facility of the April 2016 measurements. Biases in estimating emission rates between AERMOD and flux chamber in the July 2016 measurements are not at large as in the April 2016 measurements (Table III.A.5). Note that wind speed in July is significantly higher than in April measurement (4 m/s vs 2 m/s).

Among all hydrocarbon species, the best agreements are often found in alkanes and aromatics, whereas large biases are found with the alcohols.

Table III.A.5. Comparison of emission rates as estimated by flux chamber and by AERMOD inverse modeling (mg/m^2-hr).

Measurement Campaign	Means of estimation	Alkanes	Alkenes	Aromatics	Alcohols
Apr 2015	FLUX	287.5	4.7	83.8	0.5
	AERMOD	250.0	0.1	95.1	25.4
May 2015	FLUX	6879.5	3.1	1082.7	101.8
	AERMOD	32.9	18.6	25.4	3536.3
Apr 2016 – 1	FLUX	35.8	0.0	59.0	195.1
	AERMOD	714.8	1.3	628.1	312.8
Apr 2016 – 2	FLUX	30.5	0.2	43.8	126.6
	AERMOD	341.7	18.1	309.8	2673.1
Apr 2016 – 3	FLUX	26.3	0.0	60.3	224.5
	AERMOD	659.7	26.8	748.6	1729.3
Jul 2016 – 1	FLUX	22.0	0.0	63.7	105.4
	AERMOD	49.1	1.3	114.6	796.3
Jul 2016 – 2	FLUX	26.2	0.0	71.6	110.9
	AERMOD	73.7	1.4	83.5	908.4

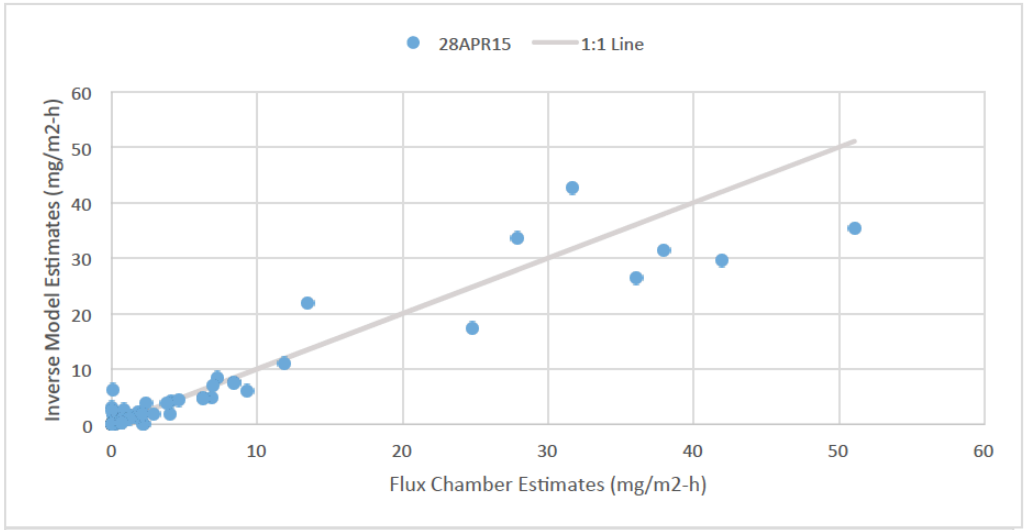

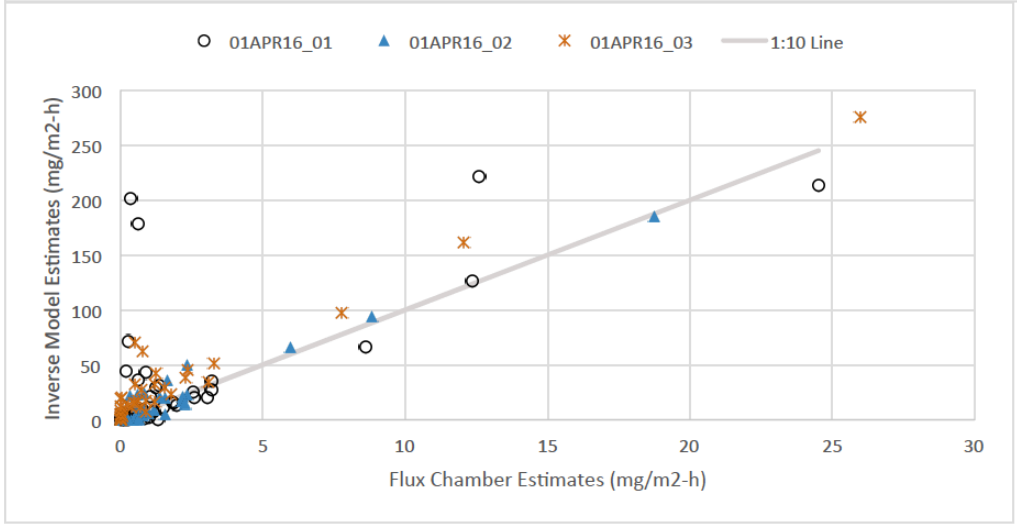

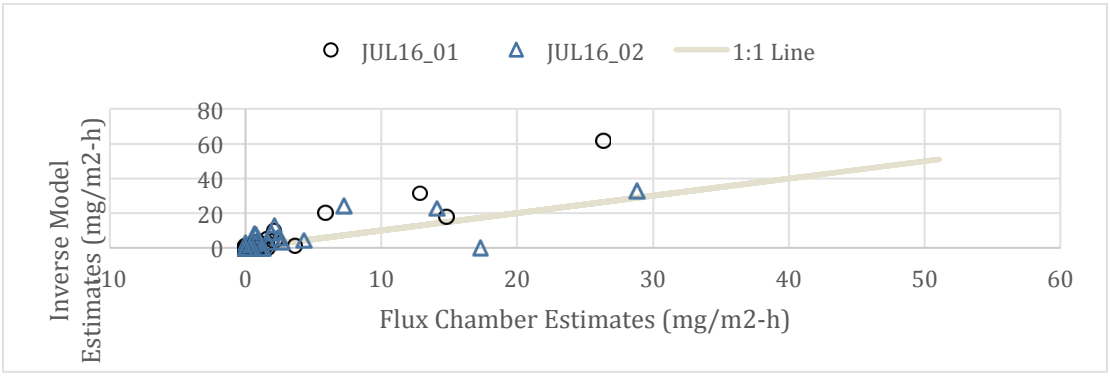

Figure III.A.29. Comparisons of emission rates of all hydrocarbon species as estimated by AERMOD and by flux chamber measurement during the April 2015, April 2016, and the July 2016 campaigns.

III.B. Natural Gas Subsurface Leakage and Natural Seepage

Measurements away from Well Pads: Baseline Determination

Methane fluxes at non-well sites were -0.1 ± 0.1 mg m^{-2} h^{-1}. Small positive and negative methane fluxes attributable to methanogenic or methanotrophic bacteria occur in any soil [Mosier et al., 1991; Striegl, et al., 1992]. Therefore, in the following, we assume that the typical baseline emission for methane in these arid basins of Eastern Utah is around ± 0.1 mg m^{-2} h^{-1}.

Measurements at Well Pads

Measurements of methane emissions at natural gas production sites have been reported [Hendler, et al., 2009; Allen et al., 2013; Brandt et al., 2014], but less work has focused on subsurface leakage [Day et al., 2014; Kang et al., 2014]. We undertook our study to add to the body of knowledge surrounding subsurface leakage and wellbore failure as well as to ascertain the impact of such leakage on local air quality. Methane fluxes at wellheads ranged from -5.6 to 7.0 × 10^4 mg m^{-2} h^{-1}; the 81st percentile was only 10 mg m^{-2} h^{-1}.

Combustible soil gas concentrations ranged from statistically zero (the lower detection limit being 10 ppm) to near total saturation, ≈ 10^6 ppm. Over 20% of samples exceeded 10^5 ppm (the explosive threshold for natural gas in air!), but many wells were selected for examination because they had previously measured high, so these results are not necessarily representative of all oil and gas wells in Utah.

Methane and other hydrocarbons are oxidized by methanotrophic bacteria in the soil [Leson & Winer, 1991; Panikov & Dedysh, 2000; Op den Camp, et al., 2009; Milucka et al., 2012; Zhang, et al., 2012]. As depicted in Figure III.B.1, leaking methane can be converted to carbon dioxide before it reaches the atmosphere. Negative methane fluxes (i.e., fluxes into the soil) occur when atmospheric methane is also consumed [Mosier et al., 1991; Striegl, et al., 1992]. At well pads, the carbon dioxide flux exceeded that of methane in 92% of cases. Carbon dioxide and methane were reasonably well correlated (r^2 = 0.42).

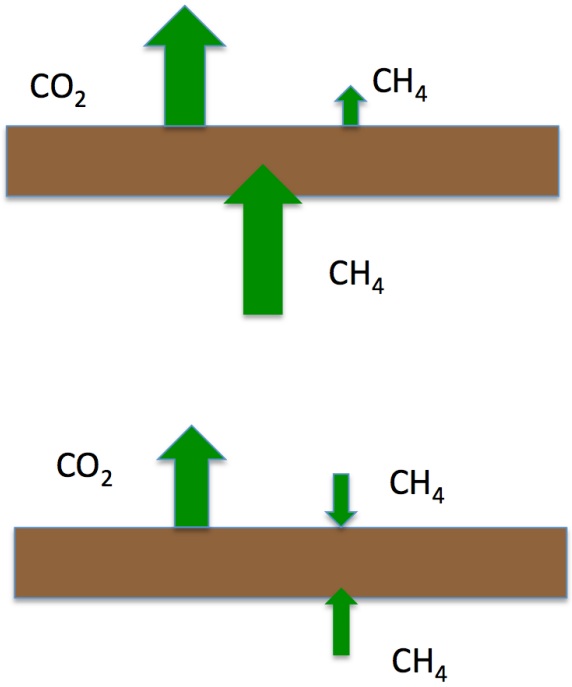

Figure III.B.1. Schematic depicting oxidation of methane to carbon dioxide by soil bacteria. Biooxidation of methane and other hydrocarbons usually produces a carbon dioxide signal stronger than that of methane.

Temperature dependence of biooxidation has also been observed. Figure III.B.2 compares winter and summer hydrocarbon fluxes measured at the same sites. Presumably a stronger hydrocarbon signal is observed in winter because biooxidation rates are suppressed [Klusman et al., 2000]. Also, we compared raw gas samples from wells at which we measured soil flux against the speciation of emission fluxes (Figure III.B.3). Raw natural gas at well sites contained very little carbon dioxide, but carbon dioxide was the majority of the emissions flux. Also, the ratio of NMHC to methane was greater in raw gas samples than in emissions, possibly because bacterial decomposition of leaked raw gas was greater for NMHC than for methane, or because of adsorption of NMHC onto soil surfaces.

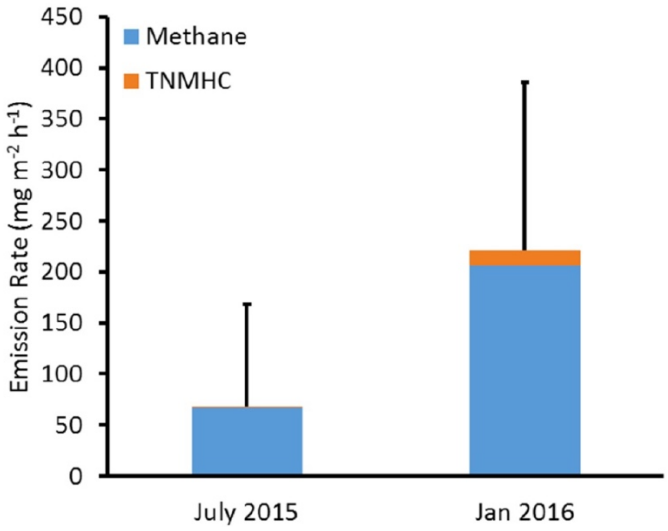

Figure III.B.2. Emissions of methane and TNMHC at the same wells during summer and winter. Whiskers represent 95% confidence intervals. The hydrocarbon flux is stronger in winter, presumably because colder temperatures suppress biooxidation.

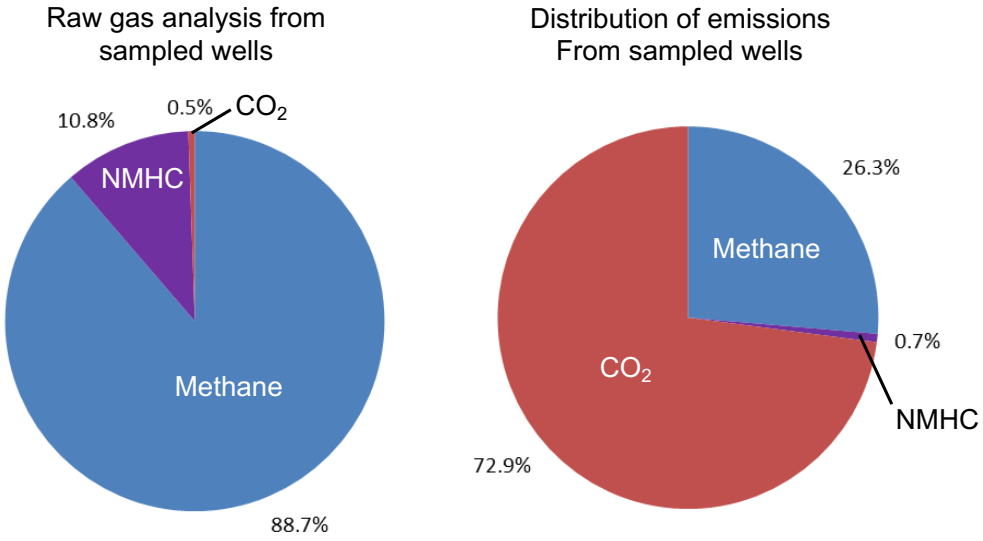

Figure III.B.3. Percentage of raw gas from gas analyses at well sites that was methane, NMHC, and carbon dioxide, and the percentage of total emission flux from well pad soils from the same wells that was from the same three components.

Flux and soil gas measurements at well pads were taken at varying distances from well heads, usually from 0.3 to 3 m. Figures III.B.4 and III.B.5 show the resulting distance profiles. Both emissions and soil gas concentrations tend to be higher near the wellhead.

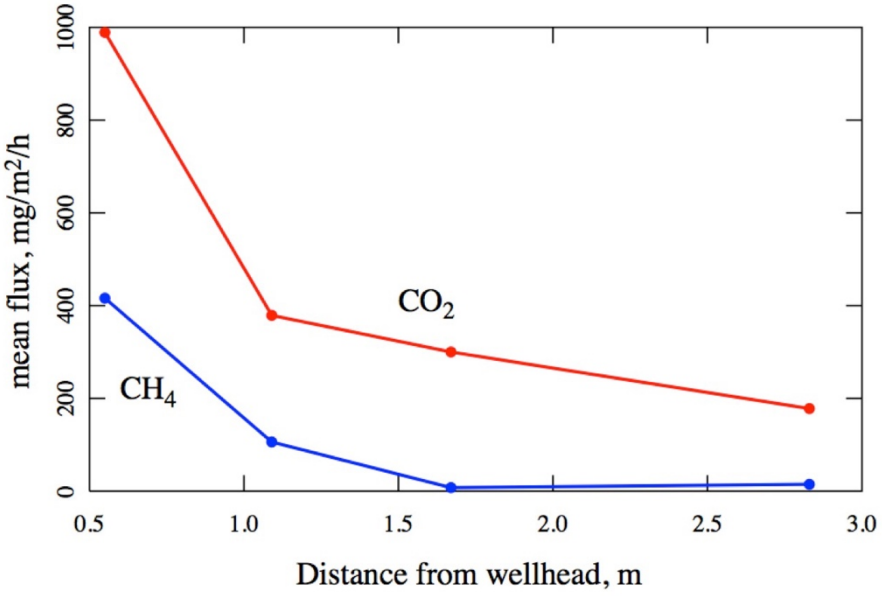

Figure III.B.4. Average fluxes drop off with distance from the wellhead.

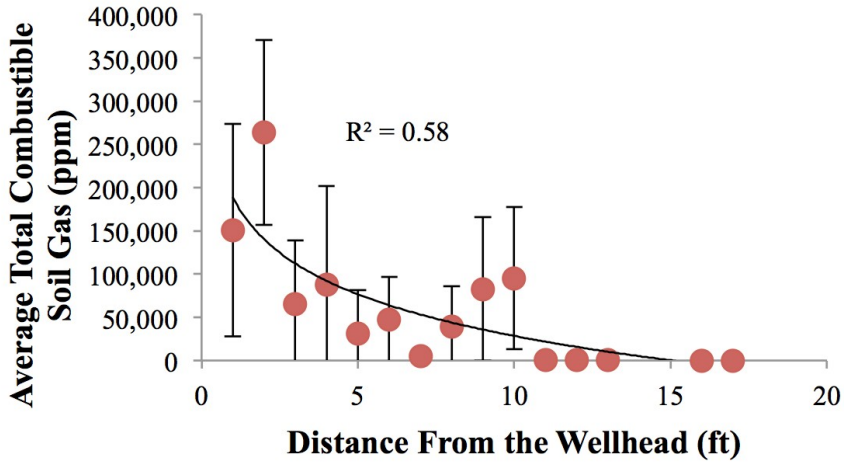

Figure III.B.5. Average combustible soil gas concentration drops off with distance from wellhead.

According to Ririe and Sweeney [1993], the composition of a soil hydrocarbon emission is a signature of its source. A natural gas leak is indicated if the methane signal is stronger than the total of other hydrocarbons—total non-methane hydrocarbons or TNMHC—while the reverse indicates outgassing from spilled hydrocarbon liquids (e.g., crude oil or gasoline).

Using this criterion, 68% the measurements were from natural gas leaks, and 32% were from liquid hydrocarbon contamination in the soil. Figure III.B.6 shows an example of TNMHC distribution of fluxes by carbon number for well pad soils that were measured during summer 2015. These results show that, to some extent, the source of fluxes from well pad soils can be determined from the speciation of emissions.

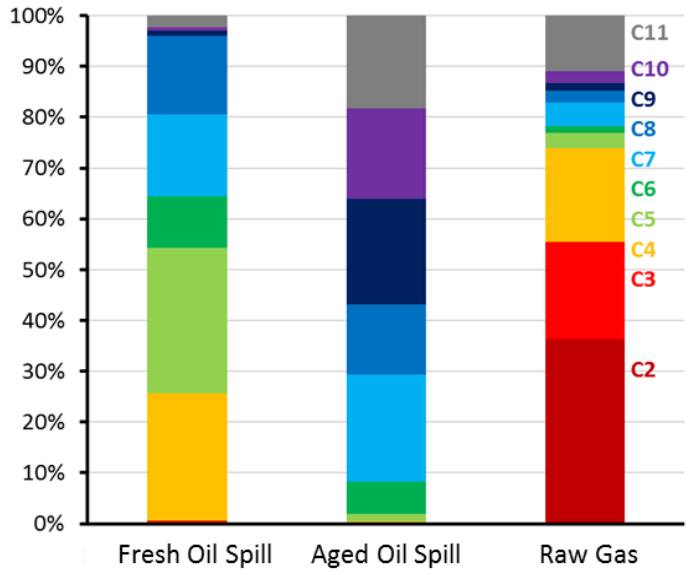

Figure III.B.6. Percent of TNMHC emissions that were due to C2-C11 hydrocarbons in fluxes from well pad soils collected during summer 2015. The two leftmost bars represent two measurement locations that were contaminated with spilled oil. The rightmost bar shows the average of all other measurements collected during summer 2015.

To examine the hypothesis that older wells might be more prone to leakage, we have plotted in Figure III.B.7 the average combustible soil gas concentration and the average methane flux against the year of completion of the well. The data points represent averages over all measurements taken at the well. Although negative and therefore trending in the expected direction, these correlations are very weak. The small values of Pearson's r^2 (0.08, 0.12) indicate that the age of the well is a poor predictor of methane flux or soil gas concentration. However, this analysis does not take into consideration any subsequent workovers or other repairs to the wells.

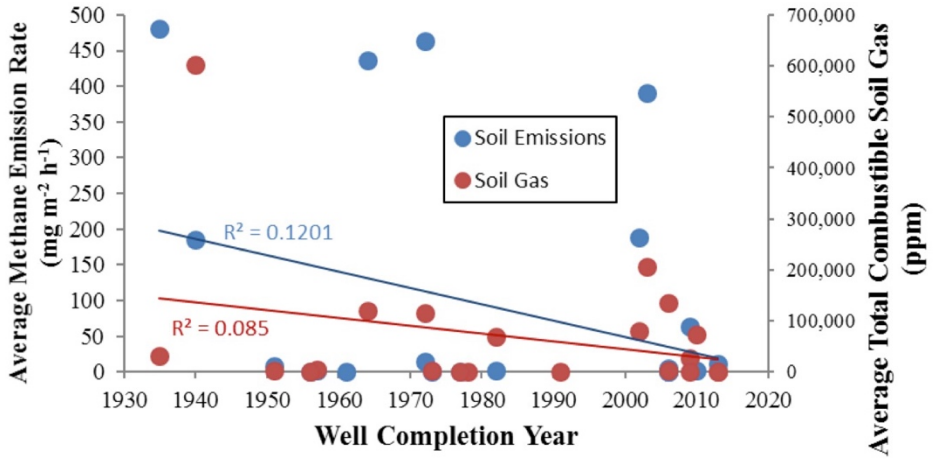

Figure III.B.7. Correlations between methane emission rate, combustible soil gas concentration, and well age.

Figure III.B.8 shows methane fluxes from producing, shut-in, and natural gas storage wells. While the sample size is small, especially for storage wells, it does appear that producing oil and gas wells have lower soil emissions than the other well types. This could explain the weak trend observed in Figure III.B.7. Newer wells are more likely to be producing, so they would be less likely to have higher soil emissions. Alternatively, it could be that older wells are more likely to have leaks, and they are also more likely to be shut-in or used for storage, so those well types tend to leak more. It may be that storage and shut-in wells experience higher reservoir pressure and so are more likely to leak, but the correlation between methane emissions and well pressure was weak ($r^2 = 0.15$).

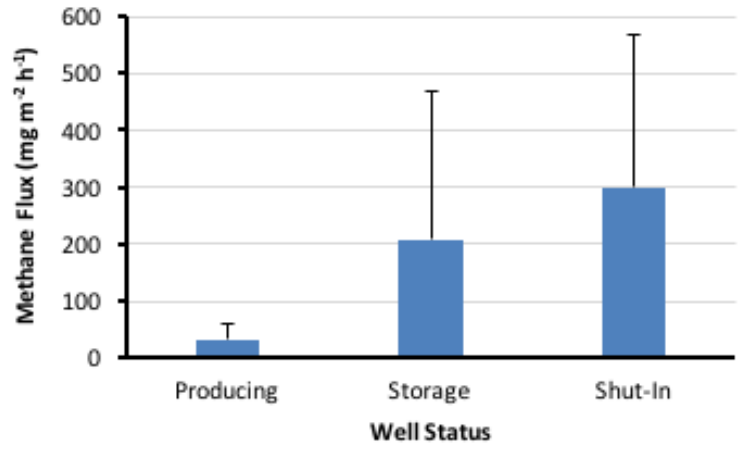

Figure III.B.8. Average methane flux from producing, storage, and shut-in wells. Whiskers show 95% confidence intervals.

One inexplicable result of this study is the lack of correlation between the combustible soil gas concentrations and the fluxes of methane into the air. Figure III.B.9 displays a rank correlation plot for these two variables. Flux measurements and soil gas measurements were usually within 0.3 m of each other, but they were never perfectly collocated. It is possible that the poor correlation between flux and soil gas is due to a highly variable and inhomogeneous spatial distribution of emissions on well pad soils.

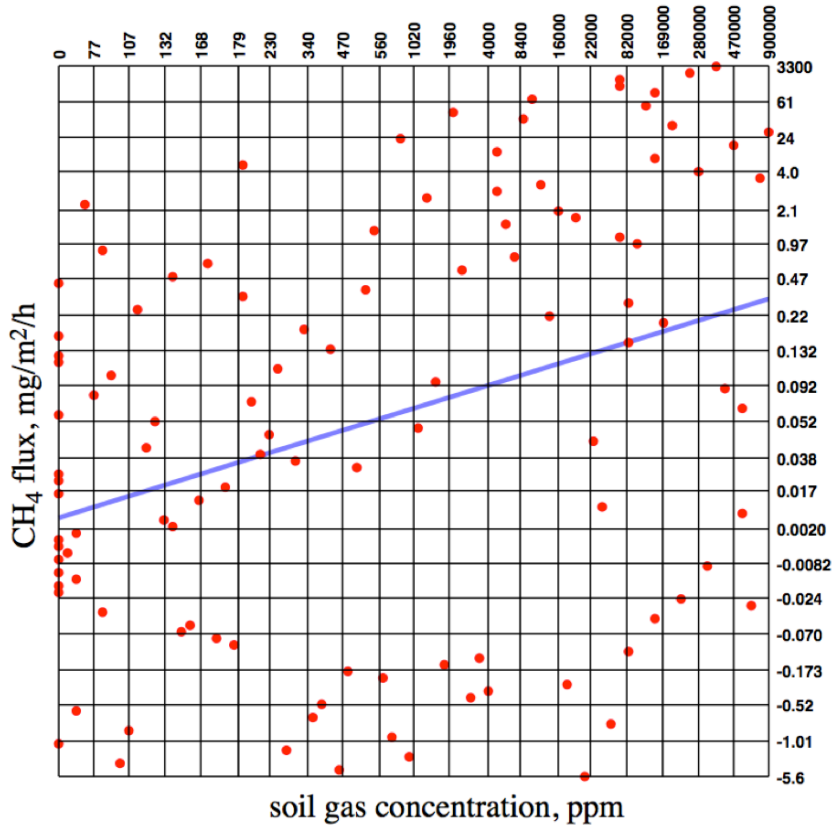

Figure III.B.9. Rank correlation plot between methane flux and combustible soil gas concentration. Pearson's R^2 = 0.12.

To better determine the spatial variability in methane fluxes from soils, we measured fluxes at 23 locations around a shut-in well. We visited the well shortly after a rainfall, and it displayed obvious bubbling through standing rainwater. Figure III.B.10 displays a graphic of the methane emissions measured that day. One very high methane emission location (ca. 7×10^4 mg m^{-2} h^{-1}) is seen WNW of the wellhead, and two moderately high emissions are seen to the SSW. We can estimate the net flux of methane from this well if we assume that the hotspot to the WNW dominates and if we treat it as a point source (meaning that its

effective area is the surface area covered by the flux chamber). The result is about 9 g h^{-1}. (A few more g h^{-1} are probably also contributed by the spots to the SSW.)

These measurements indicate several things. Although Figures III.B4 & 5 imply that on average higher emissions occur closer to the wellhead, the emission pattern at any given time and at any given well may be asymmetric and centered away from the wellhead, presumably because rising gas follows the path of least resistance through micro-channels in the soil. Also any water descending into the soil will displace soil gas upwards [Hillel, 1998], implying that larger than typical fluxes of soil gas can occur during and immediately after rainfall or a rapid snowmelt. This result shows that emissions can be very spatially inhomogeneous at well pad soils, and movement of measurement location by only a short distance can lead to very different results.

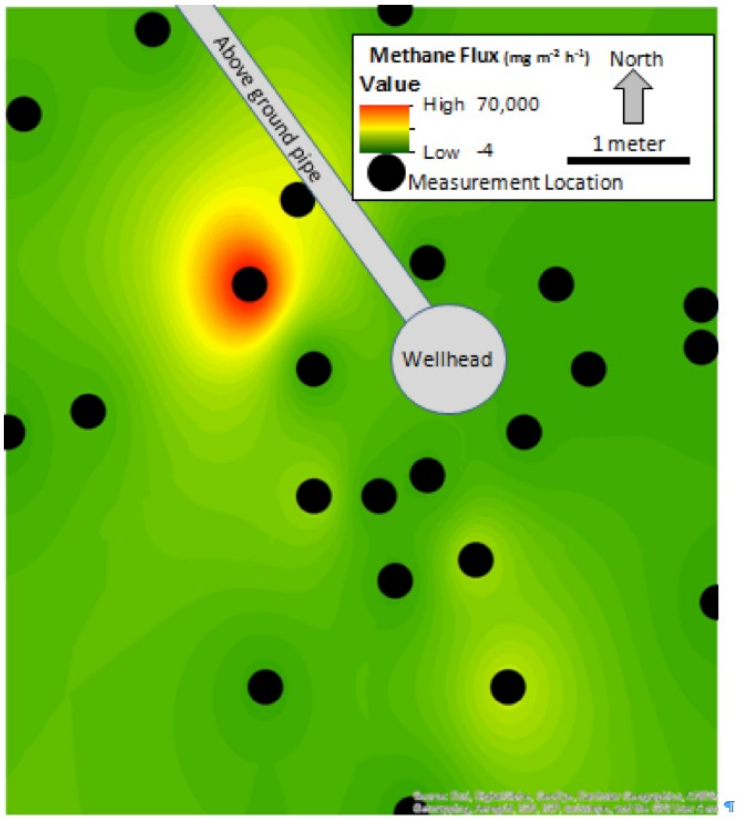

Figure III.B.10. Emissions from a shut-in well observed shortly after a rainstorm. The coloring shows a spatial extrapolation of emissions measured at indicated measurement locations. Placement of measurement locations on the map was determined from GPS measurements that had >1 m accuracy.

Other studies have indicated that emissions from the soil to the atmosphere are influenced by changes in barometric pressure [Kirchgessner et al., 2000; Xu et al., 2014]. The so-called

barometric pumping phenomenon occurs when a falling barometer leads to soil gas being drawn out of the soil and vice versa. We have searched for correlations between the data appearing in Figure III.B.6 and both the barometric pressure and its rate of change, but have observed no improvement in the correlation. There may be other confounding variables, such as the compaction or moisture content of the soil. Furthermore, as pointed out above, in about one-third of the measurements, the TNMHC flux exceeds that of methane. In such cases, it stands to reason that TNMHCs are also a large component of the combustible soil gas. Perhaps a stronger correlation would emerge if we were to compare soil gas methane concentration against methane flux.

Natural Seepage Measurements

It has been argued that natural methane seepage is a non-negligible fraction of the global methane budget [Etiope & Klusman, 2000; Etiope, 2004, 2005]. One study suggests that geologic formations in the Uintah Basin have been leaking natural gas since the early Tertiary [Johnson & Roberts, 2003] although it has also been argued that natural seepage in the Uintah Basin is too slow to have any impact on the chemistry or physics of the atmosphere [Mansfield, 2014]. In any case, we took a total of 14 measurements at six "geologically interesting" sites looking for evidence of natural seepage. These included the damage zone of the Uintah Basin boundary fault, and solid hydrocarbon outcroppings; either coal, oil shale, or gilsonite. (Gilsonite is a solid hydrocarbon mineral found almost exclusively in the Uintah Basin in surface-exposed veins [Monson & Parnell, 1992].) The measured methane fluxes at all these sites were statistically zero.

Basin-Scale Emissions

We can estimate the total average emission per well by integrating surface profiles. In other words, we can write

$$F = \int_0^\infty 2\pi r\, f(r)\, dr$$

where $f(r)$ represents the average flux at a distance r from the wellhead, i.e., one of the traces appearing in Figure III.B.4, and where F represents the total emission from the well. When $f(r)$ is measured in mg m^{-2} h^{-1}, Φ has units mg h^{-1}. The results of this integration appear in Table III.B.1.

Table III.B.1. Estimates of total average emission rates per well, for three categories of well.

Well status	Sample size	CH_4 g/h	CO_2 g/h
Gas storage	23	4	6
Producing	117	0.3	7
Shut-in	55	2	22

We can multiply the entries in Table III.B.1 by the total numbers of gas storage, producing, and shut-in wells in the Uintah Basin (0, 5640, and 452, respectively [Utah-DOGM]) to obtain basin-wide emissions estimates for the Uintah Basin: 2.6 kg CH4 hr^{-1} and 49 kg CO2 hr^{-1}. Our sample size is too small, the emissions are too spatially variable, and our sampling protocol is too non-random for us to put much faith in these numbers, but they are probably reasonable order-of-magnitude estimates. The 2.6 kg hr^{-1} estimate is only 0.004% of the total Uintah Basin methane flux as estimated by aircraft measurements [Karion, et al, 2013]. Furthermore, if we assume that the complete carbon dioxide emission results from the oxidation of methane that has leaked, then the total methane loss due to subsurface well-bore leakage is 20 kg h^{-1} = 180 tonne y^{-1}, only about 0.0003% of the Uintah Basin annual natural gas production [Utah- DOGM].

III.C. Land Farm Emissions

We measured emissions from a land farm facility in the Uintah Basin during fall 2014, spring 2015, and spring 2016 (21 total flux chamber measurements). We also estimated emissions from the facility using plume characterization/inverse modeling during spring 2015. The facility consisted of two land farms—one that had been remediated and contained some vegetation, and another that was actively receiving oil and gas solid waste.

Methane, hydrocarbon, and alcohol fluxes from the remediated land farm were -0.54 ± 1.41, -0.14 ± 1.04, and -0.03 ± 0.92 mg m^{-2} h^{-1}, respectively, indicating that volatile organics in the solid waste added to this section of the facility had decomposed or volatilized.

Fluxes from the active land farm were extremely variable, and are shown in Table III.C.1. Measurement locations on the active land farm were randomly distributed, and some measurements were collected on soils that were black with visible oil, while others were indistinguishable from natural soil. The location to which fresh waste was added varied over the three visits to the facility, and soil and solid waste at the land farm were regularly mixed and tilled, so the spatial distribution of fluxes was variable.

Table III.C.1. Summary of fluxes measured from an active land farm.

mg m^{-2} h^{-1}	Average	95% conf.	10^{th} percentile	90^{th} percentile
Methane	1.40	1.92	0.02	2.92
Carbon dioxide	3260.80	2965.74	508.35	5219.48
Total hydrocarbons	197.96	137.50	57.60	456.15
Alkanes	156.58	99.64	48.56	386.63
Alkenes	1.68	1.96	0.01	6.61
Aromatics	39.70	38.93	8.98	66.22
Alcohols	4.18	9.00	-1.12	11.27

Methane emissions from the active land farm were higher than at the remediated land farm, but were low compared to emissions of other organics. Alkanes made up more than 75% of the total organic compound flux from the active land farm, and aromatics accounted for 20% (Figure III.C.1). C1-C5 alkanes made up a very small portion of the total organic compound flux, probably because these volatile compounds were emitted from the solid waste either prior to their disposal at the land farm or after disposal but prior to our measurements. Similarly, benzene and toluene (C6 and C7 aromatics in Figure III.C.1), comprised a minority of the aromatic flux, which was dominated by C8 and C9 aromatics.

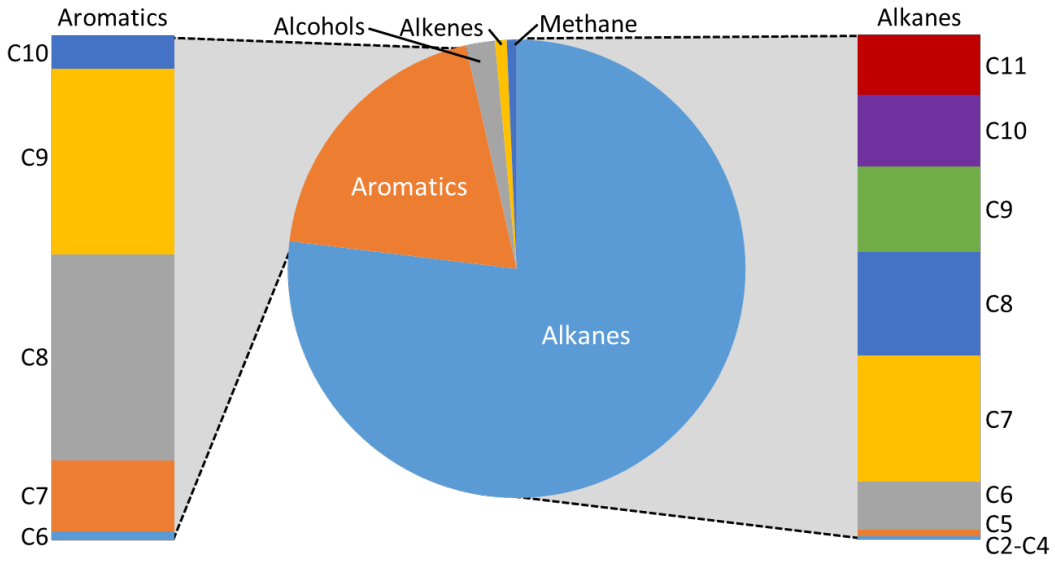

Figure III.C.1. Fraction of emissions from an active land farm that was due to alkanes, aromatics, alkenes, alcohols, and methane. Fractions of alkane and aromatic emissions are also broken down by carbon number.

Land farms in the Uintah Basin commonly cover 1-3 ha. Assuming the fluxes shown in Table III.C.1 occur over the area of a 2 ha land farm, that land farm would emit 95.0 ± 66.0 kg day^{-1} of total hydrocarbons. Fluxes of methanol, benzene, and total BTEX (benzene, toluene, ethylbenzene, and xylenes) would be 0.1 ± 0.4, 0.4 ± 0.4, and 11.1 ± 1.5 kg day^{-1}, respectively. For comparison, flux of BTEX from active land farms in Louisiana was measured by Pardue and Valsaraj [2000]. Application of those fluxes over a 2 ha area would result in total BTEX emissions of 3.2 ± 3.2 kg day^{-1}.

III.D. Snowpack Emissions

We performed a number of flux chamber experiments in Clay Basin and in the Uintah Basin with the chamber situated over snow. This occurred either 10 feet or less from a natural gas well, on snow-covered soil very near produced water ponds, directly on a snow-and-ice covered produced water pond, or at locations within the natural gas field that were neither near a pond nor a well.

As mentioned previously, in each experiment we determine emissions for approximately 57 VOC species by collecting air in canisters that are subsequently analyzed by GCMS. We then determine total non-methane hydrocarbon (TNMHC) emissions by summing the contributions of each VOC. Therefore, one way of analyzing the emission spectrum during any particular run is to take the measured emission of any one of the 57 VOCs during a run as a single data point, and then assemble a complete dataset from a series of runs. Figures III.D.1-4 display the histograms that result. For comparison, the histogram of data obtained from teflon blank runs are also shown. Because the distributions are broad and heavy-tailed, it is difficult to display all the data in a single histogram. Therefore the central part of each dataset is displayed in a histogram spanning the range ±0.12 mg m^{-2} h^{-1}. Outliers are then indicated separately. Since the PTFE blank is expected to emit nothing, it indicates the detection limits of our system, and any non-zero measurements that it gives should be interpreted as being statistically zero. Obviously the mode and mean of the teflon measurements are both very near zero, and although there are a small percentage of outliers lying many standard deviations away from the mode, these experiments indicate that any VOC measurement with a magnitude greater than about ±0.05 mg m^{-2} h^{-1} is almost certainly statistically different from zero.

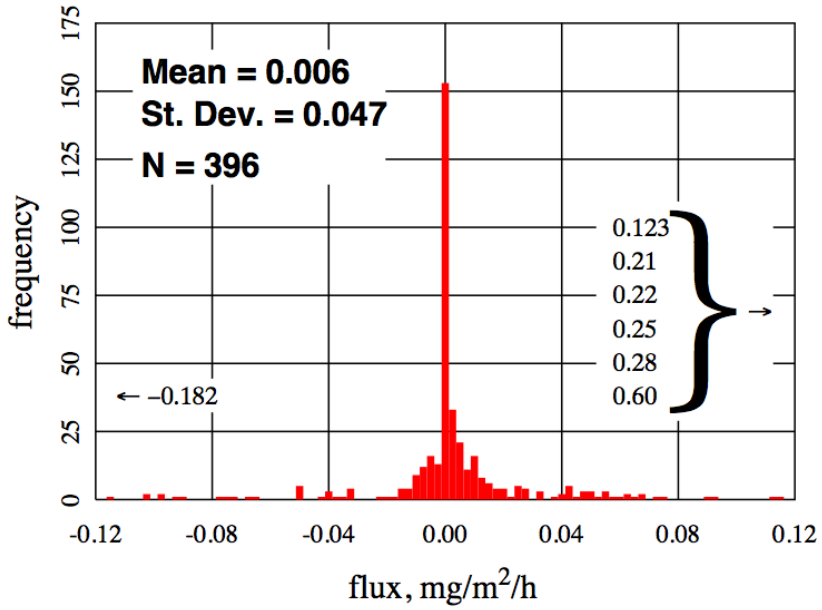

Fig. III.D.1. Histogram of the measured VOC fluxes during experiments on PTFE sheets, performed as a null test of the system. Seven outliers are indicated by the left- or right-pointing arrows. Statistics tabulated in the upper left apply to the full dataset, including outliers.

Figures III.D.2 displays the histogram obtained from snow packs near neither gas wells nor produced water ponds, and Figure III.D.3 displays the results for snow packs either on a frozen, snow-covered pond or snow packs within a few meters of the edge of a pond.

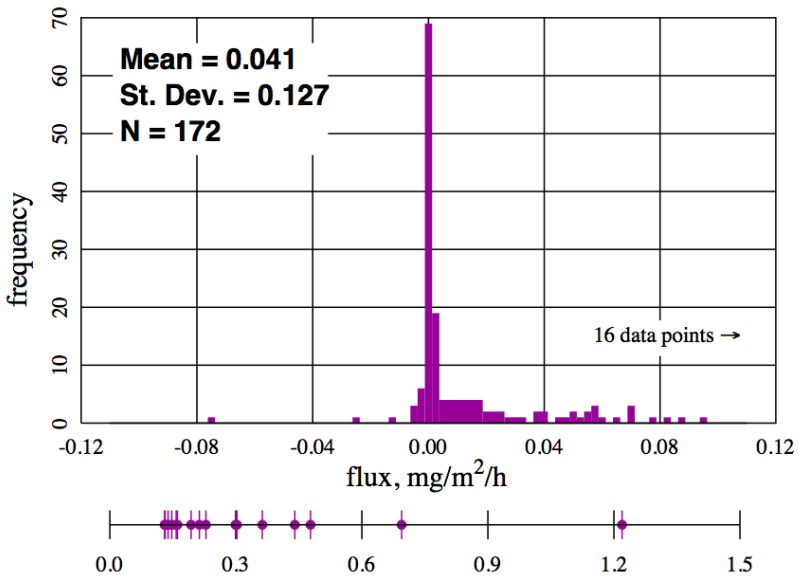

Figure III.D.2. Histogram of the measured VOC fluxes from snow packs distant either from gas wells or produced water ponds. 16 outliers are displayed on a separate linear scale below. Five of the outliers represent alcohols (methanol or ethanol) two are alkenes (1-propene or 1-hexene), one aromatic, and the remaining six are alkanes. Statistics tabulated in the upper left apply to the full dataset, including outliers.

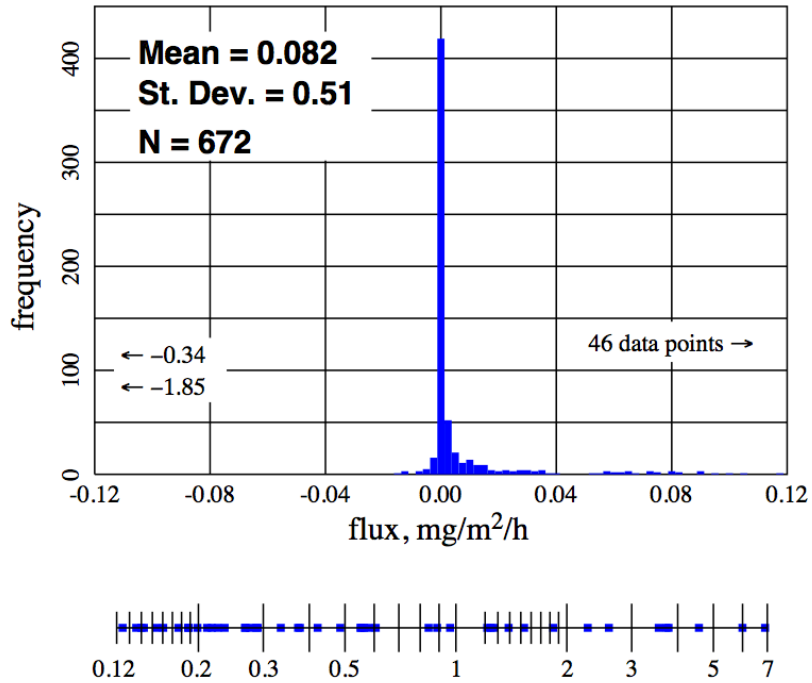

Figure III.D.3. Histogram of the measured VOC fluxes from snow packs on or near produced water ponds. Two negative outliers, indicated by left-pointing arrows, represent methanol uptake by the snowpack. 46 positive outliers are displayed separately on a logarithmic scale below. The positive outliers represent methanol (8), aromatic (14), and alkane (24) compounds.

Both snowpack datasets are characterized by a large central peak near zero, similar to the peak seen with the PTFE blanks, implying that many VOC species have statistically zero

emissions. However, both datasets also have heavy positive tails that are almost certainly not statistically zero indicating that these snow packs are discharging gases to the atmosphere.

It is difficult to know with certainty the ultimate carbon source of these emissions, but an appropriate hypothesis is that they result from organics that had previously adsorbed onto or dissolved into the snowpack. This would explain, for example, why the emission from snow near the produced water ponds is stronger. One possible scenario is that organics adsorb or dissolve overnight and then are emitted upon sublimation of the snow during the day. All our experiments occurred in daylight hours, but a possible outcome is that nighttime chamber experiments would see more negative fluxes.

It is interesting to compare these results with flux chamber measurements taken on snow-covered ground near natural gas wells. Those results are shown in Figure III.D.4. The large peak near 0 still appears, but both the positive and negative tails are heavier than in the preceding two examples.

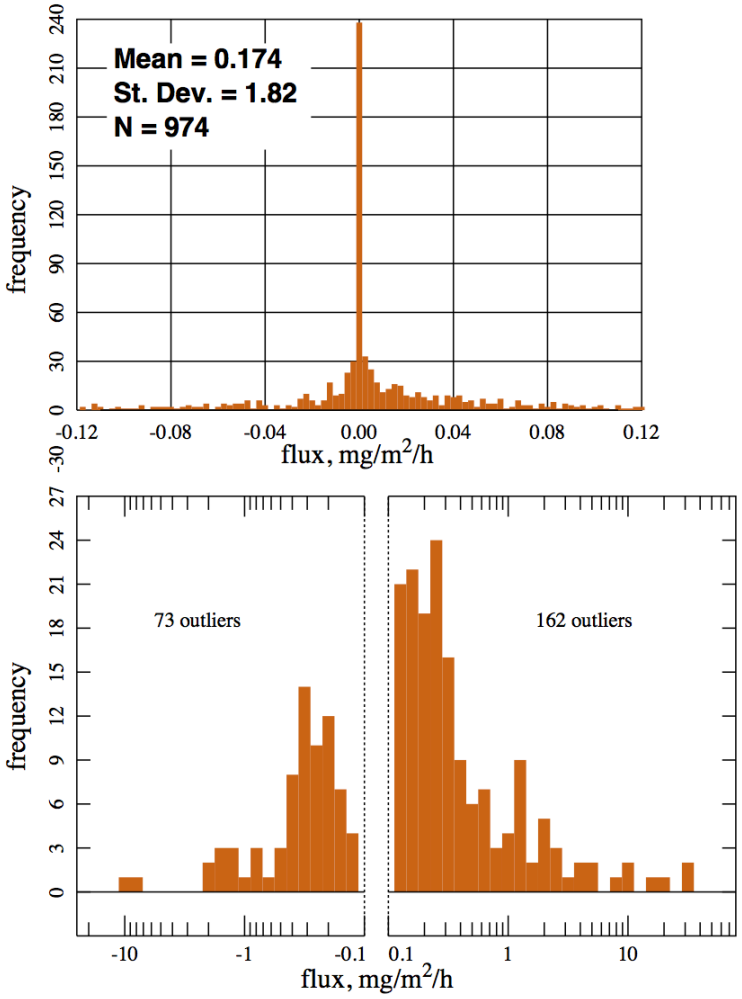

Figure III.D.4. Histograms representing VOC flux measurements on snow-covered ground within 10 feet of natural gas wells. Three separate histograms are used to represent the central, negative, and positive branches of the dataset. Outliers are represented by alkanes (169), aromatics (43), alkenes (8), and alcohols (15). Note the different vertical scales used for these histograms, and that the outlier histograms are plotted on a logarithmic mantissa.

Because the emission spectrum in Figure III.D.4 is statistically very different than Figure III.D.2 or III.D.3, the best interpretation is that the snowpack in the vicinity of a well generates emissions by two separate mechanisms. One mechanism is essentially identical to the process observed in other snowpacks, i.e., VOCs that entered the pack from the atmosphere and that are now being re-emitted. The other is identical to the process discussed in Section III.B, i.e., VOCs that entered the pack from the soil and that are subsequently transmitted to the atmosphere.

The statistical data reported in each of the four figures above is duplicated in the first three columns of Table III.D.1. The next column reports the number of total runs that contributed to each dataset. Methane fluxes are measured separately through detection by the LGR gas analyzer and the mean value over all runs in the category is reported in column 5. The mean TNMHC (excluding alcohols) appears in the last column.

Table III.D.1. Statistics of flux chamber measurements on snowpacks

	Number of canister samples	Mean of all VOC species mg m^{-2} h^{-1}	Std. Dev. mg m^{-2} h^{-1}	Total runs	Mean CH_4 mg m^{-2} h^{-1}	Mean TNMHC mg m^{-2} h^{-1}
PTFE	396	0.006	0.047	7	0.026	0.28
Snow distant from wells and ponds	172	0.041	0.127	3	-0.0051	1.68
Snow near ponds	672	0.082	0.51	12	0.029	2.2
Snow near wells	974	0.172	1.82	17	161	9.9

TNMHC emissions around 2 mg m^{-2} h^{-1} seem low in comparison to the produced water pond data reported above, but obviously, the total surface area of the snowpack is much larger than that of the ponds. If a snowpack of total area 10^3 km^2 emits VOCs at a rate of 2 mg m^{-2} h^{-1}, then its total VOC emission rate is 2×10^3 kg/h. By comparison, aircraft measurements performed in February 2013 lead to an estimate that the natural gas field in Uintah County, Utah has a methane emission rate of $(5.5 \pm 1.5) \times 10^4$ kg/h [Karion et al., 2014]. The emission rate of other VOCs might be about 4% of the methane emission rate, also about 2×10^3 kg/h. Our measurements suggest that VOCs cycling in and out of the snowpack is an important component of the VOC budget in the basin, but more measurements are needed to confirm this.

One could argue that these data are artificially high because the dome generates a greenhouse effect, heating the snow beneath it. However, that only means that the chamber experiments overestimate VOC emission rates. It does not alter the observation that the snowpack is emitting VOCs.

Photochemical grid models include deposition effects, meaning that molecules coming in contact with the ground or the snow are removed from the model at some given rate. However, it seems that more realism can be achieved by permitting some of those molecules to return to the atmosphere. More extensive measurements of VOC fluxes in and out of the snow, as well as of water vapor freezing and sublimation rates on and off the snowpack, are needed to inform these models.

IV. SUMMARY

We have measured emissions of hydrocarbons and greenhouse gases to the atmosphere from several uncharacterized area sources associated with the natural gas or oil production industry. The geographic setting of the study was several gas or oil producing basins in Eastern Utah (Uintah, Clay, and Paradox Basins) and West Central Wyoming (Upper Green River Basin). These sources include produced water surface impoundments ("ponds"), subsurface leakage from natural gas wells, natural seepage, land farms, and emissions from the snowpack. We have also measured concentrations of hydrocarbons in produced water ponds. The measurement techniques consisted of flux chamber and plume characterization combined with inverse modeling.

Produced Water Impoundments

A common technique for handling produced water, especially in the arid Western USA, is to place it in open-pit ponds, either for evaporation or for storage before re-injection. Prior to our study, very little was known about the emissions of these ponds.

Most produced water facilities that we studied have a common layout. Water arrives by tanker truck and is collected first into a small *skim pond*, used to skim off crude oil for re-sale. The skimmed water then proceeds to one or more *active ponds*, i.e., ponds that are actively receiving produced water. Larger facilities also have *inactive ponds*, or ponds that have received no new water for several weeks or months and from which water is being allowed to evaporate. We found that the strongest emissions (per unit area) occurred from the skim ponds and the weakest from the inactive ponds, presumably because most volatile hydrocarbons breathe out shortly after reaching the facility. The relative contributions of skim, active, and inactive ponds are about 15%, 83%, and 2%, respectively.

The emissions from the ponds included methane, non-methane hydrocarbons (NMHC), alcohols, and carbon dioxide. The NMHC emission had a relatively constant speciation, persisting over all facilities, over many orders of magnitude in the total emission, and over all seasons, dominated by BTEX aromatics and C5 to C8 alkanes. This constant speciation implies that fluxes of different NMHCs are correlated. On the other hand, emissions of methane, the alcohols, and carbon dioxide were poorly correlated with the NMHC emission. As far as methane and carbon dioxide are concerned, we attribute this to the fact that methane and carbon dioxide are the by-products of bacterial action and their fluxes are determined by other factors, including dissolved oxygen and temperature. The alcohol emission was dominated by methanol, but also included smaller amounts of ethanol and isopropanol. The lack of correlation between NMHC and methanol is more difficult to explain, and may result from the fact that spent methanol is also discharged into the ponds. Our measurement procedures included attempts to detect alkenes, but these had no detectable emission, as is typical of oil and gas emissions.

We also examined the relationship between concentrations of organics dissolved in the water and their fluxes into the atmosphere. We found, as predicted by mass-transfer laws, that the concentration of any compound in the water was proportional to its flux, within

about an order of magnitude, and that standard models (e.g., WATER9) can predict the mass-transfer coefficients to within about an order of magnitude. This implies that it should be possible to estimate fluxes by measuring water concentrations.

The facilities we studied covered about 25% of the 174 hectares of produced water ponds that we identified in the Uintah Basin. Assuming that our results can scale to all the ponds in the Uintah Basin, we estimate total emissions of about 240, 3000, 1000, 800, and 1000 tonnes/year of methane, carbon dioxide, alkanes, aromatics, and alcohols, respectively, and a total non-methane organic emission of 2800 tonnes/year. The methane emission constitutes 0.1% and 0.2%, respectively, of two separate emissions inventories, while the non-methane organic emission constitutes 1.5% and 2.8%, respectively.

To obtain a complementary analysis, we have also measured plume concentrations at a number of ponds and employed an inverse modeling technique. We found that the model estimations are highly sensitive to the complexity of the ponds and meteorological conditions. Agreement between inverse modeling and flux chamber is best under steady wind condition at facilities consisting of a single pond. We recommend that the inverse-modeling technique should only be used as a means to verify other measurement techniques (e.g., flux chamber, open-path Fourier transform infrared) rather than being used as an estimation tool for organic compound emissions from produced water ponds.

Subsurface Leakage from Natural Gas Wells and Natural Seepage

This study was stimulated in part by the observation [Stolp et al., 2006] that methane in high concentrations can be found in the soil near well pads. It was also stimulated by reports [Etiope & Klusman, 2000; Etiope, 2004, 2005] that natural seepage has been observed in oil- and gas-producing basins and that it may constitute an important part of the global methane emission.

We measured methane emissions at 27 different wells at various times over the course of the study, for a total of 195 flux measurements on well pads. For many of these measurements, the corresponding total combustible soil gas concentration was also measured. Flux measurements were observed over a range from -5.6 to $+7.0 \times 10^4$ mg m^{-2} h^{-1}, although the distribution is heavy-tailed, with the 81st percentile being only 10 mg m^{-2} h^{-1}. Combustible soil gas concentrations ranged from statistically zero to near total saturation ($\approx 10^6$ ppm). Over 20% of samples exceeded 10^5 ppm. However, sampling of wells was non-random, intentionally including a significant fraction of wells with high soil gas. We also observed that both methane emissions and combustible soil gas concentrations fall off, on average, with distance from the well head.

We observed evidence of oxidation of methane to carbon dioxide in the soil. In over 90% of the measurements, the carbon dioxide flux exceeded that of methane. This is due to oxidation of methane by soil bacteria. Further evidence of this is that the CO_2 signal weakens relative to CH_4 in winter, when cold temperatures suppress bacterial action.

We also measured non-methane hydrocarbon (NMHC) fluxes at these sites. In about 1/3 of the measurements, the NMHC flux exceeds that of methane, which is evidence that the

emission is primarily caused by hydrocarbons, e.g., crude oil or gasoline, that had been previously spilled onto the soil.

Inexplicably, we find no significant correlation between total combustible soil gas concentrations and methane fluxes, even when we controlled for variation in atmospheric pressure. We assume there must be other confounding variables, such as soil compaction and soil moisture.

When these results are scaled up to the entire Uintah Basin, we find that this leakage mode is an insignificant contribution (≈ 0.004%) to the total CH_4 flux. It is also an insignificant portion (≈ 0.0003%) of total natural gas production.

In an effort to detect natural seepage, we deployed the flux chamber over surface outcrops of coal, oil shale, gilsonite, and over a fault system. No significant fluxes of methane or NMHC were observed.

Land Farms

We performed 21 flux chamber measurements at a facility that contained two land farms. One had been remediated and contained some vegetation, while another continued to receive solid hydrocarbon waste. Fluxes from the remediated farm were low, indicating that most of its VOCs had decomposed or volatilized. Fluxes from the active land farm were extremely variable, presumably because the operators vary the discharge point for solid waste in the farm. Land farms in the Uintah Basin have areas in the range of 1 to 3 ha. We estimate that a 2 ha land farm would emit about 100 kg/day of total hydrocarbons, including about 10 kg/day of BTEX compounds.

Snowpack Emissions

It is well known that exchange of compounds between the atmosphere and the snowpack in polar regions influences the chemistry and physics of the troposphere. Measurements of such effects in temperate regions are less extensive, and we are aware of none in oil- and gas-producing basins. We performed a number of flux chamber measurements with the chamber situated over snow in either Clay Basin or the Uintah Basin. These occurred either 10 feet or less from a natural gas well, on snow-covered soil or ice near produced water ponds, and also at locations within the natural gas field near neither ponds nor wells.

At first glance, the emissions seem inconsequential, but upon closer inspection, we see that they have heavy-tailed distributions that are statistically distinct from the PTFE blank experiments reported above, indicating that something is happening. For example, the average NMHC emission (including methanol) from snowpacks not near wells or ponds is about 2 mg m^{-2} h^{-1}. This seems small in comparison to the pond emissions reported above, until we remember that the snowpack covers the entire basin. Over an area of 10^3 km^2, this equates to a total NMHC emission of 2×10^3 kg/h, which should not be ignored in any effort to understand the winter ozone problem in the Uintah Basin. The mechanism of this emission is not understood, but we hypothesize that organics in the atmosphere adsorb or dissolve onto the snowpack and are re-emitted when ice crystals sublime.

V. APPENDIX: COMPOUNDS DETECTED BY THE FLUX CHAMBER

CO_2 CH_4

ALKANES

ethane	propane	n-butane
n-pentane	n-hexane	n-heptane
n-octane	n-nonane	n-decane
n-undecane	n-dodecane	isobutane
isopentane	2,2-dimethylbutane	2,3-dimethylbutane
2-methylpentane	3-methylpentane	2-methylhexane
2,3-dimethylpentane	3-methylhexane	2,2,4-trimethylpentane
2,3,4-trimethylpentane	2,4-dimethylpentane	2-methylheptane
cyclopentane	methylcyclopentane	cyclohexane
methylcyclohexane	3-methylheptane	

AROMATICS

benzene	toluene	ethylbenzene
o-xylene	m-xylene	p-xylene
isopropylbenzene	n-propylbenzene	o-ethyltoluene
m-ethyltoluene	p-ethyltoluene	1,3,5-trimethylbenzene
1,2,4-trimethylbenzene	1,2,3-trimethylbenzene	m-dethylbenzene
p-diethylbenzene	styrene	

ALKENES

ethylene	propylene	acetylene
1-butene	trans-2-butene	cis-2-butene
1-pentene	trans-2-pentene	cis-2-pentene
isoprene	1-hexene	

ALCOHOLS

methanol	ethanol	isopropanol

CARBONYLS

formaldehyde	acetaldehyde	acrolein/acetone
propinalehyde	crotonaldehyde	butyraldehyde
benzaldehyde	valeraldehyde	p-tolualdehyde
hexaldehyde		

VI. REFERENCES

Allen, D. T.; Torres, V. M.; Thomas, J.; Sullivan, D. W.; Harrison, M.; Hendler, A.; Herndon, S. C.; Kolb, C. E.; Fraser, M. P.; Hill, A. D., Measurements of methane emissions at natural gas production sites in the United States. *Proceedings of the National Academy of Sciences* **2013,** *110* (44), 17768-17773.

Ahmadov, R.; McKeen, S.; Trainer, M.; Banta, R.; Brewer, A.; Brown, S.; Edwards, P. M.; de Gouw, J. A.; Frost, G. J.; Gilman, J.; Helmig, D.; Johnson, B.; Karion, A.; Koss, A.; Langford, A.; Lerner, B.; Olson, J.; Oltmans, S.; Peischl, J.; Petron, G.; Pichugina, Y.; Roberts, J. M.; Ryerson, T.; Schnell, R.; Senff, C.; Sweeney, C.; Thompson, C.; Veres, P. R.; Warneke, C.; Wild, R.; Williams, E. J.; Yuan, B.; Zamora, R., Understanding high wintertime ozone pollution events in an oil- and natural gas-producing region of the western US. *Atmospheric Chemistry and Physics* **2015,** *15* (1), 411-429.

Ausma, S.; Edwards, G. C.; Wong, E. K.; Gillespie, T. J.; Fitzgerald-Hubble, C. R.; Halfpenny-Mitchell, L.; Mortimer, W. P. A micrometeorological technique to monitor total hydrocarbon emissions from landfarms to the atmosphere. *J. Environ. Qual.* **2001,** *30* (3), 776-785.

Ausma, S.; Edwards, G. C.; Fitzgerald-Hubble, C. R.; Halfpenny-Mitchell, L.; Gillespie, T. J.; Mortimer, W. P. Volatile hydrocarbon emissions from a diesel fuel-contaminated soil bioremediation facility. *J. Air Waste Manage. Assoc.* **2002,** *52* (7), 769-780.

Ausma, S.; Edwards, G. C.; Gillespie, T. J. Laboratory-scale measurement of trace gas fluxes from landfarm soils. *J. Environ. Qual.* **2003,** *32* (1), 8-22.

Bartels-Rausch, T.; Jacobi, H.-W.; Kahan, T.F.; Thomas, J.L.; Thomson, E.S.; Abbatt, J.P.D.; Ammann, M.; Blackford, J.R.; Bluhm, H.; Boxe, C.; Dominé, F.; Frey, M.M.; Gladich, I.; Guzmán, M.I.; Heger, D.; Huthwelker, Th.; Klán, P.; Kuhs, W.F.; Kuo, M.H.; Maus, S.; Moussa, S.G.; McNeill, V.F.; Newberg, J.T.; Pettersson, J.B.C.; Roeselová, M.; Sodeau, J.R. A review of air-ice chemical and physical interactions (AICI): liquids, quasi-liquids and solids in snow. *Atmospheric Chemistry and Physics*, **2014**, 14, 1587-1633.

Benko, K. L.; Drewes, J. E., Produced water in the Western United States: geographical distribution, occurrence, and composition. *Environmental Engineering Science* **2008,** *25* (2), 239-246.

Boudries, H.; Bottenheim, J.; Guimbaud, C.; Grannas, A.; Shepson, P.; Houdier, S.; Perrier, S.; Dominé, F. Distribution and trends of oxygenated hydrocarbons in the high Arctic derived from measurements in the atmospheric boundary layer and interstitial snow air during the ALERT2000 field campaign. *Atmos. Environ.* **2002,** *36* (15), 2573-2583.

Brandt, A.; Heath, G.; Kort, E.; O'Sullivan, F.; Pétron, G.; Jordaan, S.; Tans, P.; Wilcox, J.; Gopstein, A.; Arent, D., Methane leaks from North American natural gas systems. *Science* **2014,** *343* (6172), 733-735.

Brymer, D. A.; Ogle, L. D.; Jones, C. J.; Lewis, D. L. Viability of using SUMMA polished canisters for the collection and storage of parts per billion by volume level volatile organics. *Environ. Sci. Technol.* **1995,** *30* (1), 188-195.

Callaham, M. A.; Stewart, A. J.; Alarcón, C.; McMillen, S. J. Effects of earthworm (Eisenia fetida) and wheat (Triticum aestivum) straw additions on selected properties of petroleum-contaminated soils. *Environ. Toxicol. Chem.* **2002,** *21* (8), 1658-1663.

Chidsey, T., Oil and Gas in the Uinta Basin, Utah: What to Do with the Produced Water. In *American Association of Petroleum Geologists Annual Convention*, Denver, Colorado, 2015.

Clark, C.; Veil, J. *Produced water volumes and management practices in the United States*, Argonne National Laboratory (ANL): 2009.

Colborn, T.; Schultz, K.; Herrick, L.; Kwiatkowski, C.; An exploratory study of air quality near natural gas operations. *Human and Ecological Risk Assessment: An International Journal* **2014,** *20* (1), 86-105.

Conley, S.; Franco, G.; Faloona, I.; Blake, ,D.R.; Peischl, J.; Ryerson, T.B., Methane emissions from the 2015 Aliso Canyon blowout in Los Angeles, CA, Science, 351, 1317-1320 (2016).

Day, S.; Dell'Amico, M.; Fry, R.; Tousi, H.J., *Field measurements of fugitive emissions from equipment and well casings in Australian coal seam gas production facilities: Report to the Department of Environment*, CSIRO, Australia, 2014.

de Gouw, J. A.; Howard, C. J.; Custer, T. G.; Fall, R. Emissions of volatile organic compounds from cut grass and clover are enhanced during the drying process. *Geophys. Res. Lett.* **1999,** *26* (7), 811-814.

Denmead, O. Approaches to measuring fluxes of methane and nitrous oxide between landscapes and the atmosphere. *Plant Soil* **2008,** *309* (1-2), 5-24.

Dicataldo, G.; Richins, G. H.; Spiroff, K. J.; Nelson, M. B., Produced-water VOC, HAP emissions, concern Rocky Mountain regulators. *Oil & Gas Journal* **2009,** *107* (25), 41-41.

Dórea, H. S.; Bispo, J. R.; Aragão, K. A.; Cunha, B. B.; Navickiene, S.; Alves, J. P.; Romão, L. P.; Garcia, C. A., Analysis of BTEX, PAHs and metals in the oilfield produced water in the State of Sergipe, Brazil. *Microchemical Journal* **2007,** *85* (2), 234-238.

Dupont, R.R. Evaluation of air emission release rate model predictions of hazardous organics from land treatment facilities. *Environ. Prog.* **1986,** *5* (3), 197-206.

Edwards, P. M.; Brown, S. S.; Roberts, J. M.; Ahmadov, R.; Banta, R. M.; deGouw, J. A.; Dube, W. P.; Field, R. A.; Flynn, J. H.; Gilman, J. B.; Graus, M.; Helmig, D.; Koss, A.; Langford, A. O.; Lefer, B. L.; Lerner, B. M.; Li, R.; Li, S.-M.; McKeen, S. A.; Murphy, S. M.; Parrish, D. D.; Senff, C. J.; Soltis, J.; Stutz, J.; Sweeney, C.; Thompson, C. R.; Trainer, M. K.; Tsai, C.; Veres, P. R.; Washenfelder, R. A.; Warneke, C.; Wild, R. J.; Young, C. J.; Yuan, B.; Zamora, R., High winter

ozone pollution from carbonyl photolysis in an oil and gas basin. *Nature* **2014,** *514* (7522), 351-354.

Eklund, B. Practical guidance for flux chamber measurements of fugitive volatile organic emission rates. *J. Air Waste Manage. Assoc.* **1992,** *42* (12), 1583-1591.

EPA, *Air Emissions Models for Waste and Wastewater*, United States Environmental Protection Agency: Research Triangle Park, North Carolina, 1994, Document No. EPA-453/R-94-080A, http://www3.epa.gov/ttn/chief/software/water/air_emission_models_waste_wastewater.pdf

EPA, U. S. Method 8015B: Nonhalogenated Organics Using GC/FID, United States Environmental Protection Agency: Research Triangle Park, North Carolina, 1996a, http://www.caslab.com/EPA-Methods/PDF/8015b.pdf.

EPA, U. S. Method 8260B: Volatile Organic Compounds by Gas Chromatography/Mass Spectrometry (GC/MS), United States Environmental Protection Agency: 1996b, http://www.epa.gov/wastes/hazard/testmethods/sw846/pdfs/8260b.pdf.

EPA, *Technical Assistance Document for Sampling and Analysis of Ozone Precursors*, United States Environmental Protection Agency: Research Triangle Park, North Carolina, 1998, Document No. EPA/600-R-98/161, http://www.epa.gov/ttn/amtic/files/ambient/pams/newtad.pdf.

EPA, *Compendium Method TO-15: Determination of Volatile Organic Compounds (VOCs) in Air Collected in Specially-Prepared Canisters and Analyzed by Gas Chromatography/Mass Spectrometry (GC/MS)*, United States Environmental Protection Agency: Cincinnati, Ohio, 1999, http://www.epa.gov/ttn/amtic/files/ambient/airtox/to-15r.pdf.

EPA, *User's Guide for WATER9 software, Version 2.0.0*, United States Environmental Protection Agency: Research Triangle Park, North Carolina, August 16, 2001, https://www3.epa.gov/ttnchie1/software/water/water9/water9%20manual.pdf

EPA, *AERMOD: Description of Model Formulation*, United States Environmental Protection Agency, Document No. EPA-454/R-03-004, September 2004. http://www.epa.gov/scram001/7thconf/aermod/aermod_mfd.pdf.

Etiope, G.; Klusman, R.W. Geological emissions of methane to the atmosphere. *Chemosphere*. **2000**, 49, 777-789.

Etiope, G. GEM -- Geologic Emissions of Methane, the missing source in the atmospheric methane budget. *Atmospheric Environment* **2004**, 38, 3099-3100.

Etiope, G. Mud volcanoes and microseepage: The forgotten geophysical components of atmospheric methane budget. *Ann. Geophys.* **2005**, 48, 1.

Evans, D.J.; West, J.M., An appraisal of underground gas storage technologies and incidents, for the development of risk assessment methodology, British Geological Survey, 2008, http://www.hse.gov.uk/research/rrpdf/rr605.pdf.

Flesch, T.K.; Harper, L.A.; Powell, J.M.; Wilson, J.D. Inverse dispersion calculation of ammonia emissions from Wisconsin dairy farms. *Transactions of the ASABE*, **2009**, 52, 253-265.

Friesen, R.; Parikh, R.; Grant, J.; Bar-Ilan, A.; Pollack, A.; Henderer, D.; Pring, D.; Sgamma, K.; Schlagel, P., Development of Baseline 2006 Emissions from Oil and Gas Activity in the Uinta Basin. *Prepared for Western Regional Air Partnership* **2009**.

Grannas, A.M.; Jones, A.E.; Dibb, J.; Ammann, M.; Anastasio, C.; Beine, H.J.; Bergin, M.; Bottenheim, J.; Boxe, C.S.; Carver, G.; Chen, G.; Crawford, J.H.; Dominé, F.; Frey, M.M.; Guzmán, M.I.; Heard, D.E.; Helmig, D.; Hoffmann, M.R.; Honrath, R.E.; Huey, L.G.; Hutterli, M.; Jacobi, H.W.; Klán, P.; Lefer, B.; McConnell, J.; Plane, J.; Sander, R.; Savarino, J.; Shepson, P.B.; Simpson, W.R.; Sodeau, J.R.; von Glasow, R.; Weller, R.; Wolff, E.W.; Zhu, T. An overview of snow photochemistry: evidence, mechanisms and impacts," *Atmos. Chem. Phys*., **2007**, 7, 4327-4373.

Gurska, J.; Wang, W.; Gerhardt, K. E.; Khalid, A. M.; Isherwood, D. M.; Huang, X.-D.; Glick, B. R.; Greenberg, B. M. Three year field test of a plant growth promoting rhizobacteria enhanced phytoremediation system at a land farm for treatment of hydrocarbon waste. *Environ. Sci. Technol.* **2009,** *43* (12), 4472-4479.

Hafner, S. D.; Montes, F.; Rotz, C. A.; Mitloehner, F., Ethanol emission from loose corn silage and exposed silage particles. *Atmospheric environment* **2010,** *44* (34), 4172-4180.

Hejazi, R. F.; Husain, T.; Khan, F. I. Landfarming operation of oily sludge in arid region—human health risk assessment. *J. Hazard. Mater.* **2003,** *99* (3), 287-302.

Hendler, A.; Nunn, J.; Lundeen, J. *VOC emissions from oil and condensate storage tanks. Final report prepared for Texas Environmental Research Consortium.*, Texas Environmental Research Consortium: 2009.

Hensen, A.; Loubet, B.; Mosquera, J.; van den Bulk, W.C.M.; Erisman, J.W.; Dämmgen, U.; Milford, C.; Löpmeier, F.J.; Cellier, P.; Mikuka, P.; Sutton, M.A. Estimation of NH_3 Emissions from a Naturally Ventilated Livestock Farm Using Local-scale Atmospheric Dispersion Modeling. *Biogeosciences Discussions,* **2009***,* 6, 825 – 862.

Hillel, D. *Environmental Soil Physics*, Academic Press, San Diego, CA (1998).

Howarth, R. W.; Santoro, R.; Ingraffea, A., Methane and the greenhouse-gas footprint of natural gas from shale formations. *Climatic Change* **2011,** *106* (4), 679-690.

Johnson, R. C.; Roberts, S.B.; *The Mesaverde total petroleum system, Uinta-Piceance Province, Utah and Colorado: Petroleum systems and geologic assessment of oil and gas in the Uinta-*

Piceance province, Utah and Colorado, US Geological Survey Digital Data Series DDS-69-B (2003).

Joye, S.B. A piece of the methane puzzle. *Nature* **2012**, 491, 538-539, doi: 10.1038/nature11749

Kampbell, D. H.; Vandegrift, S. A. Analysis of dissolved methane, ethane, and ethylene in ground water by a standard gas chromatographic technique. *J. Chromatogr. Sci*. **1998**, 36 (5), 253-256.

Kang, M.; Kanno, C. M.; Reid, M. C.; Zhang, X.; Mauzerall, D. L.; Celia, M. A.; Chen, Y.; Onstott, T. C., Direct measurements of methane emissions from abandoned oil and gas wells in Pennsylvania. *Proceedings of the National Academy of Sciences of the United States of America*, **2014**, 111(51), 18173–18177. http://doi.org/10.1073/pnas.1408315111

Karion, A.; Sweeney, C.; Petron, G.; Frost, G.; Hardesty, R. M.; Kofler, J.; Miller, B. R.; Newberger, T.; Wolter, S.; Banta, R.; Brewer, A.; Dlugokencky, E.; Lang, P.; Montzka, S. A.; Schnell, R.; Tans, P.; Trainer, M.; Zamora, R.; Conley, S., Methane emissions estimate from airborne measurements over a western United States natural gas field. *Geophys. Res. Lett.* **2013,** *40* (16), 4393-4397.

Kasimir, A. Greenhouse gas emissions from farmed organic soils: a review. *Soil use and management* **1997,** *13*, 250.

Kirchgessner, D. A.; Piccot, D.A.; and Sushma S. M., An improved inventory of methane emissions from coal mining in the United States, *Journal of the Air & Waste Management Association*, **2000**, 50.11, p. 1904-1919.

Klusman, R.W., Leopold, M.E. and LeRoy, M.P., Seasonal variation in methane fluxes from sedimentary basins to the atmosphere: Results from chamber measurements and modeling of transport from deep sources, *Journal of Geophysical Research*, **2000**, 105(D20), pp.24661-24670.

Leduc, R.; Fécil, B.; Leconte, C.; Normandin, Y.; Pagé, T. Odour and VOC impact assessment and air quality monitoring program at a municipal solid waste landfill. *Water Practice and Technology* **2009,** *4* (2), wpt2009032.

Leson, G., and Winer, A.M. Biofiltration: An Innovative Air Pollution Control Technology For VOC Emissions, *Journal of the Air & Waste Management Association*, **1991**, 41.8, p. 1045–1054.

Lu, J.; Wang, X.; Shan, B.; Li, X.; Wang, W., Analysis of chemical compositions contributable to chemical oxygen demand (COD) of oilfield produced water. *Chemosphere* **2006,** *62* (2), 322-331.

Lyman, S.; Tran, T., Inversion structure and winter ozone distribution in the Uintah Basin, Utah, USA. *Atmospheric Environment* **2015,** *123*, 156-165.

Mansfield, M.L. Kerogen maturation data in the Uinta Basin, Utah, USA, constrain predictions of natural hydrocarbon seepage into the atmosphere, *Journal of Geophysical Research: Atmospheres*., **2014**, 119, p. 3460–3475, doi: 10.1002/2013JD020148.

Marchant, C.; Moore, K.; Wojcik, M.; Martin, R.; Pfeiffer, R.; Prueger, J.; Hatfield, J. Estimation of dairy particulate matter emission rates by lidar and inverse modeling. *Transactions of the ASABE* **2011,** *54* (4), 1453-1463.

McDuffie, E. E.; Edwards, P. M.; Gilman, J. B.; Lerner, B. M.; Dubé, W. P.; Trainer, M.; Wolfe, D. E.; Angevine, W. M.; deGouw, J.; Williams, E. J., Influence of oil and gas emissions on summertime ozone in the Colorado Northern Front Range. *Journal of Geophysical Research: Atmospheres* **2016**. 121, 8712-8729, doi: 10.1002/2016JD025265.

Milucka, J.; Ferdelman, T.G.; Polerecky, L.; Franzke, D.; Wegener, G.; Schmid, M.; Lieberwirth, I., Wagner, M.; Widdel, F.; Kuypers, M.M.M. Zero-valent sulphur is a key intermediate in marine methane oxidation. *Nature*, **2012,** 491, 541-546, doi: 10.1038/nature11656.

Miyazaki, B., Well Integrity: An overlooked source of risk and liability for underground natural gas storage. Lessons learned from incidents in the USA, in *Underground Gas Storage: Worldwide Experiences and Future Development in the UK and Europe*, D.J. Evans and R.A. Chadwick, eds., The Geological Society, London, Special Publications, 313, 163-172 (2009)

Monson, B.; Parnell, J., The origin of gilsonite vein deposits in the Uinta Basin, Utah, in *Hydrocarbon and Mineral Resources of the Uinta Basin, Utah and Colorado: Utah Geological Association Guidebook 20;* Fouch, T.D; Nuccio, V.F.; Chidsey, T.C.Jr., eds.; Salt Lake City, Utah; p.257-270 (1992).

Mosier, A.; Schimel, D.; Valentine, D.; Bronson, K.; Parton, W. "Methane and nitrous oxide fluxes in native, fertilized and cultivated grasslands. *Nature*, **1991**. 350, 330-332.

Neff, J.; Lee, K.; DeBlois, E. M., Produced water: overview of composition, fates, and effects. In *Produced water*, Springer: 2011; pp 3-54.

Op den Camp, H.J.M.; Islam, T.; Stott, M.B.; Harhangi, H.R.; Hynes, A.; Schouten, S.; Jetten, M.S.M.; Birkeland, N.-K.; Pol, A..; Dunfield, P.F. Environmental, genomic and taxonomic perspectives on methanotrophic *Verrucomicrobia*. *Environ. Microbiol. Rep*., **2009**, 1, 293-306. doi: 10.1111/j.1758-2229.2009.00022.x.

O'Shaughnessy, P.T.; Altmaier, R. Use of AERMOD to determine a hydrogen sulfide emission factor for swine operations by inverse modeling, *Atmospheric Environment,* **2011**, 45, 4617-4625.

Panikov, N.S. and Dedysh, S.N., Cold season CH_4 and CO_2 emission from boreal peat bogs (West Siberia): Winter fluxes and thaw activation dynamics. *Global Biogeochemical Cycles*, **2000**, 14(4), pp.1071-1080.

Pape, L.; Ammann, C.; Nyfeler-Brunner, A.; Spirig, C.; Hens, K.; Meixner, F. An automated dynamic chamber system for surface exchange measurement of non-reactive and reactive trace gases of grassland ecosystems. *Biogeosciences* **2009,** *6* (3), 405-429.

Pardue, J. H.; Valsaraj, K. Assessment of Air Emissions at the US Liquids Exploration and Production Land Treatment Facility. **2000**.

Parker, D.; Ham, J.; Woodbury, B.; Cai, L.; Spiehs, M.; Rhoades, M.; Trabue, S.; Casey, K.; Todd, R.; Cole, A. Standardization of flux chamber and wind tunnel flux measurements for quantifying volatile organic compound and ammonia emissions from area sources at animal feeding operations. *Atmos. Environ.* **2013,** *66*, 72-83.

Pate, B.; Jayanty, R.; Peterson, M. R.; Evans, G. Temporal stability of polar organic compounds in stainless steel canisters. *J. Air Waste Manage. Assoc.* **1992,** *42* (4), 460-462.

Petrenko, V.F.; Whitworth, R.W. *Physics of Ice*, Oxford University Press, Oxford 1999.

Post, L., ed., 1994, *HGSYSTEM 3.0 Technical Reference Manual*, Report No. TNER.94.059, Shell Research Limited, Thornton Research Centre, P.O. Box 1, Chester, England, Shell Internationale Research Maatschappij B.V.

Prenni, A.; Day, D.; Evanoski-Cole, A.; Sive, B.; Hecobian, A.; Zhou, Y.; Gebhart, K.; Hand, J.; Sullivan, A.; Li, Y., Oil and gas impacts on air quality in federal lands in the Bakken region: an overview of the Bakken Air Quality Study and first results. *Atmospheric Chemistry and Physics* **2016,** *16* (3), 1401-1416.

Rappenglück, B.; Ackermann, L.; Alvarez, S.; Golovko, J.; Buhr, M.; Field, R.; Soltis, J.; Montague, D. C.; Hauze, B.; Adamson, S., Strong wintertime ozone events in the Upper Green River basin, Wyoming. *Atmospheric Chemistry and Physics* **2014,** *14* (10), 4909-4934.

Ririe, G.T.; Sweeney, R.E.,. Comparison of hydrocarbon gases in soils from natural seeps and anthropogenic sources, in *Proceedings of the 1993 Petroleum Hydrocarbons and Organic Chemicals in Ground Water: Prevention, Detection, and Restoration*. November, 1993.

Sander, R. Compilation of Henry's Law Constants for Inorganic and Organic Species of Potential Importance in Environmental Chemistry, Version 3, 1999. http://www.henrys-law.org/henry-3.0.pdf

Schwarzenbach, R.P.; Gschwend, P.M.; Imboden, D.M. *Environmental Organic Chemistry*, 2nd ed., Wiley-Interscience, Hoboken, NJ (2003).

Selley, R.C. *Elements of Petroleum Geology*, W.H. Freeman and Company, New York (1985).

Stoeckenius, T.; McNally, D.; Eds. *Final Report: 2013 Uinta Basin Winter Ozone Study*, March 2014, http://rd.usu.edu/htm/reports.

Stolp, B.J.; Burr, A.L.; Johnson, K.K. Methane Gas Concentration in Soils and Ground Water, Carbon and Emery Counties, Utah, 1995-2003, Scientific Investigations Report 2006–5227, US Geological Survey, 2006.

Striegl, R.G.; McConnaughey, T.A.; Thorstenson, D.C.; Weeks, E.P.; Woodward, J.C. Consumption of atmospheric methane by desert soils, **1992**, *Nature*, 357, 145-147.

Sumner, A.L.; Shepson, P.B. Snowpack production of formaldehyde and its effect on the Arctic troposphere, **1999**, *Nature*, 398, 230.

Theobald, M. R.; Løfstrøm, P.; Walker, J.; Andersen, H. V.; Pedersen, P.; Vallejo, A.; Sutton, M. A. An intercomparison of models used to simulate the short-range atmospheric dispersion of agricultural ammonia emissions. *Environ. Model. Software* **2012,** *37*, 90-102.

Thibodeaux, L.; Hwang, S. Landfarming of petroleum wastes—modeling the air emission problem. This natural treatment process has vapor emission problems that may be reduced dramatically by subsurface injection. *Environ. Prog.* **1982,** *1* (1), 42-46.

Thoma, E. *Measurement of emissions from produced water ponds: upstream oil and gas study #1*, U.S. Environmental Protection Agency: Cincinnati, Ohio, October 2009, http://nepis.epa.gov/Adobe/PDF/P100EACG.pdf.

Tibbetts, P. J. C.; Buchanan, I. T.; Gawel, L. J.; Large, R., A Comprehensive Determination of Produced Water Composition. In *Produced Water*, Ray, J.; Engelhardt, F. R., Eds. Springer US: 1992; Vol. 46, pp 97-112.

Tissot, B.P.; Welte, D.H. *Petroleum Formation and Occurrence*, 2nd ed., Springer-Verlag, Berlin (1984).

Twine, T. E.; Kustas, W.; Norman, J.; Cook, D.; Houser, P.; Meyers, T.; Prueger, J.; Starks, P.; Wesely, M. Correcting eddy-covariance flux underestimates over a grassland. *Agricultural and Forest Meteorology* **2000,** *103* (3), 279-300.

Utah Division of Oil, Gas and Mining (DOGM), oilgas.ogm.utah.gov/Statistics/Statistics.cfm

Utvik, T. I. R., Chemical characterisation of produced water from four offshore oil production platforms in the North Sea. *Chemosphere* **1999,** *39* (15), 2593-2606.

Veil, J. A.; Puder, M. G.; Elcock, D.; Redweik Jr, R. J., A white paper describing produced water from production of crude oil, natural gas, and coal bed methane. *Argonne National Laboratory, Technical Report* **2004**.

Vulindlu, M.; Charlett, A.: Surman, S.; Lee, J. V. Comparison of agar-based methods for the isolation and enumeration of heterotrophic bacteria with the new Multidose IDEXX SimPlate method. Water Sci. Tech. **2004**, 50 (1), 277-280.

Wang, D.; Austin, C. Determination of complex mixtures of volatile organic compounds in ambient air: canister methodology. *Anal. Bioanal. Chem.* **2006,** *386* (4), 1099-1120.

Wang, T.; Sattayatewa, C.; Venkatesan, D.; Noll, K. E.; Pagilla, K. R.; Moschandreas, D. J., Comparison of two dynamic measurement methods of odor and odorant emission rates from freshly dewatered biosolids. *Journal of Environmental Monitoring* **2011,** *13* (6), 1746-1752.

Warneke, C.; Geiger, F.; Edwards, P. M.; Dube, W.; Petron, G.; Kofler, J.; Zahn, A.; Brown, S. S.; Graus, M.; Gilman, J. B.; Lerner, B. M.; Peischl, J.; Ryerson, T. B.; de Gouw, J. A.; Roberts, J. M., Volatile organic compound emissions from the oil and natural gas industry in the Uintah Basin, Utah: oil and gas well pad emissions compared to ambient air composition. *Atmospheric Chemistry and Physics* **2014,** *14* (20), 10977-10988.

Xu, L., Lin, X., Amen, J., Welding, K. and McDermitt, D., Impact of changes in barometric pressure on landfill methane emission. *Global Biogeochemical Cycles*, **2014**, 28(7), 679-695.

Zhang, Y.; Gable, C. W.; Zyvoloski, G. A.; Walter, L. M., Hydrogeochemistry and gas compositions of the Uinta Basin: A regional-scale overview. *AAPG bulletin* **2009,** *93* (8), 1087-1118.

Zhang, Y.; Li, B.-Z.; Yang, J.-S.; Wang, S.-Q.; Yuan, H.-L. Diversity of culturable butane-oxidizing bacteria in oil and gas field soil, *Huanjing Kexue/Environ. Sci*., **2012**, 33, 299-304.